Centralised vs decentralised PI control for an islanded multi-inverter microgrid

AF Jordaan

orcid.org/0000-0001-7827-6902

Dissertation accepted in fulfilment of the requirements for the degree *Master of Engineering in Computer and Electronic Engineering* at the North-West University

Supervisor:	Prof KR Uren
Co-supervisor:	Prof G van Schoor
Co-supervisor:	Dr MG Botha

Graduation:	June 2023
Student number:	29685036

Abstract

Energy supply security is arguably one of the most pressing challenges for both emerging and established countries around the world, as technology grows increasingly reliant on reliable energy. With the increase of Renewable Energy Sources (RES), low maintenance costs in comparison with utility grids, and low energy losses, microgrids are a preferred solution for addressing energy security. Microgrids are not without their challenges, therefore, a lot of research is focused explicitly on the voltage and frequency stability of a microgrid.

This study aims to compare the performance of a centralised and decentralised controller for an island multi-inverter microgrid. Microgrid control is frequently complex, financially and computationally expensive, and difficult to scale as the microgrid grows, therefore, a simple control technique (PI controller) will be used in both configurations to determine if it can be used to maintain stability within a microgrid after being subjected to various types of disturbances.

The current challenges in microgrid control are firstly identified from literature. A simulation model from the literature is retrieved, however, due to model constraints, a mathematical model must be derived that can be used to approximate the simulation model before any sort of control can be implemented. The mathematical model is used to design the control systems, which are then applied to the simulation model in the Simulink environment.

To compare the centralised and decentralised control strategies, an experimental design is created in which scenarios are built to assess the performance of the control systems under extreme conditions derived from the literature. The results of each scenario will be analysed to determine the best performing approach for each scenario/application, and the techniques will be rated based on their capacity to minimise disruptions.

This work underlines the importance of simplicity; the fact that a basic PI controller can sustain stability in a multi-inverter microgrid demonstrates the effectiveness of resilient control techniques. Future research may include the integration of Neural Networks into the control system to allow for approaches such as load forecasting, although this will significantly increase the control system's complexity.

Keywords: Islanded microgrid, decentralised control, microgrid stability, low-voltage, load management

Contents

List of Figures

List of Tables

Acronyms

AC	Alternating Current.
AI	Artificial Intelligence.
ANOVA	Analysis of Variance.
CCHP	Combined Cooling Heating and Power.
CCT	Critical Clearing Time.
CHP	Combined Heat and Power.
DC	Direct Current.
DCL	Digital Communication Link.
DER	Distributed Energy Resource.
DERs	Distributed Energy Resources.
DG	Distributed Generation.
DSM	Demand-Side Management.
EMS	Energy Management System.
ESS	Energy Storage System.
FFT	Fast Fourier Transform.
IAE	Integral Absolute Error.
ISE	Integral Squared Error.
MAS	Multi-Agent System.
MPPT	Maximum Power Point Tracking.
NERSA	National Energy Regulator of South Africa.
PCC	Point of Common Coupling.
PI	Proportional-Integral.
PID	Proportional-Integral-Derivative.
pu	per unit.
PV	Photovoltaic.
PWM	Pulse Width Modulation.
RES	Renewable Energy Sources.
ROCOF	Rate of Change of Frequency.
SoC	State of Charge.
SPOF	Signle Point of Failure.
THD	Total Harmonic Distortion.
USA	United States of America.
V2G	Vehicle-to-Grid.

Chapter 1

Introduction

This chapter will provide some background on microgrids, their operation, and control. The problem statement is discussed along with the research objectives and research methodology. This chapter will conclude with an outline for the rest of this dissertation.

1.1 Background

Energy supply security is currently a major concern for both developed and developing countries worldwide, as extensive disruptions could have a huge impact on global economies. Energy security can be defined as reliable, adequate, and affordable energy for both private and industrial consumers [1].

Various factors might jeopardise the security of energy in every country; consequently, these problems should be noted to ensure that they are addressed in future solutions to this challenge. One of the known energy security risks includes physical security threats such as sabotage, natural disasters, and theft. Another risk is the technical failures of systems such as power outages caused by malfunctions [1].

The rest of this chapter will provide some background on microgrids and their control. This is not an in-depth discussion since the detail will be covered in chapter 2, but it will provide a broad overview of microgrids and their control. The problem statement is also present in this chapter, although the literature supporting the problem statement is discussed in chapter 2. This chapter will conclude with the research objectives and methodology of this study.

1.1.1 Microgrids

Some solutions have been implemented to try and mitigate the risks associated with energy security; one of which is the introduction of Renewable Energy Sources (RES). RES are widely used for electricity generation since they can minimise both transmission losses and overall costs when they are located close to the consumers [1]. A typical configuration of multiple RES is also known as a microgrid, which is described by [2] as a localised collection of interconnected energy sources and loads that operate as a single controllable unit which is synchronous with the main grid in grid-tied operation. One of the main advantages of microgrids is the fact that they can disconnect from the utility grid and function autonomously (also known as islanded mode) as the physical and/or economic conditions dictate [2]. The grid-tied mode of operation of a microgrid refers to the operation in which energy can be exchanged with the utility grid, whereas in islanded mode, the microgrid does not have any connection with the utility grid [3]. The typical microgrid primarily consists of five main elements, which can be derived from figure 1.1 [4]:

- Distribution network (Electrical feeder)
- Distributed generation units (Wind/PV/Synch. Gen.)
- Energy storage units (ESS)
- Controllable and uncontrollable loads (Load)
- Control system (Primary control)

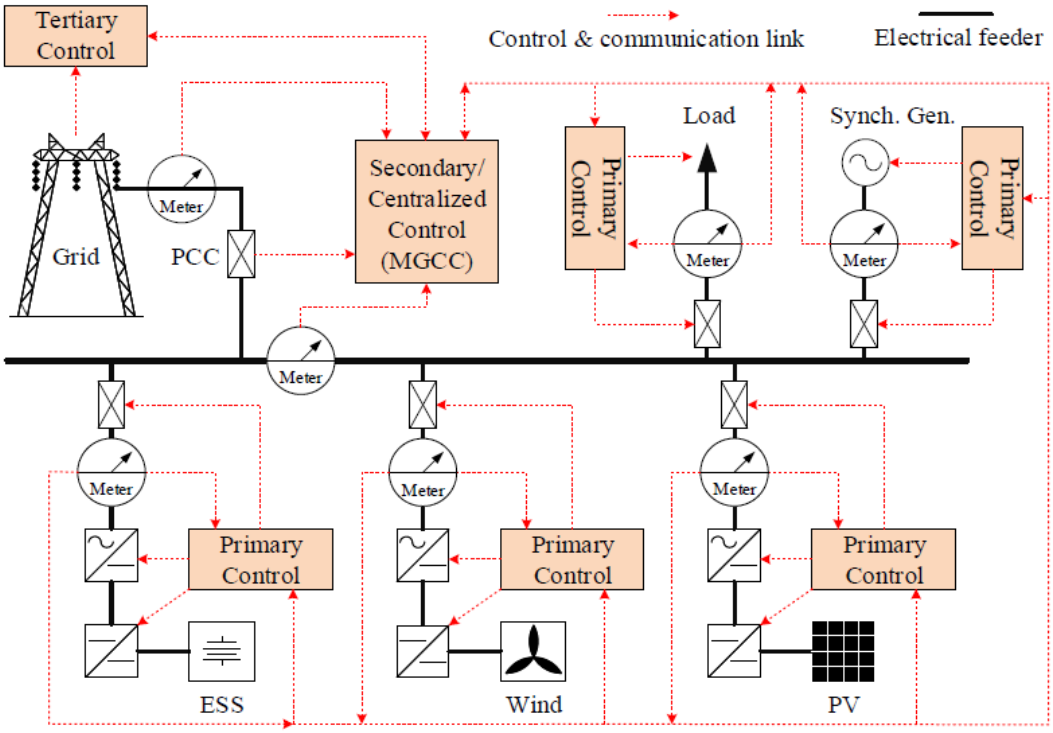

Figure 1.1: Typical configuration of a microgrid. From [4].

Distributed Generation (DG) in microgrids refers the power generation at close proximity to the consumption sites [2]. When comparing DG to central generation, it is clear that DG can eliminate some of the transmission, distribution, and generation costs while increasing the overall efficiency by removing elements of inter-dependency [2].

From all the above it becomes clear that microgrids consist of multiple individual units that are interconnected to operate together to ensure energy security. The problem with such a diversified system is it is quite hard to control so many individual components effectively such that the entire system is within voltage and frequency standards, as depicted by the National Energy Regulator of South Africa (NERSA) in [5]. If the microgrid does not comply with the standards of the utility grid, it will not be allowed to operate, therefore, the control system in a microgrid is one of the most important elements.

1.1.2 Microgrid control

A microgrid, in its grid-tied mode, is relatively stable and the control of such a system is effortless in comparison to the islanded microgrid. Whenever it is required of the microgrid to disconnect itself from the utility grid, it is required of the microgrid to establish the system bus voltage and frequency while, at the same time, providing the demanded active and reactive power to the loads within the set of IEEE standards [6].

The islanded operation of the microgrid is where the most challenges originate since the bus voltage and frequency are dependent on the load connected to the microgrid. If the load is small, the microgrid will be able to supply the load with the required power, but as the load increases, the microgrid may not be able to keep supplying the load with the adequate amount of power, which may lead to voltage and frequency deviations [6]. The variation of voltage and frequency within a microgrid is also dependent on numerous factors such as the short circuit capacity of the system, the inertia in the microgrid, and the active-reactive power balance in the system [4], [7], [8].

The configuration used in a microgrid will often determine whether or not the microgrid can be expanded. Since a microgrid is usually a cluster of individual units connected, it is possible to increase the capacity of a microgrid by adding components/units. This is highly useful in most microgrids; however, the control system of such a microgrid must be robust to withstand the disruption induced into the system. This is because one of the primary issues in a microgrid setup is the interaction between Distributed Energy Resources (DERs) [9]. The interaction between the DERs in this context refers to the adding and removing of elements in the system.

There are several different control strategies developed over the years to try and maintain the bus frequency and voltage at the required reference values, but since there is not a single microgrid configuration, the control system implemented may have to be adapted to fit each configuration. Therefore, one needs to assess the configuration of the microgrid before choosing a control technique to apply.

1.2 Problem statement

The load connected and interaction between inverters in a multi-inverter microgrid is currently a major cause of voltage and frequency instability in a microgrid. To find the best suitable controller for each application and configuration, centralised and decentralised control strategies must be tested on a multi-inverter microgrid with ideal sources to determine the impact of different disturbances.

1.3 Research objectives

To ensure this study is done using a systematic approach, four milestones, or objectives, were identified; the model development of an islanded microgrid, sensitivity analysis, control strategy development, and the evaluation of the developed control system. This section will describe these objectives after which the methodology to complete each objective will be discussed in section 1.4. An overview of the storyline of this dissertation, which includes the following objectives, is shown in figure 1.2.

1.3.1 Model development of an islanded microgrid

This study will be done in a simulation environment only, therefore, a representative model of an actual microgrid is needed. The model should include a load that can be connected or disconnected from the microgrid. The microgrid model should also contain multiple inverters that can be added or removed from the system at any given time, as dictated by the conditions. These conditions refer to the scenario in which the capacity of the microgrid is not large enough to supply the load in which case more inverters should be added to the microgrid to increase the capacity. Should one of the inverters fail or require maintenance, the inverter should be removed from the microgrid. The final element that should be included is an Energy Storage System (ESS). The model should allow for adjustments in the load's characteristics as well as the characteristics of each inverter in order to create different scenarios for which the control system can be tested.

1.3.2 Identification of instability contributors

Once the model is developed, a sensitivity analysis should be performed. The sensitivity analysis aims to identify factors (with regards to the sizing of the system components as well as operation of the system) that will contribute significantly toward the voltage and frequency stability of the microgrid. These factors may include the size of the load, how and when different inverters are connected and disconnected from the microgrid, the size of the ESS, and the size of each inverter. Different scenarios should be evaluated to determine the characteristics of an unstable system and also to determine the sensitivity of the system to the different sizing and operational factors.

1.3.3 Control strategy development

The two control techniques that will be evaluated are centralised and decentralised PI control. Centralised control will be used to control all the inverters in the same microgrid with the same control loop. Decentralised control will also control all the inverters in the microgrid, but in this control technique, each inverter has its control loop instead of one control loop for all the inverters. These separate control loops all form part of the decentralised control system. The verification of the control system will be completed in this objective.

1.3.4 Evaluation of control systems

Once the control systems are developed, they will be implemented on the microgrid model in the simulation environment. Different scenarios will be created in which the control techniques' performance will be measured against stability criteria. The stability criteria will be derived from literature and microgrid simulations without control techniques implemented. The controllers' performance under different circumstances will then be evaluated. The validation of the control system will be completed in this objective.

1.4 Research methodology

This section will describe the methodology that will be used to address the different objectives described in the preceding section.

1.4.1 Model development for an islanded microgrid

The modelling of an islanded microgrid requires extensive knowledge of fundamental electrical systems, which can make the modelling process difficult. The literature will be consulted to find adequate knowledge on the elements needed to understand and model the microgrid in Simulink. Previous studies will also be consulted to find information as well as existing building blocks for a microgrid. Since this study aims to investigate the different control philosophies, it is not required to develop the model from first principles, but previously developed and verified blocks can be used to compose the Simulink model.

Simulink is the choice of simulation software since it has great support and a good database of existing building blocks that can be used to construct any simulation model. There are also electrical toolboxes that will be used to simplify the process. Simulink also simplifies the process of adding and removing inputs and/or disturbances which ensures a good and reliable simulation environment.

Since the goal is not to develop the microgrid model from scratch, it will be necessary to ensure that the system dynamics are accurate. This will be accomplished by developing a mathematical state-space model of a single inverter and comparing it to the Simulink model to verify the dynamics of the microgrid. Once this is done, it can be assumed that the model is valid and the next step can proceed.

1.4.2 Identification of instability contributors

The simulations for the sensitivity analysis will also be done in the MATLAB/Simulink environment. This analysis will only commence once the model is operating according to specification. At this stage, the control development/implementation will not be done as this sensitivity analysis aims to find the sensitive parameters in the microgrid which will later be used in the control development. There are specialised analysis techniques such as Analysis of Variance (ANOVA) and Monte Carlo, but these methods are not used in this sensitivity analysis since ANOVA models apply best to data that is presented in groups [10], while the Monte Carlo method is optimised for mathematical problems which make use of random samples [11]. Neither of these methods can be applied to this sensitivity analysis without adjustments to the model.

The sensitivity analysis entails that different predefined scenarios are simulated to observe the behaviour of the microgrid subjected to different disturbances related to the load's magnitude and the number of inverters connected. These scenarios will test the durability of the system; for example, different disturbances will be introduced into the system which may cause the system to become unstable. Some of these scenarios will originate from literature in which the output of the simulations will be compared to the results in literature as another verification step to ensure the model is operating as expected. The results from these simulations will be carefully analysed to discover which system characteristics are critical for system stability.

1.4.3 Control strategy development

The control of the microgrid will also be done in the MATLAB/Simulink environment. As discussed in the preceding sections, centralised- and decentralised control will be examined as control approaches. The data extracted from the sensitivity analysis will be used to choose the suitable design technique to design/develop the PI controllers for the centralised- and decentralised control systems.

These controllers will then be implemented on the simulation model and the same scenarios will be used to test the effectiveness of each controller as was used in the sensitivity analysis. The system will also be tested in a few extra scenarios to test the robustness of the control system under extreme circumstances. The centralised controller will be developed first. This controller will receive the desired reference voltage and frequency values as input. It will then calculate the error signal from the measurements at the Point of Common Coupling (PCC) and the given reference input.

The decentralised controller will also receive the desired voltage and frequency values as inputs, but the error signals will be calculated from the measurements at the output of each inverter. The result being each inverter has its control system that will maintain that inverter at the desired reference point. This would result in a small steady-state error for each inverter, but the bus voltage and frequency may deviate from the reference point.

The results of these simulations will be used in the control system's verification process. To ensure that the control system is influencing the inverters in the desired way, the output waveforms of the Simulink model will be compared to a reference.

1.4.4 Evaluation of control systems

The evaluation of the control systems will entail that the performance of each controller is compared to the other control system as well as to the benchmark (microgrid with no control). Since the performance of each controller cannot simply be measured by output graphs alone, methods found in literature will be used to quantify the performance of each control technique.

The controllers will be evaluated on their ability to withstand disturbances and configuration changes. The error- and control signals of each controller alongside the output voltage and frequency values of the entire system will be used to calculate the performance of the controllers. The performance measures that will be used in this study are provided by the South African grid code [5]:

- Voltage
  - Can the control system maintain the voltage within the specified range?
  - Range: 218.5 V $\leq$ Voltage $\leq$ 241.5 V.
- Frequency
  - Can the control system maintain the frequency within the specified range?
  - Range: 49.5 Hz $\leq$ Frequency $\leq$ 50.5 Hz.

Once the comparison is done, the best controller for each application and configuration can be decided. The validation of the control system will be completed by determining the performance of the control system after being subjected to various undesired circumstances.

The storyline of this study is presented in figure 1.2. The first two objectives are completed in chapter 3, since the modelling and sensitivity analysis are done in this chapter. The third objective is completed in chapter 4 where the control system is designed and implemented on the Simulink model.

The verification of the control system is also done in chapter 4. The verification of the control system is done by examining whether or not the influence of the control system is as specified by the design requirements. The final objective is done in chapter 5 in which the control system is evaluated. The validation of the control system is also done along with the evaluation. The validation of the control system is done by determining whether or not the control system is able to maintain stability within the microgrid without violating the specified operating ranges.

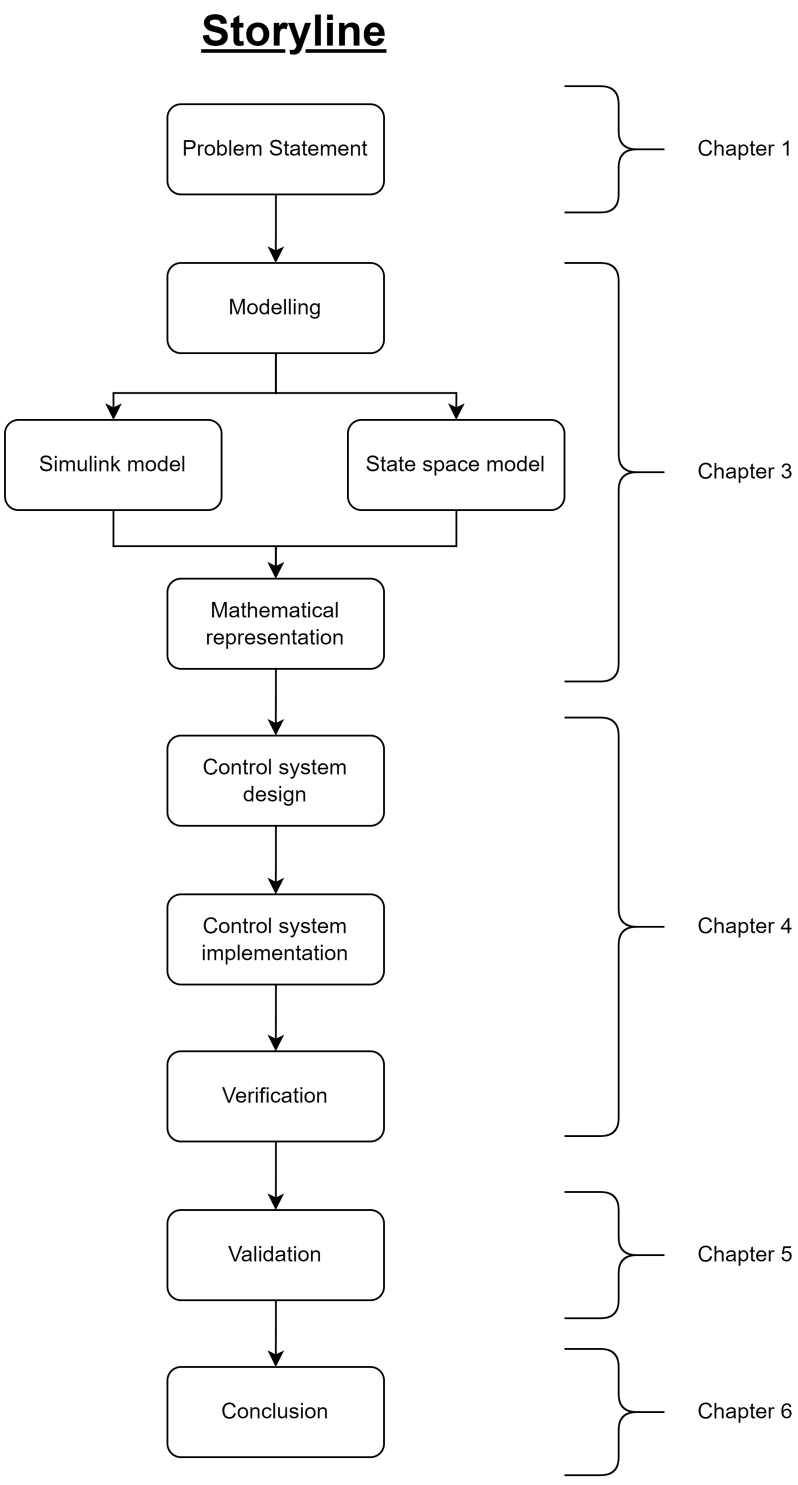

Figure 1.2: Storyline for this dissertation

1.5 Dissertation outline

Chapter 1 discussed the problem statement along with the research objectives for this study. The research methodology is also discussed in chapter 1.

Chapter 2 focuses on the literature on microgrids and the challenges associated with microgrid stability and control. The current challenges are highlighted in this study and the possible control techniques are also discussed from literature and previous studies.

Chapter 3 describes the modelling process that was followed to obtain a representative mathematical state-space model of an inverter in the Simulink model. The state-space model was derived in a symbolic format before it was converted to a numerical state-space model using the parameters obtained from the Simulink model.

Chapter 4 depicts the design procedure of an adequate PI control system. All the design assumptions and choices are explained and the implementation of the control system in Simulink is detailed as well. The verification of the PI control system is also done in chapter 4.

Chapter 5 discusses the results obtained from the simulations performed to asses the performance of the control system. An experimental design is developed in which different scenarios are identified that will test the overall performance of the centralised and decentralised control system. The validation of the control system is done in chapter 5.

Chapter 6 concludes this dissertation. A final overview is provided of the results obtained during the dissertation, along with some of the shortcomings. The possibilities for future research are also discussed in this final chapter.

Chapter 2

Literature Study

This chapter will describe some of the phenomena, challenges, and control strategies commonly found in microgrids. First, some of the technologies used in microgrids are discussed after which the different modes of operation for microgrids will be explained. The stability concerns will be detailed and some control solutions will be discussed from literature.

2.1 Introduction

This chapter aims to provide enough information from the literature on microgrids to identify some flaws in microgrid control and operation.

This chapter opens with microgrid technology sections in which Photovoltaic (PV) generation, energy storage, and load management are discussed. The section on PV is a summary of how this technology works and how it is typically implemented in the conventional microgrid. The energy storage is then analysed in which the options for energy storage are discussed, and the expectations from the energy storage are also listed. Load management is the final element in the technology section that will be considered. Load management proof to be a powerful tool when considering microgrid control. This is discussed and explained along with the possible forms of load management in a microgrid.

The next section is on the grid-tied and islanded operational modes of a microgrid in which the differences, advantages, and disadvantages are listed. This is followed by microgrid stability, which is quite significant in the context of this study. The stability covers voltage stability and frequency stability while the effect of power sharing on the stability is also discussed.

The chapter concluded with the control of a microgrid. In this section, the different control techniques, namely droop control, centralised- and decentralised control, multi-agent system control, and PID control are discussed and compared with one another. The interaction between different DERs in a microgrid is also listed, which is also significant for this study.

2.2 Microgrid Technology

The typical microgrid consists of an ESS, a Distributed Energy Resource (DER), and a load connected to the microgrid. The DER is responsible for the generation of energy while the ESS is responsible for the storage of energy. There are numerous renewable sources used in microgrids such as wind, fuel cells, Combined Heat and Power (CHP), etc. but they are not relevant to this study. The sections to follow will elaborate on the basic technologies of a microgrid relevant to this study.

2.2.1 Photovoltaic generation

The typical microgrid configuration will consist of a PV array that will convert the photovoltaic energy to Direct Current (DC) electric energy. Since the output energy of the PV array is not constant, a DC-DC converter with a Maximum Power Point Tracking (MPPT) scheme is added to the output of the PV array. This will ensure that the PV array is operating at maximum capacity while maintaining a stable voltage to the DC-AC inverter that will convert the DC voltages into Alternating Current (AC) voltages that can be introduced to the PCC [12], [13].

A PV cell can be considered a current source, as illustrated in figure 2.1. The series resistance R_s accounts for the voltage drop observed in PV cells due to the structural resistance while the shunt resistance R_p represents the voltage loss due to the diode leakage current [12].

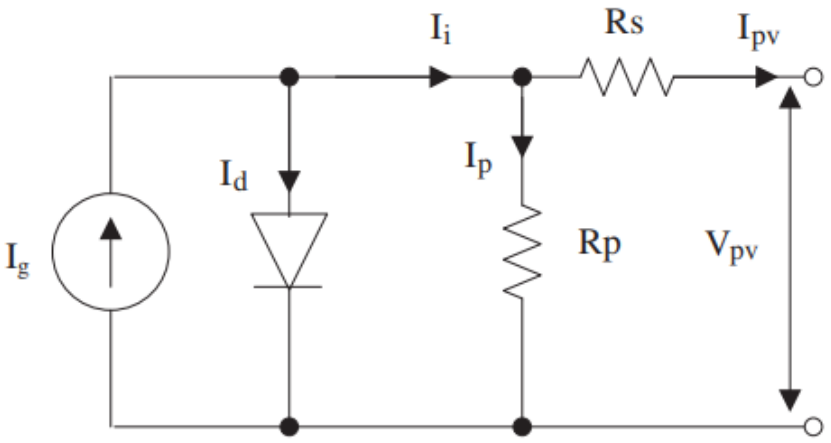

Figure 2.1: Equivalent circuit of a PV cell. From [12].

The fact that the PV cells can be considered current sources will introduce some non-linear behaviour. The output voltage is dependent on the output current, which in turn is dependent on elements such as irradiance and cell temperature [12], [14]. When the I-V (current-voltage) characteristics of the PV are examined, as shown in figure 2.2, the relationship between voltage and current is non-linear, as expected.

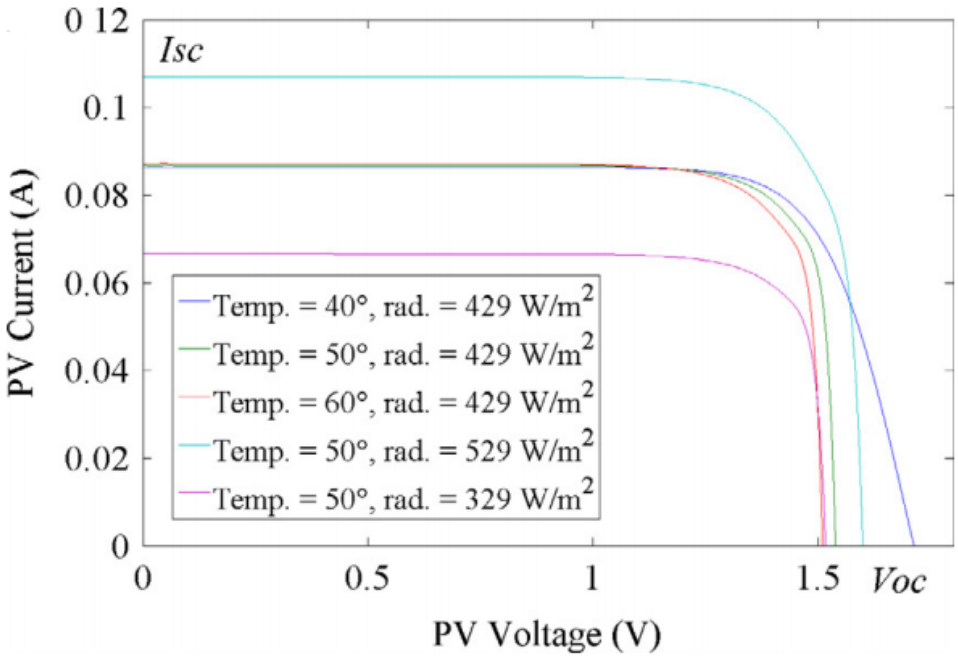

Figure 2.2: I-V characteristics of PV cell. From [12].

The I_{sc} and V_{oc} values represent the short-circuit current and open-circuit voltage respectively. The variation in output due to changes in temperature and irradiance is evident which complicates the control of such a cell. To ensure a more stable output from the PV array to the next stage in the microgrid, an MPPT system is implemented to optimise the efficiency of the PV energy conversion [12]. By using the MPPT controller, the voltage of the PV array can be adjusted to obtain maximum real power despite the natural variability while the reactive power is controlled by the constant power factor using an inverter controller [12].

2.2.2 Energy storage

The energy storage devices/technologies is a crucial factor to legitimise RES as a reliable contributor to main sources and to provide a successful operation of a microgrid [2]. Energy storage technologies are classified into three types: electrochemical systems (batteries and flow cells), kinetic energy storage systems (flywheels), and potential energy storage (pumped hydro or compressed air storage) [2], [15]. Although all the before-mentioned technologies can be used, batteries constitute the best solution to ensure the sustainability of fixed voltage and frequency operation while using RES in a microgrid [2], [15].

The requirements of the ESS in a microgrid, as described in [2], [16], can be summarised as the following:

- The most important aspect of the ESS is to provide a balance between the power generated by the RES and the power demanded from the load connected to the microgrid.
- The ESS must store all excess energy during off-peak hours to be able to supply all loads when needed.
- The ESS must be able to help meet the unpredicted and sudden demands from the loads.
- The ESS must provide smooth transition conditions from grid-tied operation to islanded operation and vice versa.
- The ESS must have the capacity to be able to accommodate the minute-hour peaks in demands during a normal day.

The design of an ESS should consider the above-mentioned requirements, but it should also consider the charge- and discharge rate, the number of charge/discharge cycles in the ESS's lifetime, and the State of Charge (SoC) [17]. The SoC refers more to the control system since the control of the ESS should maintain the ESS at a healthy SoC to ensure not shortening its lifespan.

2.2.3 Load management

There are various kinds of loads connected to a typical microgrid and they will contribute significantly toward the system's operation, stability, and control [2]. The loads connected to the microgrid can be divided into two categories: Type I controllable loads (Passive load), and Type II controllable loads (Active load) [18].

Type I controllable loads, or passive loads, largely comprise residential loads that include fridges, washing machines, air-conditioners, and water heaters [18]. One of the characteristics of these types of loads is that they cannot inject power into the grid at any time, they can only absorb power.

Type II controllable loads, or active loads, include battery storage, Vehicle-to-Grid (V2G), and Combined Cooling Heating and Power (CCHP). Unlike Type I loads, the Type II controllable loads can supply energy to the network, hence, active controllable loads [18]. According to [18], battery storage is one of the best ways to reduce renewable energy fluctuation and enhance system stability due to the battery's ability to store excess energy and inject energy into the power system during power shortage.

The development of smart meter technology has grown tremendously in the last decade which allowed the communication between the distributor operation company and the smart devices (controllable loads) to be in real-time. Therefore, the customer can also participate in Demand-Side Management (DSM) with the assistance of an Energy Management System (EMS) [18]. The DSM can only be implemented if the characteristics of a controllable load are known. The authors of [18] and [19] summarised some of the characteristics as:

- Most controllable loads that are found in a microgrid usually are small-scale and dispersed. There are also numerous types of loads connected to the microgrid, which will complicate the management of these loads using traditional control methods.
- There is always real-time information about the load available. In the typical configuration, the controllable load will receive the control demand from the upper controller and send back the measured information in real time.
- The active demand-side response by the end-user will be more beloved. With the development of smart homes and smart grids, the end-user will have more control to schedule the controllable loads to avoid having a shortage of supply.

- The controllable loads in a microgrid can usually be controlled together with distributed renewable energy.

The concept of DSM embraces all of the measures implemented by the utility grid operators to directly modify the power profiles of electricity consumers to ensure a more reliable and efficient operation of electrical grids [20]. According to [20], DSM can be classified into six separate categories, as depicted in figure 2.3:

1. Peak clipping
2. Valley filling
3. Load shifting
4. Flexible load shape
5. Strategic load-growth
6. Strategic conservation

Categories 1-4 above are considered to be part of load management, whereas categories 5 and 6 are part of strategic conservation actions.

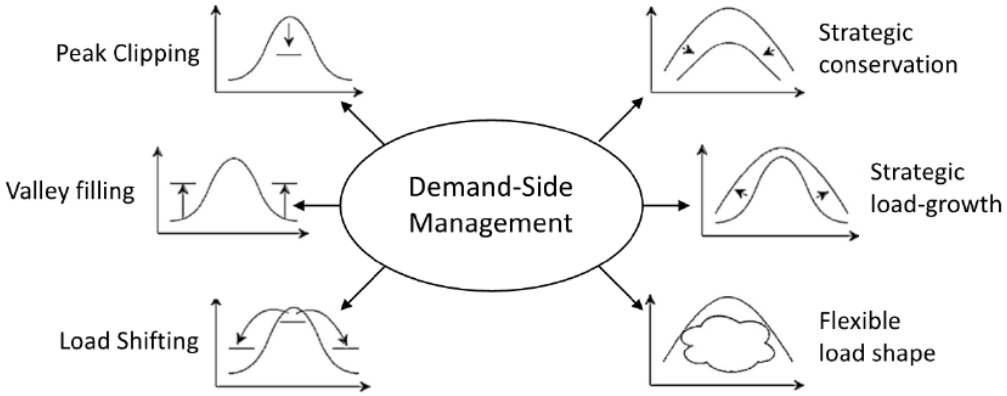

Figure 2.3: Classification of the objectives of DSM. From [20].

Peak clipping, also known as peak shaving in DSM, is the process of reducing the system peak loads which is generally required in the case of limited power capacity. Peak shaving can be obtained by either direct or indirect reduction of the power consumption of the customer where the direct reduction refers to control signals and the indirect reduction refers to price signals [20], [21]. The direct method entails that the loads are reduced by the control system after it received the control signal from the supervisory controller. The indirect method entails that the price of the electricity supplied is different during different times of the day, which will encourage the customers to limit their power usage during that time of day.

The next form of load reduction of system peak loads is known as load shifting, which aims to shift the power demand of end-users from peak times to off-peak times. This can be done by either price signals or through ESS [20]. Valley filling is the increasing power demand of customers in periods where long-run incremental costs are less than the average electricity price [20]. The final category, flexible load shape, can be considered as the combination of the three mentioned load management techniques, and aims at a more complex and flexible modification of the power demand patterns [20].

2.3 Microgrid operational modes

Depending on the present state of the electrical system, microgrids can operate in either grid-tied or islanded mode. Grid-tied operation is desired in most circumstances, however, it is not always possible, resulting in utility grid disconnection. The sections that follow will go over the problems and benefits of each style of operation.

2.3.1 Grid-tied operation

The microgrid will, in ideal circumstances, stay connected to the utility grid to operate in grid-tied mode. During the grid-tied mode of operation, the microgrid will supply the utility grid with reactive power while the bus voltage and frequency are determined by the utility grid. If the DG is reduced for any reason, the utility grid will compensate for the lack of active power in the microgrid which will result in no voltage deviations [22].

The fact that the utility grid is responsible for the bus voltage and frequency reduces the burden on microgrids, but it also contributes to the stability of a grid-tied microgrid. Since stability is usually related to voltage and/or frequency deviations/oscillations, a grid-tied microgrid cannot become unstable in this sense. The instability of a grid-tied microgrid is then reliant on the stability of the individual components in the system. Therefore, if a component such as a DER malfunctions, it may cause instability, but that is not necessarily related to a certain operating circumstance [4], [22]. Thus, the stability challenges for a grid-tied microgrid are not as severe as for an islanded microgrid.

2.3.2 Islanded operation

The microgrid will island itself when a fault occurred which means that the utility grid will not be connected to the microgrid. This will require the DGs to form the bus voltage and frequency in accordance with consumer constraints [22]. The DGs utilised in a microgrid which will operate in islanded mode are referred to as grid-forming DGs whereas DGs used when the microgrid is in grid-tied mode are referred to as grid-following DGs [23].

The stability concerns in an islanded microgrid are much more in comparison with a grid-tied microgrid. One of these concerns in islanded microgrids, especially in microgrids with small distribution systems, is their relatively low short-circuit capacity. In such systems, any small change in microgrid configuration (the start-up or shut down of a diesel generator) may result in relatively large voltage and frequency deviations which, in turn, may lead to instability [4].

Another concern of an islanded microgrid is that they have little or no inertia in the sources, meaning they cannot instantly supply large load changes [8], [22], [24], [25]. This creates challenges for achieving power balance and power sharing amongst the sources because the system frequency in the microgrid will vary until the power sourced by the microgrid and the power consumed by the load are balanced [4], [8], [3].

Load shedding is defined by [3] as a coordinated set of controls which results in a decrease of the electrical load in a power system or microgrid. As mentioned earlier, the balance between the power supply and power demand is crucial for microgrid stability. In the case of a surplus supply, the generation output can be decreased and/or the distributed storage in the microgrid can be charged to solve the imbalance between supply and demand [3]. In the case of supply shortages, generation output can be increased by adding more DGs to the microgrid and/or the distributed storage can be discharged to assist the DGs. In the case of critical supply shortages, load shedding should be applied if all other measures failed to compensate for the imbalance in the microgrid [3].

The stability of a microgrid can also be measured by means of the Critical Clearing Time (CCT), which is defined as the maximum time between initiation of the fault and the isolation/clearing of the fault such that the microgrid remains stable [4]. When considering control system stability, the CCT can be measured; if it falls below a set threshold, the system is said to be stable. [26]. Thus, the larger the CCT in a microgrid, the better the transient stability in the microgrid will be, i.e. the more stable it will be [27].

2.4 Microgrid stability

The characteristics of a microgrid mentioned in section 2.3 can be further investigated to analyse the different types of stability challenges a microgrid may encounter. The reason is that some of the stability challenges observed in large interconnected systems have not been observed in microgrids, therefore, stability in a microgrid needs to be classified [4]. In conventional grid-tied microgrids, the transient and voltage stability problems typically occur more frequently than frequency stability, whereas in islanded microgrids, the frequency stability is of higher concern due to low system inertia and the high penetration of RES [4].

Voltage and frequency are firmly coupled in microgrids, therefore, contrary to some instability phenomena in the conventional utility grid, fluctuations in all system variables will cause instability in a microgrid [4]. This makes it rather difficult to classify instability in a microgrid as "voltage instability" or "frequency instability" based solely on measurements taken of the respective variables [4]. Due to this difficulty, [4] presented an alternative classification of a microgrid, as seen in figure 2.4.

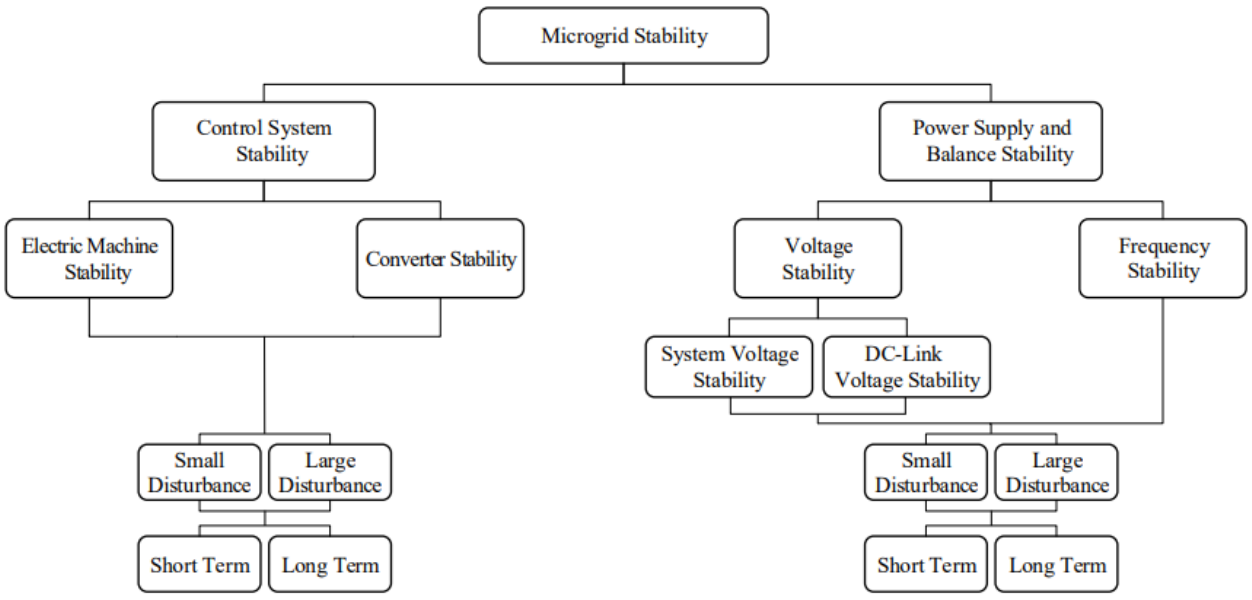

Figure 2.4: Classification of stability in a microgrid. From [4].

The classification in figure 2.4 can be divided into two categories; instability due to the equipment control systems, and instability due to active and reactive power sharing and balance. The instability in either category can be a short- or long-term phenomena in which short-term refers to a time frame of a few seconds, and long-term refers to a time frame of larger than one second [4].

2.4.1 Power sharing and balance

Power supply and balance stability pertain to the ability of the microgrid to maintain a power balance between power supply and demand and to effectively share the demanded power among DERs such that the system satisfies the operational requirements [4]. The concept of power sharing is known as Droop Control, which will be discussed later in this document [28]. These types of instability challenges are usually associated with the loss of a generational unit, violation of DERs limits, or poor power sharing among the DERs in the microgrid [4].

2.4.2 Frequency stability

The frequency regulation in a microgrid is of high concern as explained in the preceding sections. Due to the limited number of generation units in microgrids, the system is at risk of large disturbances for such disturbances can cause large frequency excursions at a high rate of change, jeopardising the system frequency stability [4], [22], [29]. In this context, the conventional control techniques may not be fast enough to overcome the rapid change in the system, especially in systems with low inertia, which will ultimately cause a change in output frequency. This can be due to the control architecture that is not optimal for the system configuration, or the control system might experience network delays which can also reduce the reaction speed of the control system [21].

Frequency instability is not always caused by frequency-related elements in the microgrid. For instance, due to the relatively small size of the microgrid, voltage changes at the terminals of the DERs in the system are almost instantaneously reflected on the load side, which can also cause variations in the output [4], [22].

2.4.3 Voltage stability

In microgrids, the limits of DERs and the sensitivity of load power consumption to supplied voltage are crucial elements in voltage instability. Thus, voltage instabilities may occur in the form of unacceptable low steady-state voltage or dynamic voltage in which the voltage rapidly changes [4], [22]. Since the power-sharing among different DERs in the system is also a known cause of voltage instability, droop control methods are being implemented in microgrids to mitigate the effect of poor power sharing since droop control will manage the output power of each DER in the microgrid [4], [22], [30].

Depending on the type of DER in the microgrid, the voltage across the dc-link capacitor is typically maintained via a buck-boost converter. This voltage may change as the power demand of the system changes, resulting in fluctuations in the active- and reactive power, as well as the output voltage of the microgrid [4]. Depending on the system response and load characteristics, voltage instability may occur following a large disturbance such as the sudden change in demand and/or output of a RES. Small disturbances such as an incremental change in the demand may also result in voltage instability, especially in microgrids that already operate close to their limit [4].

2.5 Microgrid Control

The preceding sections presented some of the stability challenges in a microgrid, but those challenges should be addressed with a suitable controller. The sections to follow will discuss control schemes which can be used to ensure voltage and frequency stability in an islanded microgrid.

2.5.1 Droop control

The droop control technique is generally used in conventional generators of power plants. In autonomous operation of converter based DG systems, droop control can be utilised to share the total load of the system between the different DGs along with controlling the voltage magnitude and frequency within the specified range [30], [31], [32].

Droop control does, however, have some shortcomings such as voltage and frequency offsets. Thus, a second layer of control needs to be implemented along with droop control to ensure a zero steady-state error in the microgrid's output [33]. This second layer of control can be realised by a Proportional-Integral (PI) controller due to their robust performance [33].

In the droop technique, the active power of the total load can be shared by drooping the frequency as a function of the output active power of the converter. The total reactive power can also be shared by drooping the voltage as a function of the output reactive power [32], [34]. As all DGs in the microgrid are integrated via inverters, an islanded microgrid can be considered equivalent to a microgrid comprising multiple inverters connected in parallel. The active and reactive output of the individual inverters can then be represented by [34]:

$$P_n = \frac{UU_n}{X_n}\delta_n \tag{2.1}$$

$$Q_n = \frac{UU_n - U^2}{X_n}, \tag{2.2}$$

where

- U : Integration voltage
- U_n : Output voltage of the inverter power supply
- X_n : Output impedance of the inverter power supply
- δ_n : Included angle between U and U_n

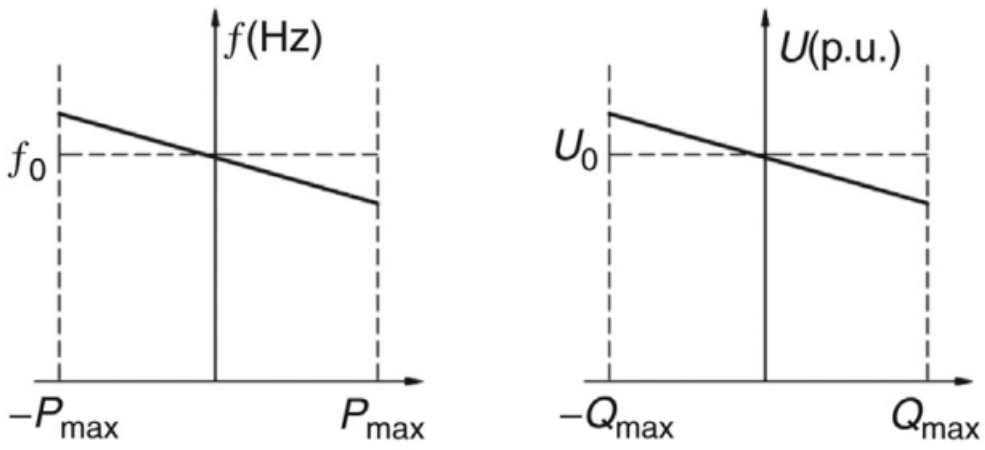

Figure 2.5: Principle of droop control. From [34].

The output voltage of the inverter can be regulated by regulating the reactive power output, while the frequency of the inverter can be regulated by controlling the active power output, as shown in figure 2.5 [34].

2.5.2 Centralised, distributed, and decentralised control

The most common types of control systems installed in microgrids are centralised and decentralised control [35]. These two control techniques are also often found in EMS where each technique has its own set of advantages and disadvantages for energy management, as discussed in [36].

2.5.2.1 Centralised control

It's first necessary to comprehend each control method's communication capabilities in order to comprehend how each will function. The centralised controller comprises a central controller that will have control over every DER in the microgrid [33]. A fundamental topology of a typical microgrid with a centralised controller is illustrated in figure 2.6. The centralised controller will gather information from the individual DERs in the microgrid, the data will be processed, and the necessary commands will be sent back to the individual DERs [33].

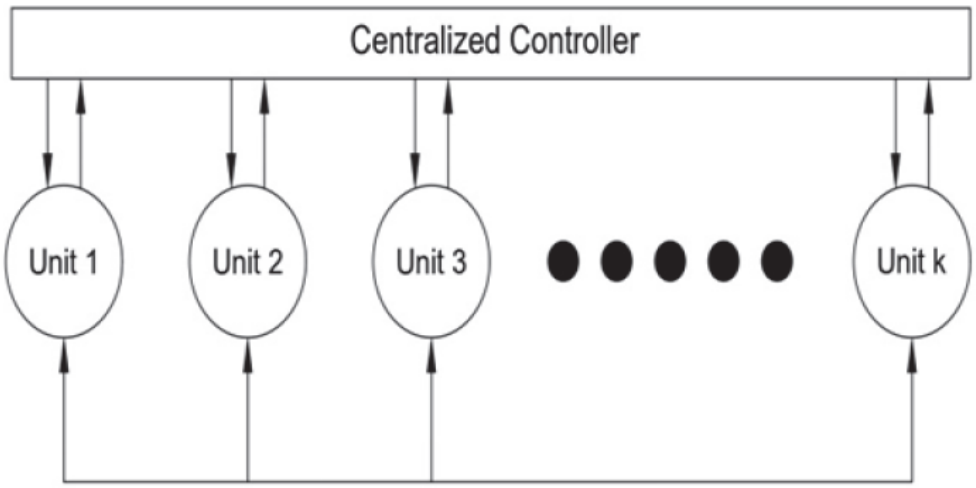

Figure 2.6: Centralised control configuration in a microgrid. From [33].

The centralised control technique is adequate to maintain a microgrid in a steady state despite disturbances in the system, but there are also several challenges associated with centralised control. This control technique is preferred for small microgrids in which low bandwidth is required [33] since the requirements of the communication network for a centralised controller are high [37].

The centralised control technique is also susceptible to a Signle Point of Failure (SPOF), which will characterise this technique as less flexible and less reliable [33]. The centralised technique will also add considerable computational overhead to the control system since all of the decisions need to be made in a central location with one algorithm [38].

2.5.2.2 Distributed control

The strategy adopted in the distributed control technique is that each controller of the DERs in the microgrid exchanges data with its neighbours using a Digital Communication Link (DCL) [33]. The topology of the distributed control system can be seen in figure 2.7.

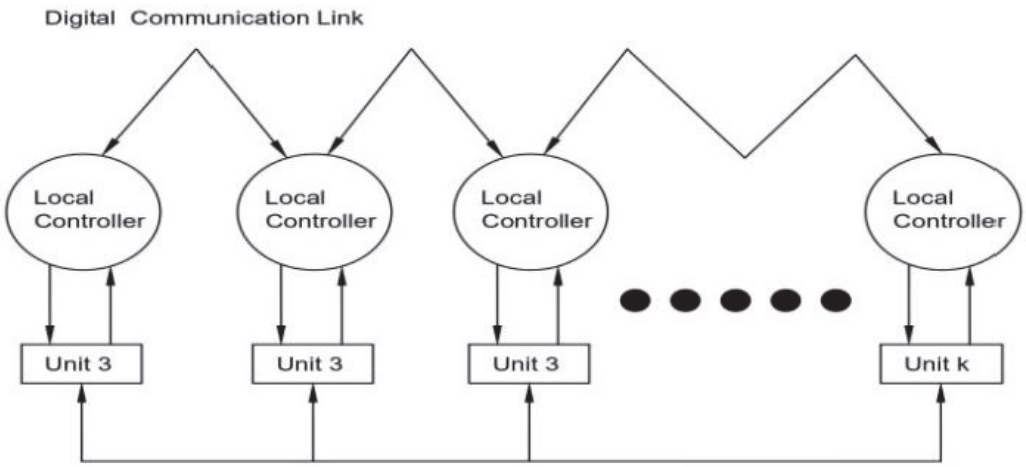

Figure 2.7: Distributed control configuration in a microgrid. From [33].

The main advantage of this system is that although some communication links may fail, the system will remain functional provided that the overall communication network remains connected [33]. This provides a benefit over the centralised controller since the chances of SPOF are mitigated by its topology and operation strategy [33]. The distributed control system also provides advantages such as dynamic flexibility and lower communication overhead [39].

2.5.2.3 Decentralised control

The decentralised control technique involves no communication between the different DERs in the microgrid. The control process of individual DERs is accomplished by local controllers installed at each DER [33]. The decentralised control technique is also considered the most reliable control method for microgrids [33], [40]. The topology of the decentralised control system can be seen in figure 2.8.

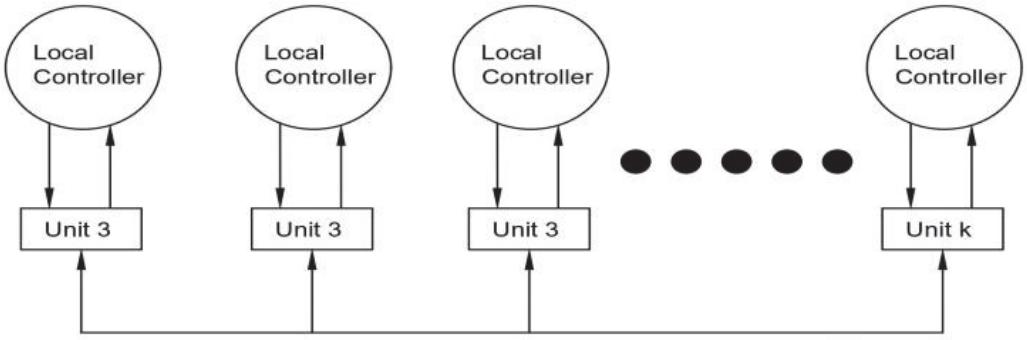

Figure 2.8: Decentralised control configuration in a microgrid. From [33]

Although the decentralised control technique has the advantages of simplicity in control and independence from digital communication technology, this control technique may suffer in performance due to the lack of information from the neighbouring DERs [33]. The lack of communication between the neighbouring DERs will complicate the process of adding more intelligence to the control system, which will decrease the decentralised controller's ability to make optimal decisions at crucial times [40].

The decentralised controller does have several advantages over the centralised and distributed control techniques. Some of these advantages, as highlighted in [40] include:

- Reliability due to no dependency on a centralised controller or communication network
- Low computational burden compared to the other techniques
- Flexibility of the control system
- Plug and play functionality can easily be achieved

In modern power systems and microgrids, the system must be able to be expanded on a regular basis, which makes the decentralised controller ideal for such a microgrid, but the control system will be lacking in complexity. [21], [40].

2.5.3 Multi-agent control system

The application of Multi-Agent System (MAS) is becoming popular in power systems and microgrids due to their inherent benefits like reactivity and increased autonomy [41]. MAS is defined as a complex system composed of several autonomous agents with local knowledge and limited abilities but can communicate with other agents to achieve a larger goal [3], [41], [42].

The agents referred to in the MAS are in a way like local controllers. They will make decisions based on the data available from the sensors in the microgrid or system [42]. Thus, a MAS can be considered both a centralised and decentralised system due to the operation of MAS. The description of distributed control will fit the description of MAS better, but the fact that the communication between agents are conditional will allow for a decentralised control system [2], [39], [43].

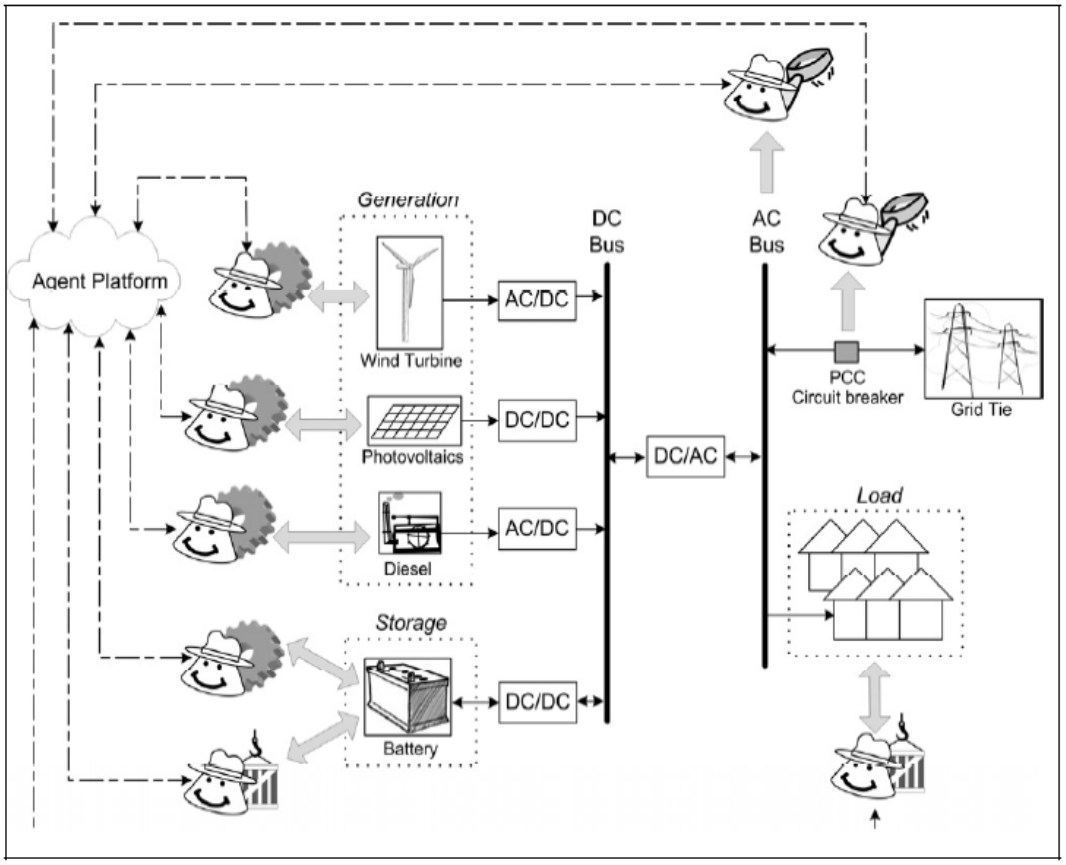

Figure 2.9: Example of a microgrid with assigned MAS agents. From [39].

Figure 2.9 illustrates how the concept of MAS would work in a microgrid. The dashed lines represent communication while the solid lines represent power flow in the microgrid. Each unit in the microgrid has its agent assigned to that unit. The agent will monitor the unit and obtain all the desired measurements and report back to the "Agent platform", which represents the next level of control. This new level is also known as the supervisory level since it does not necessarily control the microgrid but supervises all the agents controlling the microgrid [39].

To explain the use of agents in a microgrid, consider the agents illustrated in figure 2.9. There are three different types of agents; producer agents, consumer agents, and observer agents. All of these agents are connected to the same microgrid and same centralised control system, but the application of each is different. The producer agent will monitor the power generated by the DER and it will also track the power available at any time. This agent is in full control of that DER in the microgrid, so it can send the control command to shut down that DER should it be necessary [39].

The consumer agent in the microgrid will monitor the amount of power consumed by the customer. This agent is also in control of the unit assigned to it, therefore, one can, for instance, install a load-management algorithm in the control system of this agent to control the loads connected to the microgrid [39]. The third and final agent is the observer agent. This agent will monitor specific parameters in the microgrid and communicate the results back to the central controller [39]. This controller will typically monitor parameters such as bus voltage and frequency, it may also be used to monitor energy storage levels in the microgrid.

The use of a MAS will hold several advantages from a control point of view, since each of the agents is capable of acting in the environment, meaning that the agent is capable of changing its environment by its actions [42].Because multiple individual agents can be connected to a single central controller, it is possible to design complex dynamic control systems with minimal effect. This will allow for the addition of intelligence such as neural networks to the control system, but the control system will not be as flexible as a decentralised controller.

2.5.4 PID control

The Proportional-Integral-Derivative (PID) controller is a family of controllers frequently used in industrial applications as a control loop feedback mechanism. PID controllers accounts for roughly 90% of control loops current installed in industrial applications [44]. It will calculate the error value between the measured and desired set point continuously and adjust the input to the controlled system to rectify the offset [44], [45].

The main function of the proportional (P) part of the controller is to minimise the present error in the system. The output of the system may become excessively high for small changes in the error if the proportional gain of the controller is high, therefore, the P-controller may cause instability in many systems [44]. The proportional output of the P-controller is represented by [44]

$$P_{out} = K_p e(t). \tag{2.3}$$

The function of the derivative (D) part of the controller is to predict the future in the controlled system. The D-controller will have a slow rate of change due to the derivative part, therefore, this controller may reduce the overshoot of the system [44]. The derivative output of the D-controller is represented by [44]

$$D_{out} = K_d \frac{d}{dt} e(t). \tag{2.4}$$

The final part in the PID controller is the integral (I) part. The function of this part is to accumulate all the past errors observed in the control loop. This controller depends on the magnitude as well as the time duration of error, which will all be integrated and multiplied with the integral gain [44]. If the integral and proportional parts were added together, a controller capable of accelerating the process being controlled while eliminating the steady-state error will be obtained [44]. The integral output of the I-controller is represented by [44]

$$I_{out} = K_i \int_0^t e(t)dt. \tag{2.5}$$

The term $e(t)$ in (2.3), (2.4), and (2.5) represents the tracking error, which is the difference between the input $r(t)$ and the output $y(t)$ of the system. The error $e(t)$ is fed into the PID controller after which the output $y(t)$ is calculated [44]. The complete PID controller is the sum of the three separate controllers and is represented by [44]

$$y(t) = K_p e(t) + K_i \int_0^t e(t)dt + K_d \frac{d}{dt} e(t). \tag{2.6}$$

PID controllers can be used in a cascaded controller, in which the controller comprises two or more individual PID controllers. The cascaded controllers are considered to be low cost and highly efficient which may be suitable for most power systems in which stability is a concern [44].

The performance of a closed loop system can be significantly affected by non-linearities caused by signal saturation, which may originate in the controlled system [46]. These non-linearities are typically contained using saturation limits in which the output cannot expand beyond the saturation limits. This will ensure that the output is within an allowable range, but the integral action of the PI/PID controller may be affected due to the windup integrator phenomenon [46].

The integral component of the PID controller will continue to integrate the input error even if the output is saturated. This can result in an extremely high output value which is clamped by saturation, but as soon as the error signal changes its sign, the controller may not function as expected since the integral component preserves the result of the unbounded integration. Therefore, the time response of the controller will deteriorate and a specific time interval is required to recover its operation [46], [47]. Thus, the use of a PID or PI controller usually include a anti-windup controller, which can be seen in figure 2.10.

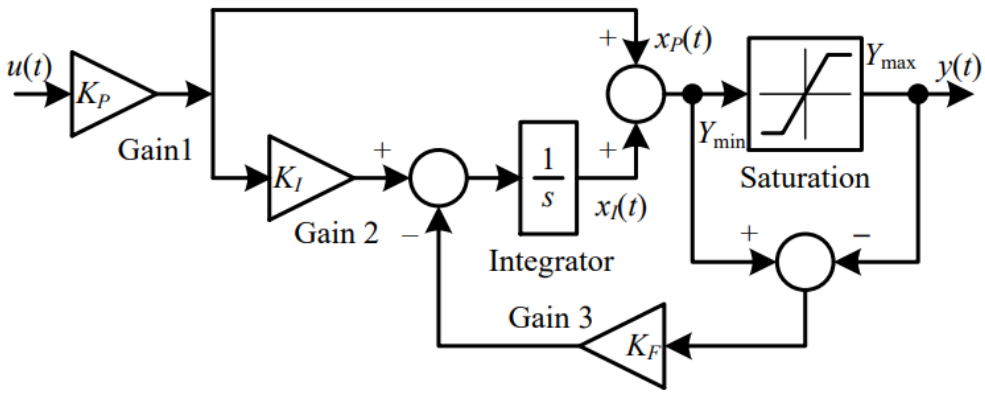

Figure 2.10: Block diagram of PI controller with integral anti-windup. From [46].

The structure of the PI controller with anti-windup in figure 2.10 includes three gain blocks (K_P, K_I, and K_F), one integrator block ($\frac{1}{s}$), one saturation block, and three adders. The input of the system is represented by $u(t)$ while the output is represented by $y(t)$.

Consequently, the input signal to the saturation block can be defined as the sum of the integral component and the proportional component. The output of the saturation is limited to the following [46]:

$$y(t) = \begin{cases} x_P(t) + x_I(t) & \text{if } Y_{min} < x_P(t) + x_I(t) < Y_{max}, \\ Y_{min} & \text{if } x_P(t) + x_I(t) \leq Y_{min}, \\ Y_{max} & \text{if } x_P(t) + x_I(t) \geq Y_{max}. \end{cases} \tag{2.7}$$

By using this anti-windup control system along with a PI or PID control system, the reliability of the overall performance of the control system will be improved [45], [46], [47].

2.5.5 Interaction between DERs

The typical microgrid typically consists of various DER units that are interconnected to supply the load connected to the microgrid with an adequate amount of power. As mentioned in [4], any change in microgrid configuration, which may indicate the start-up or shut down of certain DERs, can result in voltage and frequency deviations. This is supported by the authors of [9] which state that the interaction between DER units in a microgrid may cause instability in an islanded microgrid.

According to [9], there are three main causes for instability in an islanded microgrid if one considers a system where DER units can be added or removed at any given time. These causes are:

- Sensitivity to DER design
- Sensitivity to DER control
- Interaction between different DER units

The sensitivity to DER design refers to the various selections of DER units available on the market, each with its proprietary design and manufacturing process. This can result in different units of the same type and same ratings in the same microgrid, therefore, the microgrid needs to be robust enough to interface with all of these different DER designs while maintaining stability [9].

The sensitivity to DER control refers to the fact that each DER unit in a microgrid is developed with its internal controller and settings. The ability to change the controller settings of the DER will vary depending on the manufacturer of that DER unit while access to controller tuning is usually not available to the end user. This complicates the control system of the microgrid because of the cascaded control. The cascaded control is realised when considering the internal control system of the DER units and the control technique used in the microgrid. This presents the challenge of maintaining stability in an islanded microgrid comprising different DER units with different control systems [9].

The third cause for instability, according to [9], refers to the cases in which the total available power in the microgrid may not be enough to adequately supply the load with sufficient power. In such a case, additional DER units may be required in the microgrid to meet the increasing demand. Whenever the additional DER units are added to the microgrid, it is critical to avoid adverse interaction between the DER units already in the microgrid, and the units added to the microgrid [9].

2.6 Critical review

This section will extract the most important information from this chapter to determine the significant elements that need to be addressed in this study. This review will focus on the topology of the microgrid, what should be included in the modelling, and what to consider during the design of an adequate control system.

The following challenges were extracted from the literature study in this chapter:

- Island operation presents more stability challenges than grid-tied operation (section 2.3).
- Power sharing and power balance in the microgrid can cause instability (section 2.4.1).
- Voltage stability (section 2.4.3).
- Frequency stability (section 2.4.2).
- Interaction between DERs in a microgrid may cause instability (section 2.5.5).
- Centralised control is simple to implement with high computational overhead (section 2.5.2.1).
- Distributed control is complicated to implement with relatively high computational overhead (sections 2.5.2.2 and 2.5.3).

- Decentralised control is simple to implement and robust with no complexity (section 2.5.2.3).

When considering the operation of PV in section 2.2.1, it is clear that it is not as simple to control. When considering the modelling of PV in the Simulink model, along with other RESs such as wind or fuel cells, the modelling of the microgrid model will become extremely complex and add unnecessary elements to the model which may compromise the aim of this study. The problem statement in section 1.2 states that this study focuses on the load connected and interaction between the inverters in the microgrid, therefore, the modelling of the RES does not have to be included in the microgrid. These sources can be considered to be ideal since they will not affect the study, except for the limited capacity they will add to the system. This will be neglected since each inverter will have a maximum capacity which will serve the same purpose as the limited capacity of the sources. Therefore, the modelling of the islanded microgrid (objective in section 1.3.1) is limited to the inverter itself and the connection of multiple inverters in parallel.

The instability contributors (objective in section 1.3.2) are also limited to the power-sharing (or the load connected to the microgrid) and the interaction between inverters. Therefore, this objective will be completed by evaluating the effect of these two factors on the stability of the microgrid.

The objective described in section 1.3.3 will be completed by means of a centralised and decentralised controller. The final objective (section 1.3.4) will be completed by repeating the simulations that were done during the sensitivity analysis to determine if the controller can mitigate the challenges stated in the literature in this chapter.

Therefore, this study will focus on a microgrid limited to the following characteristics:

1. The microgrid will operate in islanded mode.
2. The microgrid will comprise several DERs (inverters in parallel) which can be added if the load demand increases.
3. The DG and ESS of each DER will be considered "ideal", meaning they will be able to supply their rated power during operation.
4. The loads connected to the microgrid will change their demand frequently.
5. The centralised and decentralised control schemes will be implemented and compared to one another.

The centralised and decentralized methodologies will be evaluated in a PI controller configuration to identify which microgrid configuration each controller is best suited for. This is done on this small-scale microgrid because centralised controllers are better suited for small systems, and by utilising a simple PI controller, the centralised controller can be compared to the decentralised controller, which is the optimal controller for microgrids (see section 2.5.2.3).

The change in load demand and the interaction between DERs (the adding of DERs in the case of a power shortage) also proved to be contributors to stability challenges, therefore, the control systems will also be tested on their ability to manage these kinds of disturbances.

Chapter 3

Modelling

This chapter will detail the modelling of an islanded microgrid. Some background will be provided on the topology of the microgrid that will be used in this study, after which the Simulink example, on which the study is based, will be discussed and explained. The mathematical modelling of a state-space model representative of the Simulink example will be done in which all the subsystems will also be discussed. This chapter will conclude with the mathematical approximation of the Simulink model and a comparison between the mathematical model and the Simulink model.

3.1 Introduction

This chapter aims to provide a comprehensive understanding of the modelling phase of this study. This chapter will not include any control system design or implementation, but it will provide the foundation for the control system design.

This phase is started with an overview of the microgrid topology that will be used in the simulation model. All the components and connections in the microgrid are explained. Since the simulation model is based on a MATLAB example, this example model is evaluated and the shortcomings that should be addressed are highlighted. Thereafter, the modified Simulink model is shown along with the operating parameters of the simulation. The subsystems of the modified simulation model are then analysed to fully understand the model and all of its components.

Since a simulation model is available, but none of the said model's dynamics are known, the mathematical state-space model of an inverter is derived. This is accomplished by constructing the state-space models for a current-, voltage-, and droop controller after which all of these are combined to create a complete inverter model. The state-space model should be representative of the simulation model, therefore, the numerical state-space model is obtained from the parameters extracted from the simulation model.

The chapter concludes with a comparison between the numerical state-space model and the simulation model to verify that the approximation is accurate.

3.2 Microgrid topology

The literature study in chapter 2 concluded that an islanded microgrid will encounter the most severe stability challenges. For this study, these challenges are limited to

1. the power-sharing among DERs in the microgrid (the size of the load connected).
2. the interaction between the DERs in the microgrid.

Therefore, a microgrid model needs to be obtained in which these stability challenges can be investigated. The microgrid topology illustrated in figure 3.1 will be used in this study.

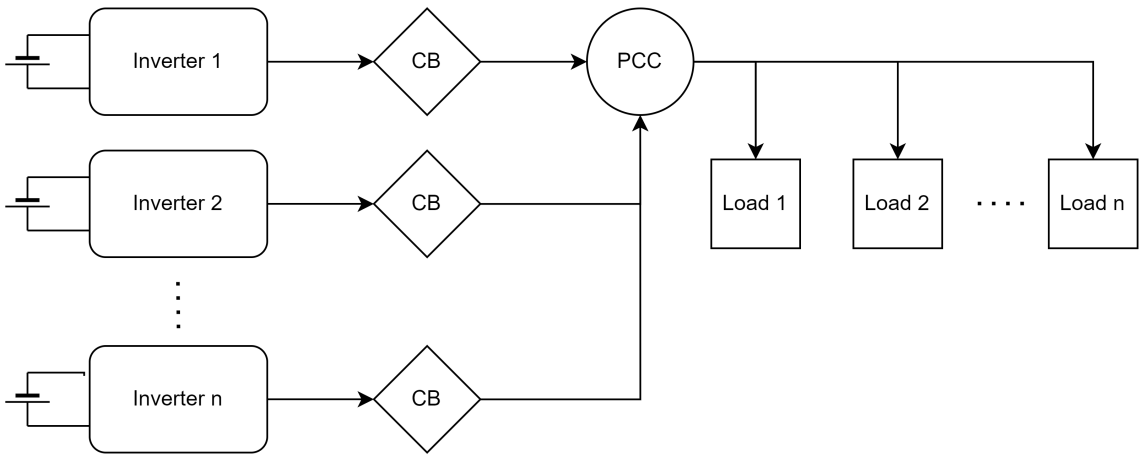

Figure 3.1: Microgrid topology that will be used in this study

The DC-source symbols next to the inverters on the left-hand side of figure 3.1 represent the ESS of each inverter. These ESSs are considered to be *ideal*, meaning that the output voltage of each ESS can be adjusted, but the capacity is considered to be infinite for this study's purpose. There can be as many inverters connected to the microgrid as the application desires, which is represented by *inverter n*. The *CB* blocks represent the circuit breakers/switches that will connect or disconnect the inverters from the PCC.

The control implementation for the microgrid has not been added to figure 3.1, but it will be discussed later in this document. The topology in figure 3.1 will be used to investigate the stability challenges, as discussed earlier, since it allows for investigating the effect when inverters are connected and disconnected, as well as the behaviour of the system when different size loads are connected. This model will be implemented in the Simulink environment, which will be discussed in the following section.

3.3 Simulink model

This section will describe the Simulink model and how it works. It is vital to note that this section does not yet feature microgrid control. All of the building blocks of the Simulink model will be discussed to ensure a good understanding of how the model operates before commencing to the next stage in this study.

3.3.1 Simulink model overview

The aim of this study is not to develop a model from first principles, therefore, if an already-developed model can be obtained on which the control can be implemented, it would be ideal. After consulting the examples of MATLAB regarding microgrids, a suitable model was found in an example [48] (see figure 3.2). This islanded microgrid model comprises three inverters connected in parallel to supply a common load. Simple centralised control was implemented, but all inverters were connected all the time and no real disturbances were introduced, therefore, it was hard to determine the effectiveness of the control system under unfavourable circumstances.

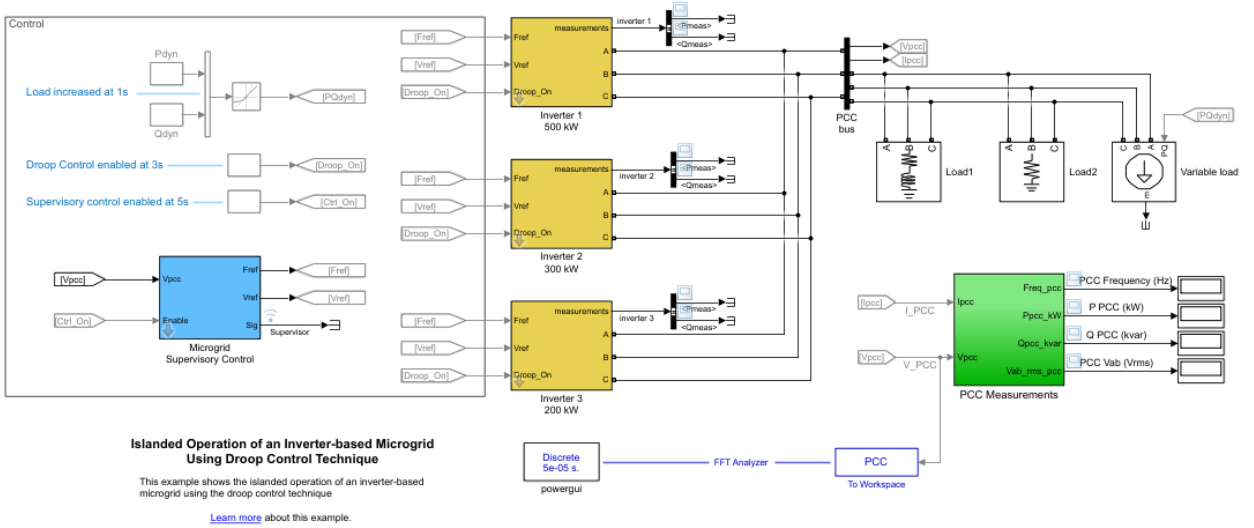

Figure 3.2: Simulink example model [48].

This model in the example already had all the electrical fundamentals built into the inverters and they were operating according to the specified parameters. Each inverter already had its internal voltage-, current-, and droop controller that will be used for power sharing. All of these parameters can be changed should it be necessary. The load connected to the microgrid consisted of a static load (a load that will not change), and a dynamic load of which one can change the characteristics. As seen in blue text in the top left corner of figure 3.2, the load can only change at $t = 1s$, which is not ideal for a dynamic load.

In this example, the inverters receive the desired voltage and frequency values as inputs after which the internal control system will aim to rectify the error between the measured values and the reference values. The droop control can also be enabled or disabled by means of a logic signal (*0* or *1*). The model allows the measurements of numerous parameters at the output of each inverter, which can be utilised should it be needed to implement a custom control system.

Although the model contains a lot of the fundamentals and it is operating as expected, there are some shortcomings which will need to be addressed. The main drawbacks of this example include:

- There is no interaction between the inverters (inverters cannot connect and disconnect from the PCC).
- There is only one type of controller that is not optimised for large disturbances.

- The magnitude of the load can be changed only once, which does not allow for full dynamic operation.
- The bus voltage and frequency are according to the standards in the United States of America (USA).

The characteristics required of the microgrid model in this study (discussed in section 2.6) can be used to test if the example model is adequate for this study. Table 3.1 provides a summary to determine whether or not the example model satisfies the required characteristics.

Table 3.1: Characteristics obtained from literature vs Simulink example

Microgrid characteristics for this study	
Defined from literature	**Simulink example model**
1. Islanded microgrid	1. Yes
2. Multiple DERs connected in parallel which can be added and removed	2. Does comprise multiple DERs, but cannot add or remove DERs
3. The ESS of each DER is considered to be ideal	3. Yes
4. The load connected can dynamically change its demand	4. No
5. Centralised and decentralised control can be compared	5. Only a centralised controller is present, but it needs optimisation

The Simulink example model satisfies 2 of the 5 requirements, as seen in table 3.1, but the remaining requirements can be added by adapting the example model. The adjustments of the example model included:

- The parallel inverters were connected via a three-phase circuit breaker to the PCC, meaning that inverters can be added or removed at any time as required by circumstances.
- The load connected was also altered to ensure it is fully dynamic. Now, the magnitude of the load and its connection or disconnection can be controlled.
- The centralised control system was optimised and the decentralised controller was added to the microgrid, but this is not covered in this chapter.

The altered microgrid that will be used in this study can be seen in figure 3.3.

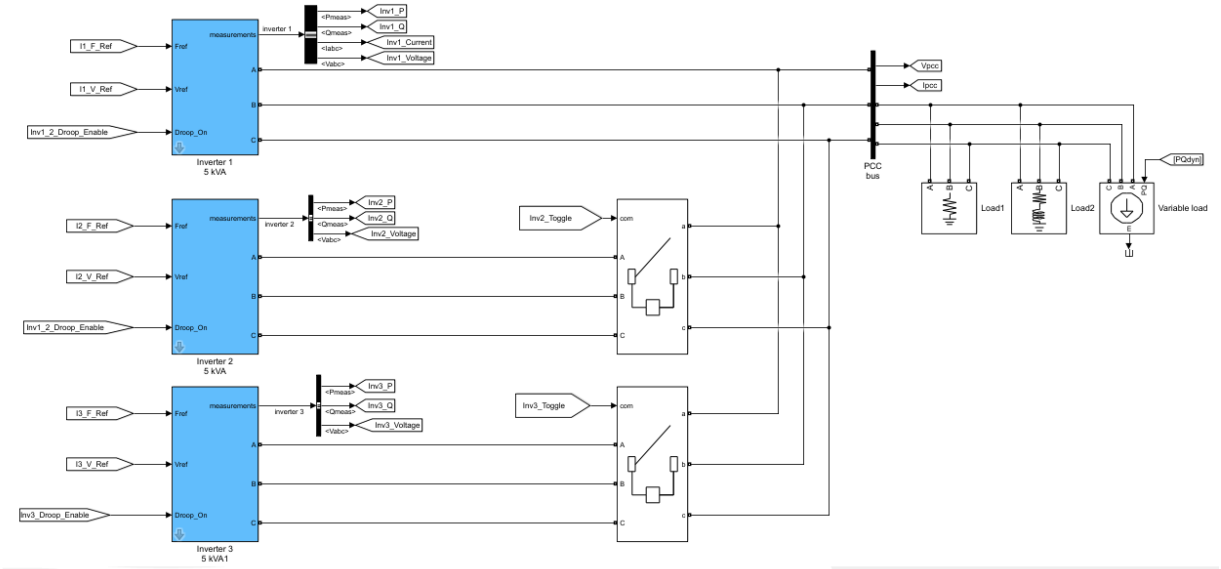

Figure 3.3: Overview of Simulink model used in this study

The three blue blocks on the left-hand side of figure 3.3 represent the three inverters (DERs). The two large blocks next to the bottom two inverters represent the circuit breakers which will connect or disconnect those inverters. The first inverter does not have a circuit breaker since this study assumes that at least one inverter should be connected at all times. The load connected to the microgrid can be seen on the right-hand side of the PCC, where the label connected to the variable load is the control signal which will control the magnitude of the load.

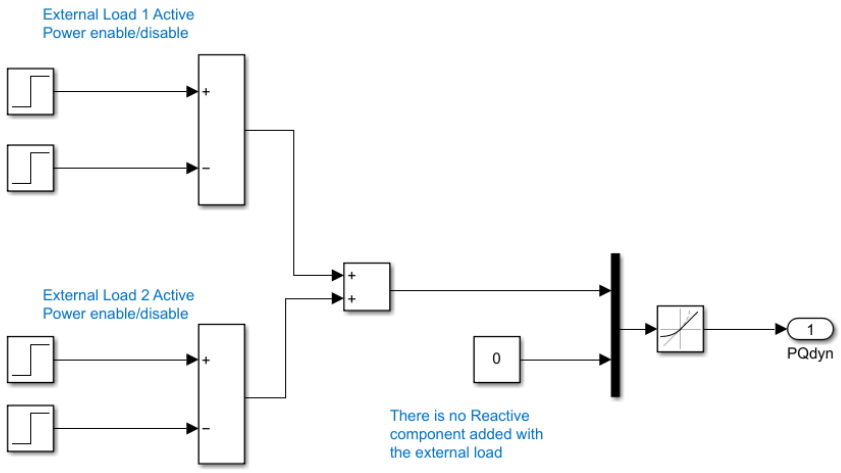

Figure 3.4: Generation of dynamic load control signal

The block diagram in figure 3.4 illustrates the way in which the control signal for the load in figure 3.3 is generated. Two additional loads can be added, external load 1, and external load 2. Each external load has two *step* blocks attached to an *add* block. The top *step* block will enable the external load with a magnitude of x, while the second *step* block will disable the external load by neutralising the first magnitude. The time and magnitude of these *step* blocks can be changed to simulate the adding and removing of loads. The output of the external load is then fed to a *mux* block which will combine the active and reactive components. This will then pass through a *rate limiter* which will create a steep slope for the output which will ensure that the change in load is not instantaneous (the transition takes 0 s to complete, which would be unrealistic).

The labels on the left-hand side of the inverters (figure 3.3) are the inputs to the inverter. The top label for each inverter represents the frequency reference, the second label is the voltage reference, and the third label is the droop enable signal, which will either enable or disable the droop control for each inverter. The droop control is discussed in chapter 3.3.3.

The model was adjusted to comply with the prerequisites and the operating conditions that will be used in this study, which can be found in table 3.2. Parameters such as the droop- and PI constants, switching frequency, and sampling time were extracted from the existing Simulink model. These parameters will be referred to in the sections to follow, where each element in the model will be discussed and explained.

Table 3.2: Parameters for Simulink microgrid model

Parameter	Value
Bus Voltage (Phase Voltage)	230 V
Bus Frequency	50 Hz
Base load (P)	3 kW
Base load (Q)	200 VAR
Dynamic load (P)	6 kW (adjustable)
Inverter power	5 kVA
DC link voltage	480 V
Voltage droop	4 %
Frequency droop	1 %
Current controller constants [P, I]	[0.3, 20]
Voltage controller constants [P, I]	[2, 14]
Inverter switching frequency	2.7 kHz
Sampling time	50 µs

3.3.2 Simulink model of an inverter

This section will detail the model of an inverter as seen in figure 3.3. When the Simulink block, also known as a mask in Simulink, is opened, the model shown in figure 3.5 is revealed. All of the inverters in the microgrid are identical, therefore, the modelling of each inverter is the same.

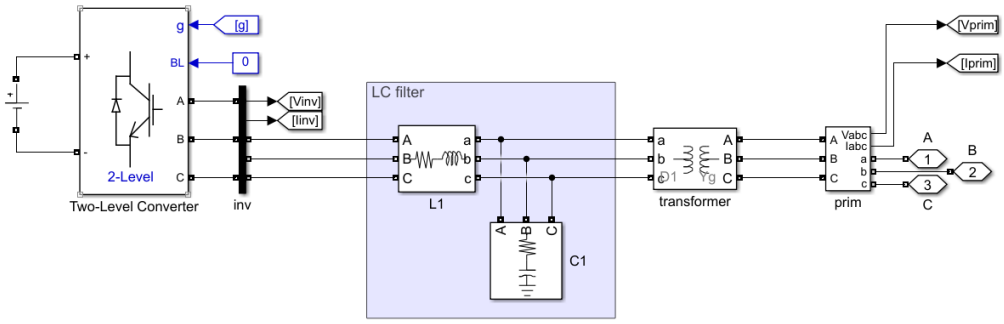

Figure 3.5: Overview of the building blocks of an inverter in Simulink

The model in figure 3.5 represents the low-level model of the inverter and ESS of the inverter while the control system can be seen in figure 3.6. The ESS of the inverter is represented by the DC-source to the left-hand side of the *Two-Level Converter*. This ESS is considered to be ideal, as discussed earlier, since the output voltage can be changed while assuming enough capacity for each application. The *Two-Level Converter* is a Simulink block which is being used to convert the DC source to a three-phase AC voltage.

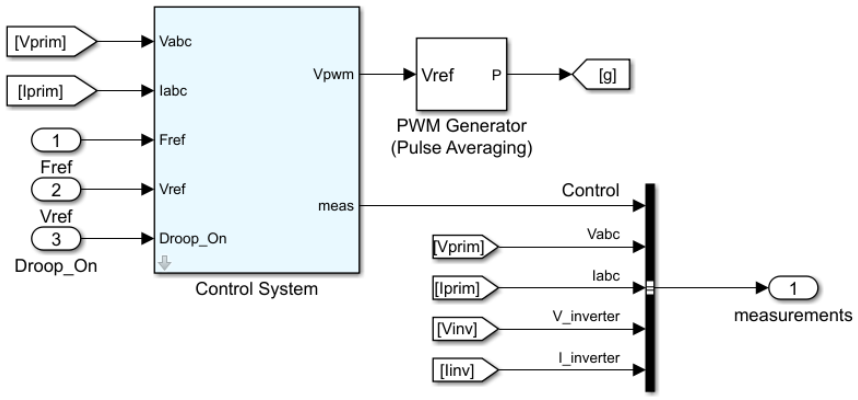

Figure 3.6: Internal control system of an inverter in Simulink

The control system in figure 3.6 will control the output voltage and current of the inverter. This is done by adapting the Pulse Width Modulation (PWM) signal to the *Two-Level Converter*, which in turn will change the output voltage of the inverter. This control system receives the reference values for the voltage and frequency, and the output measurements of the inverter as inputs. The internal control system makes use of PI controllers to obtain a small steady-state error.

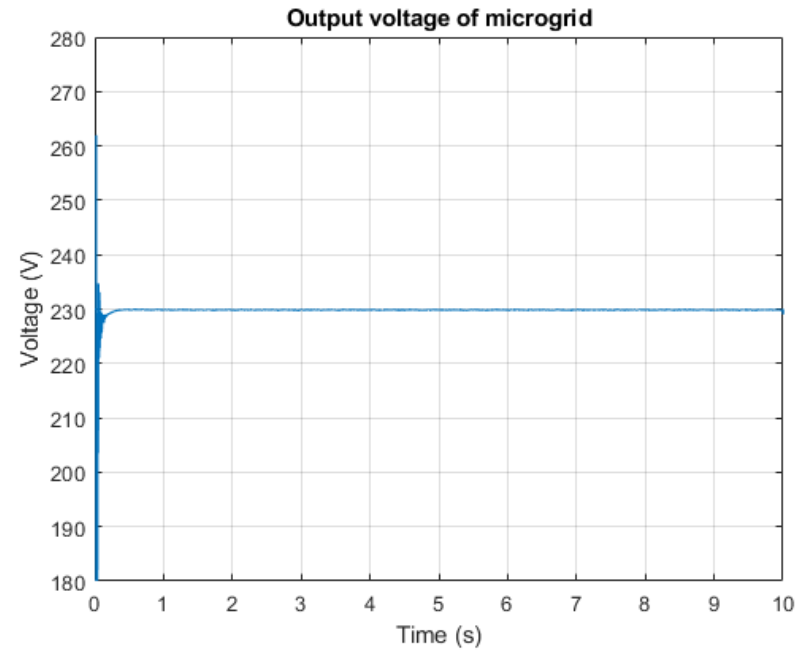

Figure 3.7: Output voltage of the Simulink model

The output voltage displayed in figure 3.7 is the measurement taken at the load when all the inverters are connected. The load is within the capabilities of the microgrid and it does not change for the duration of the simulation. The voltage is accurate and the internal control system of the inverters can maintain the bus voltage at the reference value.

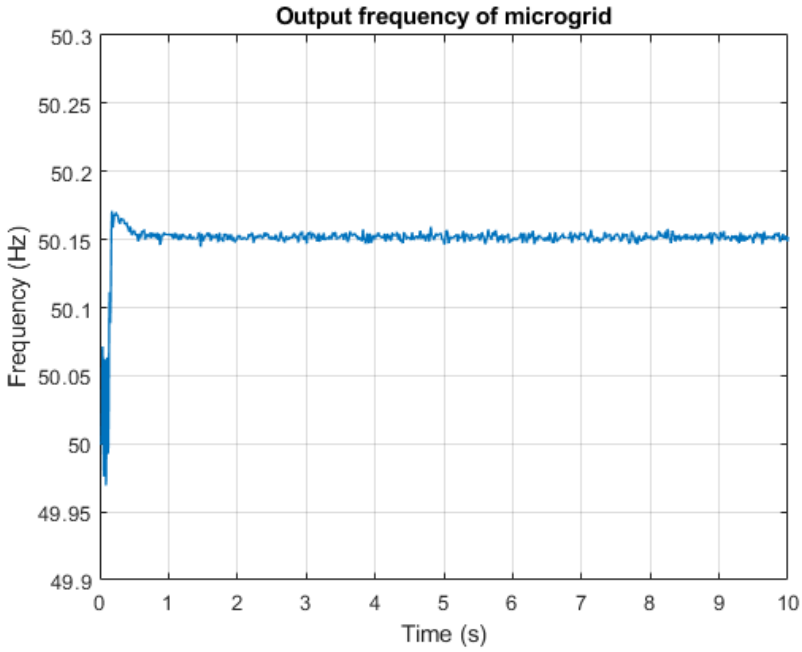

Figure 3.8: Output frequency of the Simulink model

The frequency output depicted in figure 3.8 is from the same simulation as in figure 3.7. The output frequency of the inverter is dependent on the input frequency reference and not an internal control system as for the output voltage. Since this simulation is done without any external control, the frequency reference remained at 50 Hz (the input reference is fixed if no external control is present, as seen in figure 3.3). Thus, with no PI controller to manipulate this input reference to the inverter, there is no rectification in the error observed in the output frequency, hence a drift is observed. It is expected that this drift will be rectified with an external control system. Other than the drift, the bus voltage and frequency prove to satisfy the model parameters, as detailed in table 3.2.

3.3.3 Droop control of Simulink inverter

The droop control of the inverter is also embedded within the control system in figure 3.6 and the block diagram in Simulink can be seen in figure 3.9.

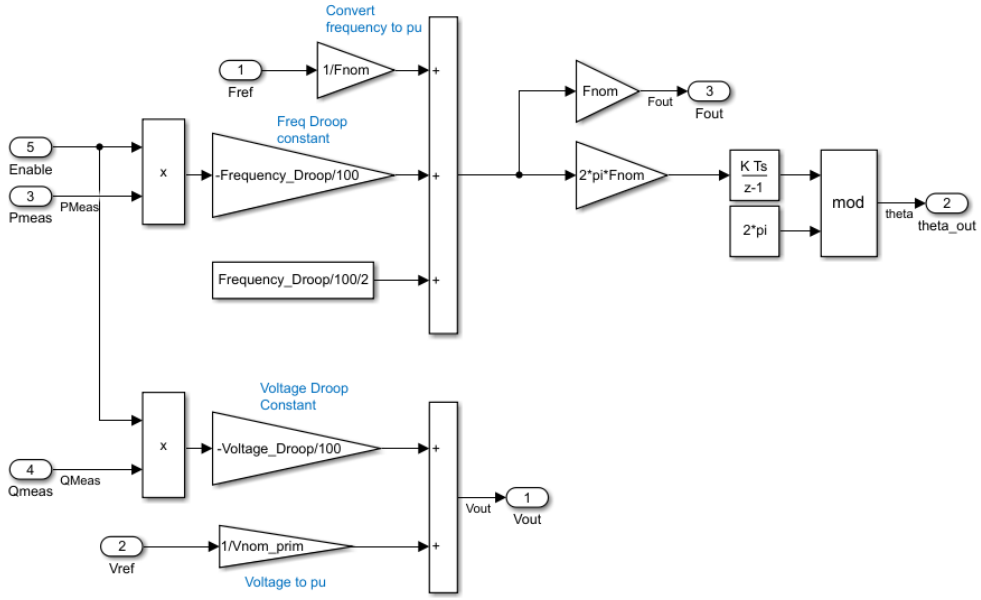

Figure 3.9: Droop control of Simulink inverter

The implementation in figure 3.9 is supported by the literature found in section 2.5.1, which states that the total active power can be controlled by drooping the frequency, while the total reactive power can be controlled by drooping the voltage. The voltage output is determined by adding the voltage (pu) to the reactive power multiplied by the negative voltage droop constant. This would imply that the voltage output would be a small margin less than the reference voltage. The larger the voltage droop constant, the larger the difference will be.

The frequency works similar to the voltage, where the output frequency is the sum of the per unit (pu) frequency, the active power multiplied by the negative frequency droop constant, and a constant. The output frequency (which is still pu) is then multiplied by the nominal frequency to obtain the new reference frequency. These voltage and frequency reference values are then fed into the rest of the control system such as the voltage and current PI controllers.

Each inverter in the microgrid has the same control system and droop control, therefore, the droop control should be able to effectively share the load amongst the inverters connected in the microgrid. The external control system may affect the effectiveness of the droop control system, but it will be discussed later in this document.

3.4 Symbolic state-space model of an inverter

The microgrid model presented in section 3.3 will be utilized to test various control strategies in the Simulink environment. The challenge, however, is to design an adequate external control system for the microgrid. To successfully design a controller, information regarding the dynamics of the system will have to be known. In this microgrid model, information regarding the dynamics are not known, since a transfer function or state-space model cannot be accurately obtained.

The step response of the system can be used to approximate some parameters, but it will still not be enough to accurately design the control system. After consulting previous studies, it became clear that a state-space model of a generic inverter can be derived and used along with the Simulink model's parameters to obtain a numerical state-space model of that inverter. This will provide the best approximation in this application while having adequate information to design the controller for a single inverter. It is important to note that the switching frequency of 2.7 kHz (table 3.2) will be neglected in the modelling of the inverter since [49] states that a high switching frequency of the inverters may be neglected.

3.4.1 Clarke, Park, and dq0 transformations

Transformations between the three-phase *abc* and *dq*0 reference frames were used to assist in the modelling and analysis of electrical machines [50]. Nowadays, *dq*0 based models are widely used in applications such as modelling and control of multi-inverter systems [50].

The diagram in figure 3.10 illustrates the transformations between the different reference frames.

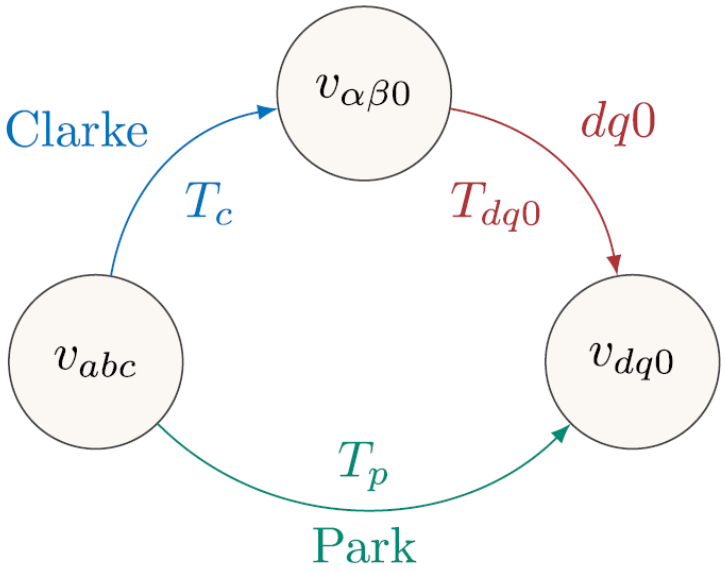

Figure 3.10: Relationship between the Clarke and Park transformations. From [50].

The Clarke transformation converts the three-phase (abc) quantities to $\alpha\beta 0$. The Park transformation converts the abc quantities to $dq0$. The $dq0$-transformation (T_{dq0}) is not equivalent to the Park transformation, but it is used in figure 3.10 to indicate the transformation between $\alpha\beta 0$ and $dq0$ [50].

3.4.2 State-space model of droop controller

The state-space model of the entire inverter will be derived in the following sections with the assistance of [49] and [51]. In these articles, an inverter is modelled using a state-space model after which the numerical state-space model is obtained. A summary of the variables that will be used in this section can be found in appendix A.

The comparison in figure 3.11 supports the idea of obtaining a generic state-space model for the Simulink model which can be used in the controller design process. The two images in figure 3.11 both have three blocks numbered from "1" to "3". The first block (block 1) represents the inverter's switching electronics. The second block (block 2) represents the output filter, and the third block (block 3) represents the control system of the inverter.

It is evident that the topology of both the inverters is the same with both inverters having a voltage-, current-, and droop controller. Therefore, it can be assumed that the approximation of the Simulink model will be accurate when using the generic model from the literature.

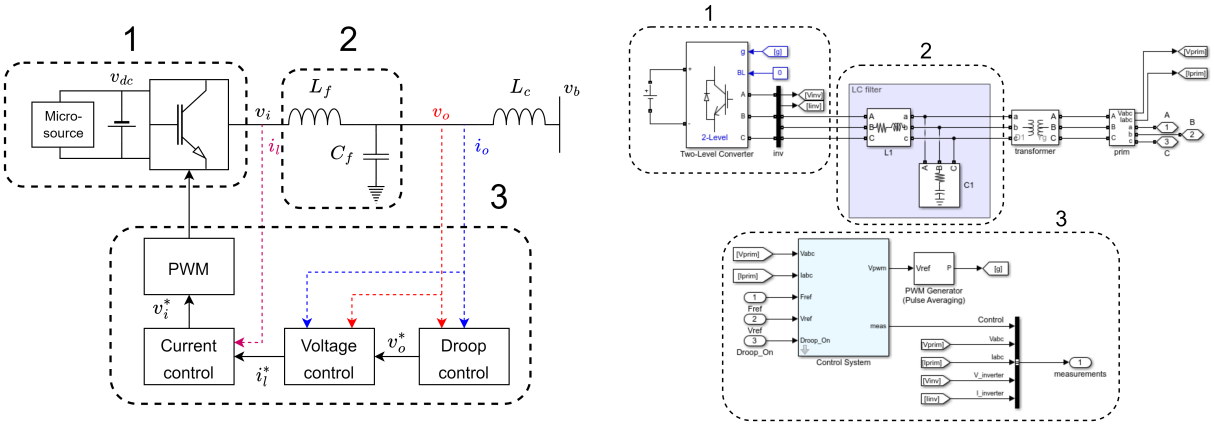

(a) Inverter model in literature **(b) Inverter model in Simulink**

Figure 3.11: Comparison between the Simulink model and the model presented in literature [49], [51].

Refer to figure 3.12 for a representation of how the inverter can be presented with all the internal control systems; the droop controller, voltage controller, and current controller. Figure 3.12 also present the low-pass filter (L_f and C_f) and coupling inductance (L_c).

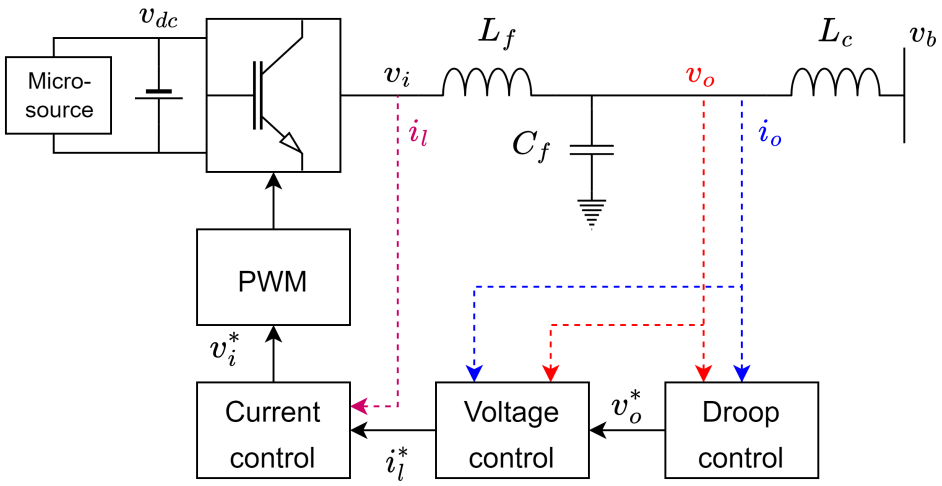

Figure 3.12: Block diagram of inverter with internal control systems. Adapted from [49] and [51].

According to the relationships between the active power and frequency, and the reactive power and voltage in section 2.5.1, these relationships can be used to realise the droop controller. The block diagram in figure 3.13 illustrates how the droop controller will control the voltage and frequency. Note that the inputs and outputs of the droop controller are in the $dq0$ reference frame.

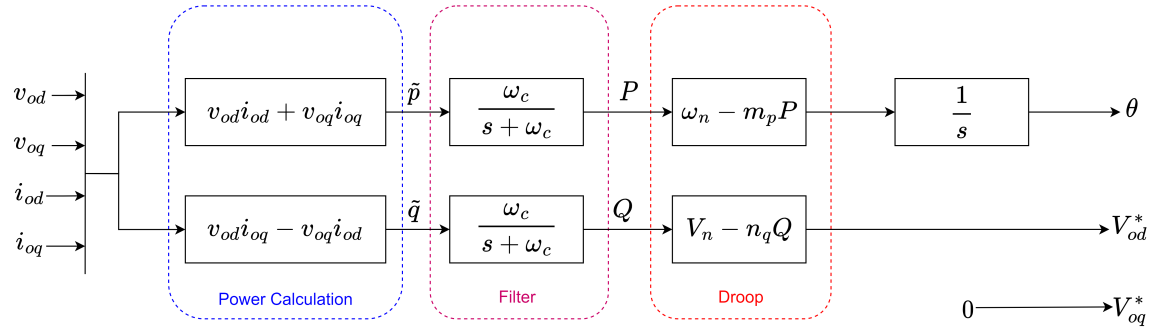

Figure 3.13: Block diagram of droop controller. Adapted from [49].

From figure 3.13, the instantaneous active and reactive power components are calculated from the measured current and voltage:

$$\begin{aligned} \tilde{p} &= v_{od}i_{od} + v_{oq}i_{oq}, \\ \tilde{q} &= v_{od}i_{oq} - v_{oq}i_{od}. \end{aligned} \tag{3.1}$$

To obtain the real and reactive power components, the instantaneous power components are passed through the low-pass filter, as illustrated in figure 3.13, which will yield:

$$\begin{aligned} P &= \frac{\omega_c}{s+\omega_c}\tilde{p}, \\ Q &= \frac{\omega_c}{s+\omega_c}\tilde{q}, \end{aligned} \tag{3.2}$$

where ω_c represents the cut-off frequency of the low-pass filter. Next, the droop gains for the voltage (n_q) and frequency (m_p) will have to be calculated:

$$\begin{aligned} m_p &= \frac{\omega_{\max} - \omega_{min}}{P_{\max}}, \\ n_q &= \frac{V_{od\max} - V_{od\min}}{Q_{\max}}. \end{aligned} \tag{3.3}$$

By introducing an artificial droop in the inverter frequency, (3.3) can express the true power sharing amongst different inverters. This is expressed in terms of the nominal frequency (ω_n) and droop gain (m_p):

$$\omega = \omega_n - m_p P. \tag{3.4}$$

Similar to (3.4), the reactive power sharing among multiple inverters can be achieved by introducing a voltage magnitude given by:

$$\begin{aligned} v_{od}^* &= V_n - n_q Q, \\ v_{oq}^* &= 0, \end{aligned} \tag{3.5}$$

where V_n represents the nominal voltage set point of the d-axis output voltage. The output voltage magnitude reference is aligned to the d-axis of the inverter reference frame, therefore, the q-axis can be set to zero (see figure 3.16).

Now that all the required parameters are calculated, the complete symbolic state-space model for the droop controller can be constructed. The outputs of the droop controller are the small signal variation in the output voltage (represented by Δv_o^*) and frequency (represented by $\Delta\omega$), as seen in figure 3.13. For simplicity, the D and Q axis components of the voltage and current are combined to form vectors as in (3.6)

$$\begin{aligned} v_{odq}^* &= \begin{bmatrix} v_{od}^* \\ v_{oq}^* \end{bmatrix}, i_{ldq} = \begin{bmatrix} i_{ld} \\ i_{lq} \end{bmatrix} \\ v_{odq} &= \begin{bmatrix} v_{od} \\ v_{oq} \end{bmatrix}, i_{odq} = \begin{bmatrix} i_{od} \\ i_{oq} \end{bmatrix}. \end{aligned} \tag{3.6}$$

The state-space model of the droop controller can then be presented by

$$\begin{aligned} \begin{bmatrix} \dot{\Delta}\delta \\ \Delta P \\ \Delta Q \end{bmatrix} &= A_P \begin{bmatrix} \Delta\delta \\ \Delta P \\ \Delta Q \end{bmatrix} + B_P \begin{bmatrix} \Delta i_{ldq} \\ \Delta v_{odq} \\ \Delta i_{odq} \end{bmatrix} \\ \begin{bmatrix} \Delta\omega \\ \Delta v_{odq}^* \end{bmatrix} &= \begin{bmatrix} C_{P\omega} \\ C_{Pv} \end{bmatrix} \begin{bmatrix} \Delta\delta \\ \Delta P \\ \Delta Q \end{bmatrix}, \end{aligned} \tag{3.7}$$

where

$$A_P = \begin{bmatrix} 0 & -m_p & 0 \\ 0 & -\omega_c & 0 \\ 0 & 0 & -\omega_c \end{bmatrix}$$

$$B_P = \begin{bmatrix} 0 & 0 & 0 & 0 & 0 & 0 \\ 0 & 0 & \omega_c I_{od} & \omega_c I_{oq} & \omega_c V_{od} & \omega_c V_{oq} \\ 0 & 0 & \omega_c I_{oq} & \omega_c I_{od} & \omega_c V_{oq} & \omega_c V_{od} \end{bmatrix} \tag{3.8}$$

$$C_{P\omega} = \begin{bmatrix} 0 & -m_p & 0 \end{bmatrix}$$

$$C_{Pv} = \begin{bmatrix} 0 & 0 & -n_q \\ 0 & 0 & 0 \end{bmatrix}.$$

3.4.3 State-space model of voltage controller

The block diagram in figure 3.14 illustrates the voltage controller of the D and Q axes voltage, including the feed-back and freed-forward terms. The output voltage control is realised with a standard PI controller, where the proportional term will speed up the response speed of the system and the integral term will eliminate the steady-state error.

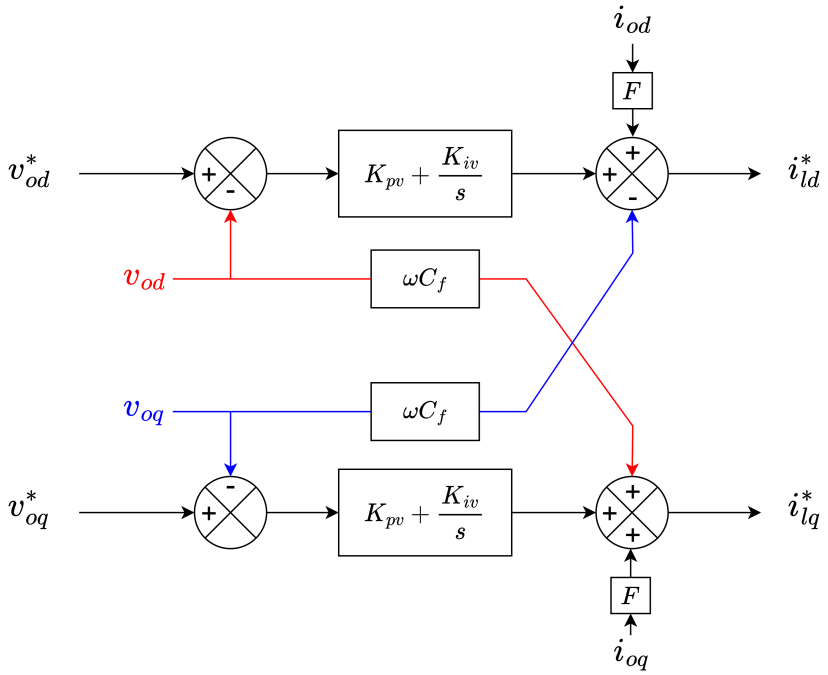

Figure 3.14: Block diagram of internal voltage controller of the inverter. Adapted from [49].

The state equations can be derived from figure 3.14 as

$$\begin{aligned} \frac{d\phi_d}{dt} &= v_{od}^* - v_{od} \\ \frac{d\phi_q}{dt} &= v_{oq}^* - v_{oq}. \end{aligned} \tag{3.9}$$

The dynamic characteristics of the voltage controller can be expressed as

$$\begin{aligned} i_{ld}^* &= Fi_{od} - \omega_n C_f v_{oq} + K_{pv}(v_{od}^* - v_{od}) + K_{iv}\phi_d \\ i_{lq}^* &= Fi_{oq} + \omega_n C_f v_{od} + K_{pv}(v_{oq}^* - v_{oq}) + K_{iv}\phi_q. \end{aligned} \tag{3.10}$$

For the state-space model, the input to the system can be divided into two terms: the reference input (B_{V1}) and the feedback inputs (B_{V2}). Therefore, the state space model for the voltage controller can be written as

$$\begin{aligned} \begin{bmatrix} \Delta\dot{\phi}_{dq} \end{bmatrix} &= \begin{bmatrix} 0 \end{bmatrix} \begin{bmatrix} \Delta\phi_{dq} \end{bmatrix} + B_{V1} \begin{bmatrix} \Delta v_{odq}^* \end{bmatrix} + B_{V2} \begin{bmatrix} \Delta i_{ldq} \\ \Delta v_{odq} \\ \Delta i_{odq} \end{bmatrix} \\ \begin{bmatrix} \Delta i_{ldq}^* \end{bmatrix} &= C_V \begin{bmatrix} \Delta\phi_{dq} \end{bmatrix} + D_{V1} \begin{bmatrix} \Delta v_{odq}^* \end{bmatrix} + D_{V2} \begin{bmatrix} \Delta i_{ldq} \\ \Delta v_{odq} \\ \Delta i_{odq} \end{bmatrix}, \end{aligned} \tag{3.11}$$

where

$$\begin{aligned} \Delta\phi_{dq} &= \begin{bmatrix} \Delta\phi_d & \Delta\phi_q \end{bmatrix}^T, B_{V1} = \begin{bmatrix} 1 & 0 \\ 0 & 1 \end{bmatrix}, \\ B_{V2} &= \begin{bmatrix} 0 & 0 & -1 & 0 & 0 & 0 \\ 0 & 0 & 0 & -1 & 0 & 0 \end{bmatrix}, \\ C_V &= \begin{bmatrix} K_{iv} & 0 \\ 0 & K_{iv} \end{bmatrix}, D_{V1} = \begin{bmatrix} K_{pv} & 0 \\ 0 & K_{pv} \end{bmatrix}, \\ D_{V2} &= \begin{bmatrix} 0 & 0 & -K_{pv} & -\omega_n C_f & F & 0 \\ 0 & 0 & \omega_n C_f & -K_{pv} & 0 & F \end{bmatrix}. \end{aligned} \tag{3.12}$$

3.4.4 State-space model of current controller

The block diagram in figure 3.15 illustrates the structure of the current controller, also comprising a standard PI controller.

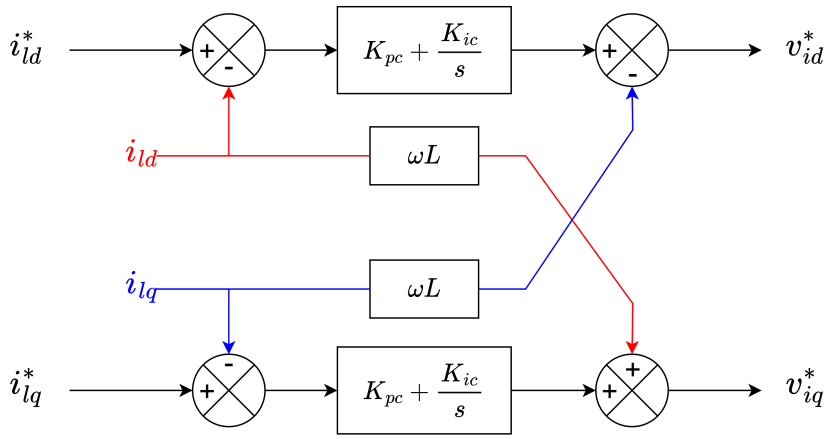

Figure 3.15: Block diagram of internal current controller of the inverter. Adapted from [49].

The state equations of the current controller are

$$\begin{aligned} \frac{d\gamma_d}{dt} &= i^*_{ld} - i_{ld} \\ \frac{d\gamma_q}{dt} &= i^*_{lq} - i_{lq}, \end{aligned} \tag{3.13}$$

and the dynamic characteristics of the controller are

$$\begin{aligned} v^*_{id} &= -\omega_n L_f i_{lq} + K_{pc}(i^*_{ld} - i_{ld}) + K_{ic}\gamma_d \\ v^*_{iq} &= \omega_n L_f i_{ld} + K_{pc}(i^*_{lq} - i_{lq}) + K_{ic}\gamma_q. \end{aligned} \tag{3.14}$$

Now that the state equations are defined and the controller's characteristics are known, the state-space model of the current controller can be expressed as

$$\begin{aligned} \begin{bmatrix} \Delta\dot{\gamma}_{dq} \end{bmatrix} &= \begin{bmatrix} 0 \end{bmatrix} \begin{bmatrix} \Delta\gamma_{dq} \end{bmatrix} + B_{C1} \begin{bmatrix} \Delta i^*_{ldq} \end{bmatrix} + B_{C2} \begin{bmatrix} \Delta i_{ldq} \\ \Delta v_{odq} \\ \Delta i_{odq} \end{bmatrix} \\ \begin{bmatrix} \Delta v^*_{idq} \end{bmatrix} &= C_C \begin{bmatrix} \Delta\gamma_{dq} \end{bmatrix} + D_{C1} \begin{bmatrix} \Delta i^*_{ldq} \end{bmatrix} + D_{C2} \begin{bmatrix} \Delta i_{ldq} \\ \Delta v_{odq} \\ \Delta i_{odq} \end{bmatrix}, \end{aligned} \tag{3.15}$$

where

$$
\begin{aligned}
\Delta\gamma_{dq} &= \begin{bmatrix} \Delta\gamma_d & \Delta\gamma_q \end{bmatrix}^T, \\
B_{C1} &= \begin{bmatrix} 1 & 0 \\ 0 & 1 \end{bmatrix}, \\
B_{C2} &= \begin{bmatrix} -1 & 0 & 0 & 0 & 0 & 0 \\ 0 & -1 & 0 & 0 & 0 & 0 \end{bmatrix}, \\
C_C &= \begin{bmatrix} K_{ic} & 0 \\ 0 & K_{ic} \end{bmatrix}, \\
D_{C1} &= \begin{bmatrix} K_{pc} & 0 \\ 0 & K_{pc} \end{bmatrix}, \\
D_{C2} &= \begin{bmatrix} -K_{pc} & -\omega_n L_f & 0 & 0 & 0 & 0 \\ \omega_n L_f & -K_{pc} & 0 & 0 & 0 & 0 \end{bmatrix}.
\end{aligned}
\tag{3.16}
$$

3.4.5 State-space model of output LC filter and coupling inductance

The state equations for the output LC filter and coupling inductance can be obtained by presuming that the inverter produces the demanded voltage, i.e. $v_i = v_i^*$. By this assumption, the state equations can be represented by:

$$
\begin{aligned}
\frac{di_{ld}}{dt} &= -\frac{\gamma_f}{L_f} i_{ld} + \omega i_{lq} + \frac{1}{L_f} v_{id} - \frac{1}{L_f} v_{od} \\
\frac{di_{lq}}{dt} &= -\frac{\gamma_f}{L_f} i_{lq} - \omega i_{ld} + \frac{1}{L_f} v_{iq} - \frac{1}{L_f} v_{oq} \\
\frac{dv_{od}}{dt} &= \omega v_{oq} + \frac{1}{C_f} i_{ld} - \frac{1}{C_f} i_{od} \\
\frac{dv_{oq}}{dt} &= -\omega v_{od} + \frac{1}{C_f} i_{lq} - \frac{1}{C_f} i_{oq} \\
\frac{di_{od}}{dt} &= -\frac{\gamma_c}{L_c} i_{od} + \omega i_{oq} + \frac{1}{L_c} v_{od} - \frac{1}{L_c} v_{bd} \\
\frac{di_{oq}}{dt} &= -\frac{\gamma_c}{L_c} i_{oq} - \omega i_{od} + \frac{1}{L_c} v_{oq} - \frac{1}{L_c} v_{bq}
\end{aligned}
\tag{3.17}
$$

The state-space model for the output LC filter and output inductance can then be expressed as

$$\begin{bmatrix} \Delta\dot{i}_{ldq} \\ \Delta v_{odq} \\ \Delta i_{odq} \end{bmatrix} = A_{LCL} \begin{bmatrix} \Delta i_{ldq} \\ \Delta v_{odq} \\ \Delta i_{odq} \end{bmatrix} + B_{LCL1} \begin{bmatrix} \Delta v_{idq} \end{bmatrix} + B_{LCL2} \begin{bmatrix} \Delta v_{bdq} \end{bmatrix} + B_{LCL3} \begin{bmatrix} \Delta\omega \end{bmatrix} \tag{3.18}$$

where

$$\begin{aligned} A_{LCL} &= \begin{bmatrix} \frac{-\gamma_{L_f}}{L_f} & \omega_0 & \frac{-1}{L_f} & 0 & 0 & 0 \\ -\omega_0 & \frac{-\gamma_{L_f}}{L_f} & 0 & \frac{-1}{l_f} & 0 & 0 \\ \frac{1}{C_f} & 0 & 0 & \omega_0 & \frac{-1}{C_f} & 0 \\ 0 & \frac{1}{C_f} & -\omega_0 & 0 & 0 & \frac{-1}{C_f} \\ 0 & 0 & \frac{1}{L_c} & 0 & \frac{-\gamma_{L_c}}{L_c} & \omega_0 \\ 0 & 0 & 0 & \frac{1}{L_c} & -\omega_0 & \frac{-\gamma_{L_c}}{L_c} \end{bmatrix}, \\ B_{LCL1} &= \begin{bmatrix} \frac{1}{L_f} & 0 \\ 0 & \frac{1}{L_f} \\ 0 & 0 \\ 0 & 0 \\ 0 & 0 \\ 0 & 0 \end{bmatrix}, B_{LCL2} = \begin{bmatrix} 0 & 0 \\ 0 & 0 \\ 0 & 0 \\ 0 & 0 \\ -\frac{1}{L_c} & 0 \\ 0 & -\frac{1}{L_c} \end{bmatrix}, \\ B_{LCL3} &= \begin{bmatrix} i_{lq} & -i_{ld} & v_{oq} & -v_{od} & i_{oq} & -i_{od} \end{bmatrix}^T. \end{aligned} \tag{3.19}$$

In the above state-space model, ω_0 represents the steady state frequency of the system at the given operating point.

3.4.6 State-space model of entire inverter

Since every component of the inverter has been defined in the sections above, it is now possible to combine the state-space models in (3.7), (3.11), (3.15), and (3.18) to obtain the state space model for the entire inverter.

To connect the inverter to the microgrid, the output variables of the inverter need to be converted to the common reference frame. The common reference frame refers to the reference frame of a single inverter. All the other inverters in the microgrid will have to be translated to this common reference frame before the modelling of those inverters can be done, but since this modelling is only for a single inverter, the other inverters will not be considered.

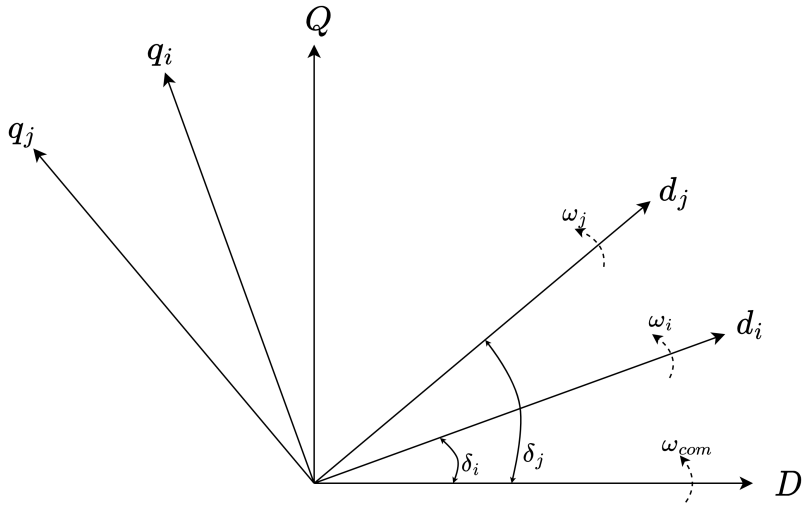

Figure 3.16: Reference frame transformation. Adapted from [49].

Figure 3.16 illustrates the transformation of the reference frame. In this figure, the axis set (D and Q) is referred to as the common reference frame rotating at a frequency ω_{com}. The axes $(d-q)_i$ and $(d-q)_j$ are the reference frame of the ith and jth inverters in the microgrid rotating at ω_i and ω_j respectively. The transformation of the inverters to the reference frame can be represented as:

$$\left[f_{DQ}\right] = \left[T_i\right]\left[f_{dq}\right] \tag{3.20}$$

where

$$\left[T_i\right] = \begin{bmatrix} \cos(\delta_i) & -\sin(\delta_i) \\ \sin(\delta_i) & \cos(\delta_i). \end{bmatrix} \tag{3.21}$$

In (3.20) and (3.21), δ_i is the angle of the reference frame of the ith inverter in the microgrid with respect to the common reference frame.

In this state-space model of an inverter, the output variables are the output currents, as represented by the vector Δi_{odq}. Now that the transformation to the reference frame is known, the output of the inverter can be converted to the $D-Q$ axis by using (3.20):

$$\left[\Delta i_{0DQ}\right] = \left[T_S\right]\left[\Delta i_{odq}\right] + \left[T_C\right]\left[\Delta\delta\right], \tag{3.22}$$

where

$$T_S = \begin{bmatrix} \cos(\delta_0) & -\sin(\delta_0) \\ \sin(\delta_0) & \cos(\delta_0) \end{bmatrix},$$
$$T_C = \begin{bmatrix} -i_{od}\sin(\delta_0) - i_{od}\cos(\delta_0) \\ i_{od}\cos(\delta_0) - i_{od}\sin(\delta_0) \end{bmatrix}. \tag{3.23}$$

The input signal to the inverter is the bus voltage v_{bDQ}, which is already on the common reference frame. Therefore, the reverse transformation should be used to convert the bus voltage to the individual reference frame:

$$\left[\Delta v_{bdq}\right] = \left[T_S^{-1}\right]\left[\Delta v_{bDQ}\right] + \left[T_V^{-1}\right]\left[\Delta\delta\right], \tag{3.24}$$

where

$$T_V^{-1} = \begin{bmatrix} -V_{bD}\sin(\delta_0) + V_{bQ}\cos(\delta_0) \\ -V_{bD}\cos(\delta_0) - V_{bQ}\sin(\delta_0) \end{bmatrix} \tag{3.25}$$

All the states, inputs, and outputs of the inverter are now known, therefore, the final symbolic state-space model for the inverter can be described. The final state-space model of the inverter is:

$$\left[\Delta\dot{x}_{\text{inv}i}\right] = A_{\text{INV}i}\left[\Delta x_{\text{inv}i}\right] + B_{\text{INV}i}\left[\Delta v_{bDQi}\right]$$
$$\begin{bmatrix} \Delta\omega_i \\ \Delta i_{oDQi} \end{bmatrix} = \begin{bmatrix} C_{\text{INV}\omega i} \\ C_{\text{INV}ci} \end{bmatrix}\left[\Delta x_{\text{inv}i}\right], \tag{3.26}$$

where

$$\Delta x_{\text{inv}i} = \begin{bmatrix} \Delta\delta_i & \Delta P_i & \Delta Q_i & \Delta\phi_{dqi} & \Delta\gamma_{dqi} & \Delta i_{ldqi} & \Delta v_{odqi} & \Delta i_{odqi} \end{bmatrix}^T, \tag{3.27}$$

and

$$A_{INVi} = \begin{bmatrix} A_{Pi} & 0 & 0 & B_{Pi} \\ B_{V1i}C_{Pvi} & 0 & 0 & B_{V2i} \\ B_{C1i}D_{V1i}C_{Pvi} & B_{C1i}C_{Vi} & 0 & B_{C1i}D_{V2i} + B_{C2i} \\ B_{LCL1i}D_{C1i}D_{V1i}C_{Pvi} + & B_{LCL1i}D_{C1i}C_{Ci} & B_{LCL1i}C_{Ci} & A_{LCLi} + \\ B_{LCL2i}[T_{Vi}^{-1} \;\; 0 \;\; 0] + & & & B_{LCL1i}(D_{C1i}D_{V2i} + D_{C2i}) \\ B_{LCL3i}C_{P\omega_i} & & & \end{bmatrix},$$

$$B_{\text{INV}i} = \begin{bmatrix} 0 \\ 0 \\ 0 \\ B_{LCL2}T_S^{-1} \end{bmatrix}, C_{\text{INV}\omega i} = \begin{bmatrix} C_{P\omega} & 0 & 0 & 0 \end{bmatrix},$$

$$C_{\text{INV}ci} = \begin{bmatrix} [T_C \;\; 0 \;\; 0] & 0 & 0 & [0 \;\; 0 \;\; T_S] \end{bmatrix}. \tag{3.28}$$

3.5 Numeric state-space model of inverter

The complete symbolic state space model can be found in (3.26), which comprises a voltage-, current-, and droop controller. This symbolic state-space model's intended use is to approximate the inverters in the Simulink model, therefore, an accurate numerical state-space model should be obtained.

The numerical values for the state-space model were obtained by studying the Simulink model. The parameters used in the Simulink model were extracted where possible and fed into the state-space model. Some of the parameters were not available for extraction, such as the voltage and current outputs, therefore, those parameters were measured in the Simulink model. The measurements were done by isolating a single inverter and completing a few simulations with this isolated inverter. The output voltages and currents were then measured, converted to the format required by the state-space model, and fed into the state-space model.

Table 3.3: Numerical values for state-space variables.

Variable	Value	Unit	Variable	Value	Unit
v_{od}	380	V	ω_n	314	rad/s
v_{oq}	0	V	K_{iv}	1	–
i_{od}	5.5	A	K_{pv}	2.35	–
i_{oq}	0.2	A	K_{ic}	400	–
ω_c	31.41	rad/s	K_{pc}	250	–
C_f	50	μF	m_p	1×10^{-4}	–
L_f	13.5	mH	n_q	2×10^{-4}	–
L_c	3.4	mH	F	0.004	–

As seen in (3.26), the two inputs to the inverter are the $D-Q$ voltage components whereas the outputs are the $D-Q$ current components along with the frequency. For this mathematical approximation, only one input and one output will be used. The D-component of the voltage will be used as the input and the D-component of the current will be used as the output.

Since the state-space model comprises all the inputs and outputs, only the data relevant to the input and output can be extracted. Therefore, the *s-domain* state-space model describing the inverter is given by:

$$\begin{aligned} \left[\Delta \dot{x}\right] &= A\left[\Delta x\right] + B\left[\Delta v_{bD}\right] \\ \left[\Delta i_{oD}\right] &= C\left[\Delta x\right], \end{aligned} \tag{3.29}$$

where

$$A = \begin{bmatrix} 0 & -0.0001 & 0 & 0 & 0 & 0 & 0 & 0 & 0 & 0 & 0 & 0 & 0 \\ 0 & -31.41 & 0 & 0 & 0 & 0 & 0 & 0 & 0 & 172.8 & 6.282 & 1.19\text{x}10^4 & 0 \\ 0 & 0 & -31.41 & 0 & 0 & 0 & 0 & 0 & 0 & 6.282 & -172.8 & 0 & 1.19\text{x}10^4 \\ 0 & 0 & -0.0002 & 0 & 0 & 0 & 0 & 0 & 0 & -1 & 0 & 0 & 0 \\ 0 & 0 & 0 & 0 & 0 & 0 & 0 & 0 & 0 & 0 & -1 & 0 & 0 \\ 0 & 0 & -0.00038 & 0.5 & 0 & 0 & 0 & -1 & 0 & -1.9 & -0.0157 & 0.21 & 0 \\ 0 & 0 & 0 & 0 & 0.5 & 0 & 0 & 0 & -1 & 0.0157 & -1.9 & 0 & 0.21 \\ 0 & 0 & -7.037 & 9259 & 0 & 2.96\text{x}10^4 & 0 & -1.85\text{x}10^4 & 0 & -3.52\text{x}10^4 & -290.7 & 3889 & 0 \\ 0 & 0.00055 & 0 & 0 & 9259 & 0 & 2.96\text{x}10^4 & 0 & -1.85e{+}04 & 290.7 & -3.52\text{x}10^4 & 0 & 3889 \\ 0 & 0 & 0 & 0 & 0 & 0 & 0 & 1.33\text{x}10^4 & 0 & 0 & 314 & -1.33\text{x}10^4 & 0 \\ 0 & 0.038 & 0 & 0 & 0 & 0 & 0 & 0 & 1.33\text{x}10^4 & -314 & 0 & 0 & -1.33\text{x}10^4 \\ 1740 & 0 & 0 & 0 & 0 & 0 & 0 & 0 & 0 & 289.9 & 0 & 8.698 & 314 \\ 1.10\text{x}10^5 & 0.00055 & 0 & 0 & 0 & 0 & 0 & 0 & 0 & 0 & 289.9 & -314 & -8.698 \end{bmatrix}, \tag{3.30}$$

$$B = \begin{bmatrix} 0 & 0 & 0 & 0 & 0 & 0 & 0 & 0 & 0 & 0 & 0 & -289.9 & 0 \end{bmatrix}^T, \tag{3.31}$$

$$C = \begin{bmatrix} 5.5 & 0 & 0 & 0 & 0 & 0 & 0 & 0 & 0 & 0 & 0 & 0 & 1 \end{bmatrix}. \tag{3.32}$$

The pole-zero plot of this state-space model is illustrated in figure 3.17. Since some of the poles and zeros are close to the origin, figure 3.17 was magnified to ensure that there are no poles on the right-hand side of the origin, which will indicate instability.

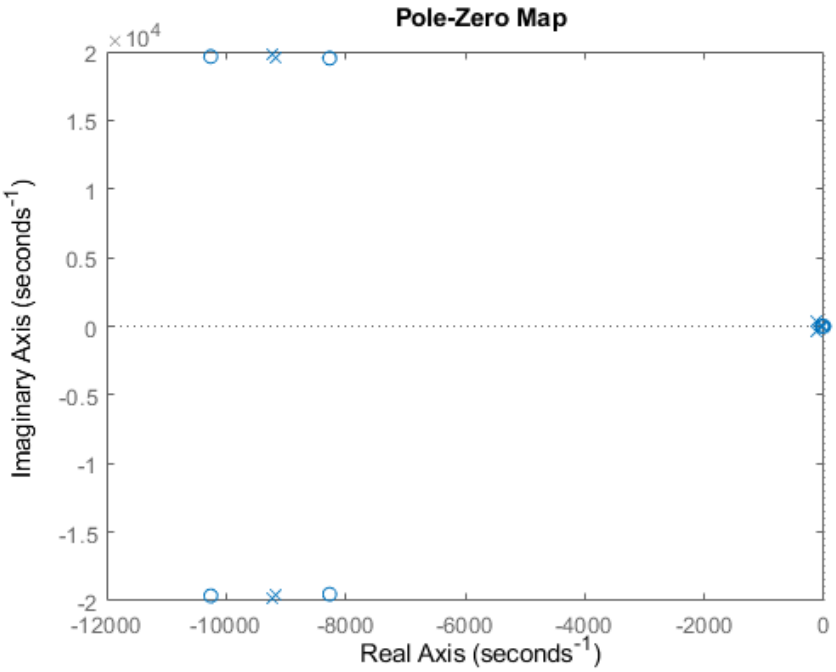

Figure 3.17: Pole-zero map of inverter's state-space model.

The magnified plot can be seen in figure 3.18. As seen, all the poles and zeros are on the left-hand side, therefore, this state-space model of the inverter will be stable. The state-space model is of 13^{th} order of which the order of the system may be reduced, but it was not done in this study. The reason being all the calculations were done in a MATLAB script, therefore, it is not needed to reduce the order. There is also a risk that the reduction is not done correctly, which may compromise the model, therefore, all the calculations were done with the original state-space model.

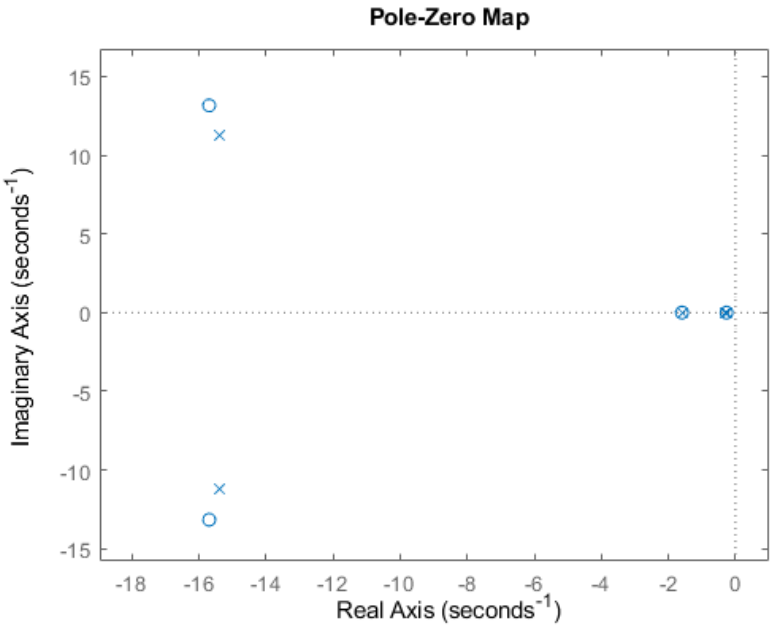

Figure 3.18: Magnified pole-zero plot of inverter's state-space model

The stability of the model can also be confirmed by means of the step response of the state-space model. The step response was plotted in MATLAB with the *step* function, as seen in figure 3.19.

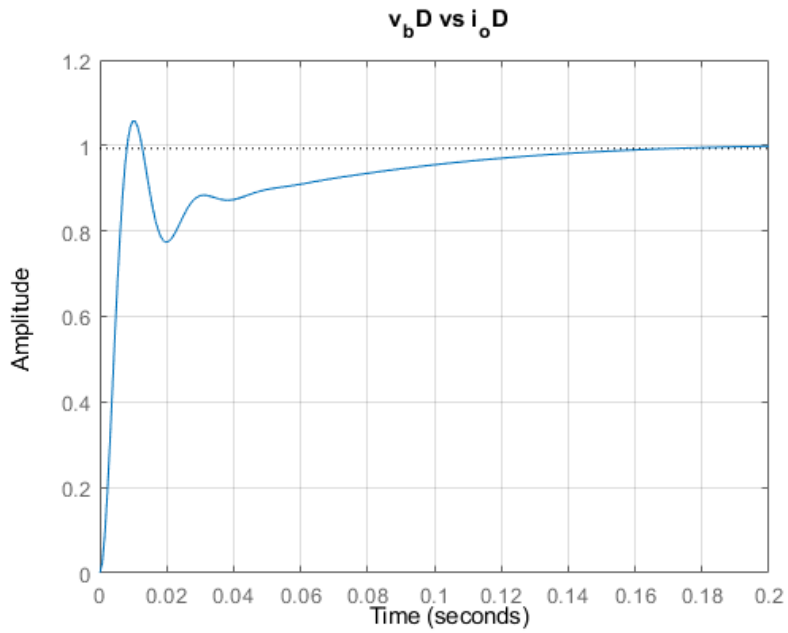

Figure 3.19: Step response of s-domain state-space model

The step response of the state-space model in figure 3.19 confirms that the model is stable. The settling time of the system is fast, which is supported by the fact that an inverter system has low to no inertia.The aim is to approximate the Simulink model with the mathematical model; thus, the *s-domain* state-space model must be transformed to the *z-domain*. The sampling time of the Simulink model is 50 µs, therefore, the sampling time of the discrete state-space model will have the same sampling time. The transformation was done in MATLAB using the *c2d* function along with the *tustin* (Bilinear method) argument. Due to the size of the discrete state-space model, it will not be displayed, but the step response will be compared to the continuous-time step response to determine if the discrete system and continuous system are the same. This comparison can be seen in figure 3.20.

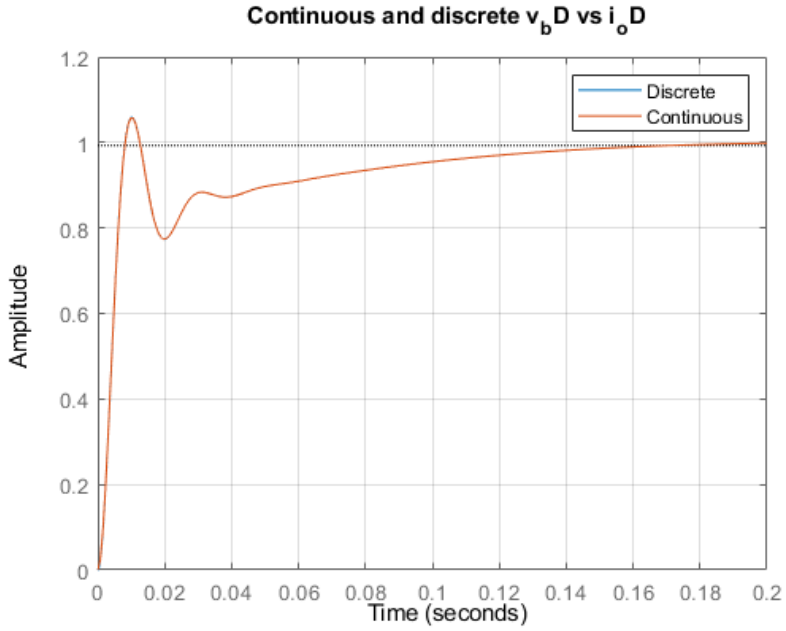

Figure 3.20: Discrete vs continuous step response of inverter model

The step response in figure 3.20 confirms the fact that the discrete and continuous state-space models are the same since the plots are the same. The steps of the discrete step response are not visible due to the small step size of the 50 µs sampling time. The state-space model is now in the correct format to compare to the Simulink model.

3.6 Mathematical approximation of the Simulink model

The preceding sections described the process by which the state-space model of an inverter was developed. This inverter model was then converted to the discrete domain, where the Simulink model is also used; thus, the two models can now be compared to determine whether or not the mathematical model is valid for the design of an adequate controller.

The input to the inverter is the D-component of the voltage, and the output is the D-component of the output current. Therefore, a single inverter in the Simulink model was isolated to simulate only a single inverter. The inverter model was adjusted such that only the voltage are provided as an input and the current was measured at the output. The output current was then converted to the *dq0* reference frame before it was used in the comparison. The *abc to dq0* Simulink block was used to do the transformation. The D-component was then isolated and plotted in figure 3.21.

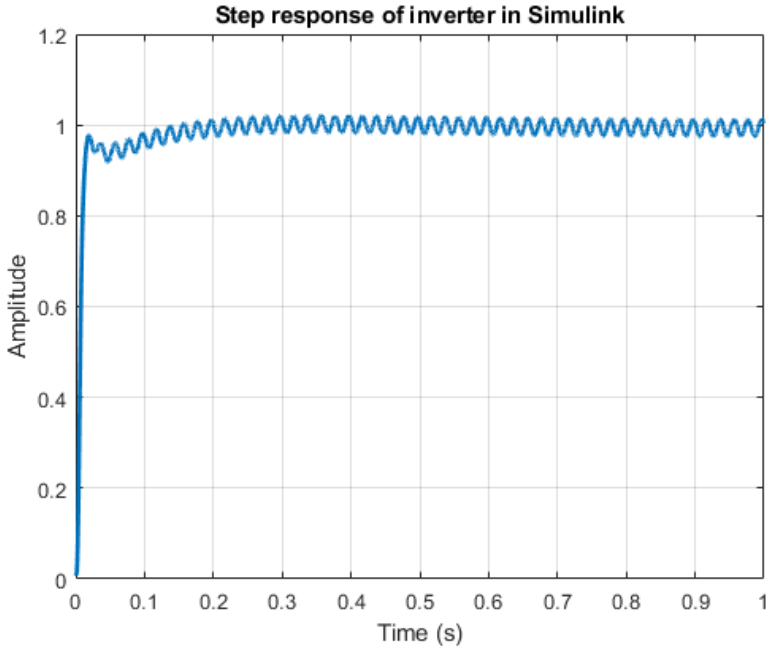

Figure 3.21: Step response of inverter in Simulink

The voltage was increased from 200 V to 230 V to simulate the step response in the input. The current was then normalised such that the maximum amplitude is 1, and plotted as seen in figure 3.21. The settling time of the step response is fast, as expected with an inverter with low to no inertia. The Fast Fourier Transform (FFT) was done on the output current, which is shown in figure 3.22.

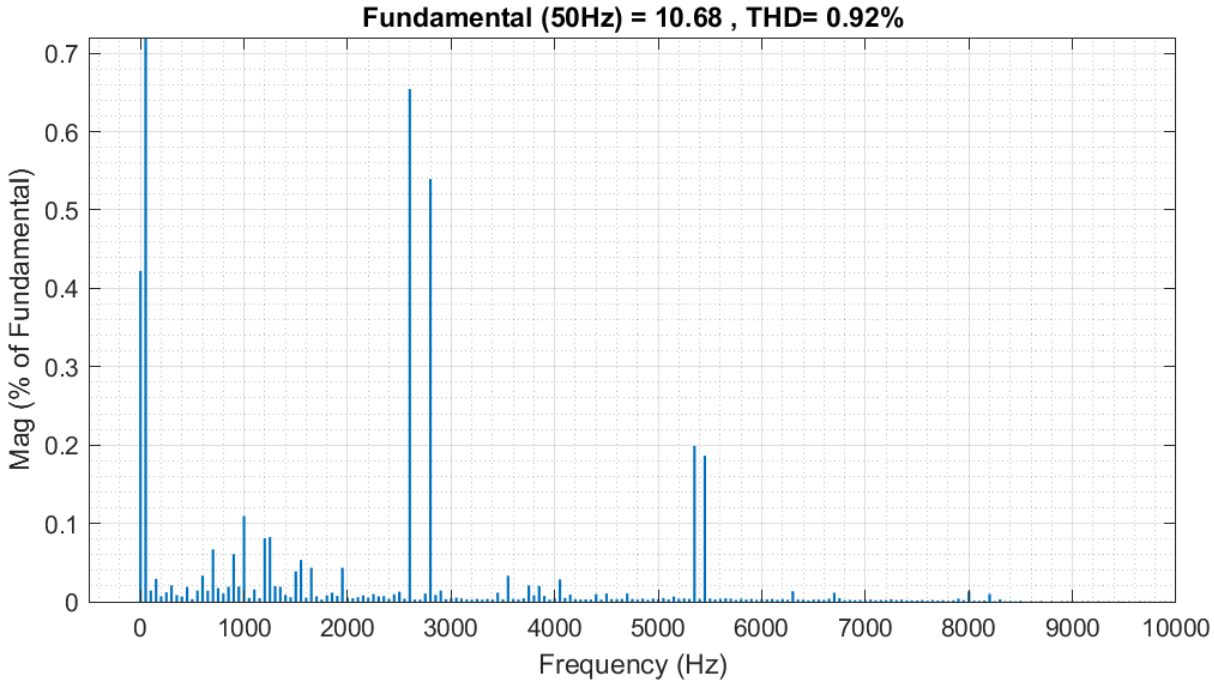

Figure 3.22: FFT of output current

The FFT was done using the *FFT Analyser App* in MATLAB on the output current obtained from Simulink. The Total Harmonic Distortion (THD) of the signal was calculated to be 0.92%, which is quite low. There were also several harmonics detected around the fundamental frequency (50 Hz) and the switching frequency (2.7 kHz), which may be the cause for the ripple in output current [50]. The ripple in the output current may also be the result of an unbalanced three phase system, as described in [50].

A comparison between the Simulink model and the mathematical state-space model can be seen in figure 3.23. There is a difference between the two models at the start, but other than that, the two models are similar. The steady-state amplitude for both models is the same and both have the same settling time, which is more significant than the small deviation at the start. Since this is an approximation from which the controller will be designed, it can be assumed that this approximation is adequate for its purpose.

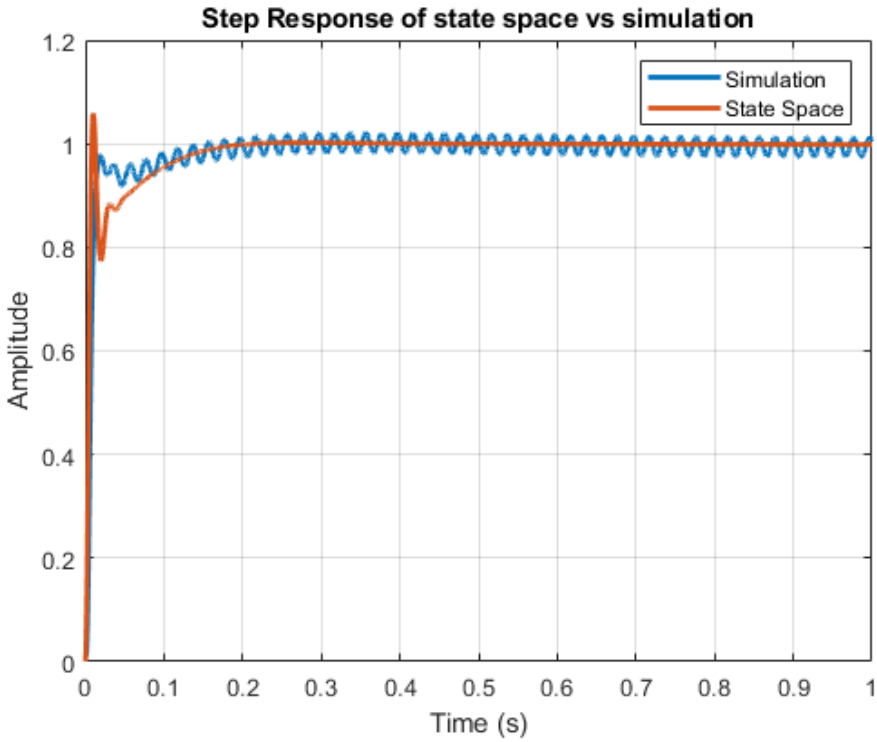

Figure 3.23: Step response of mathematical state-space vs Simulink model

3.7 Conclusion

This chapter described the entire modelling process of an inverter in an islanded microgrid. The mathematical modelling, along with all the assumptions, was described and explained. The numerical mathematical model was also compared to the Simulink model to ensure they are representatives of each other before the controller design phase can commence.

Some challenges presented themselves throughout this chapter, for example, the ripple in the output current. This ripple was assumed to be from switching harmonics in the inverter, as supported by the FFT done on the output current waveform. The mathematical model and Simulink model did also not match 100% due to some high-frequency elements, therefore, this will have to be considered in the next chapters in which the controllers will be designed.

The numerical state-space model proved to be an adequate representative of the Simulink model. This state-space model will be used in the next chapter where an adequate PI controller will be designed for this state-space model. The designed controller will be implemented on the Simulink model to control the output of the inverter within the acceptable range.

Chapter 4

Digital PI controller design

This chapter details the design of a PI controller for an inverter in Simulink. The design method, calculations, and implementation in Simulink are discussed in this chapter. The chapter concludes with the verification of the PI controller.

4.1 Introduction

The mathematical state-space model was developed in the preceding chapter and will be used in this chapter to design an adequate PI controller for the Simulink inverter. This chapter starts with a trade-off between the phase-lead and phase-lag controller. Once the desired controller is chosen, the controller is designed using the frequency response method to comply with the predefined criteria.

The implementation of the PI controller in the Simulink model is discussed for both the centralised and decentralised configuration. The overload detection that was added to the model to compensate for the dynamic load is also discussed and explained. The chapter concludes with the verification of the controller by comparing the compensated step responses to the original step responses to determine if the prerequisites were satisfied.

4.2 Design methods

The control of the inverters in the microgrid will be realised with a PI controller since it is simple to implement, cost-effective, and not computationally expensive. This means that this control system can be installed in almost any inverter due to its simplicity. The challenge, however, is to find the optimal configuration for each application, otherwise, this simple control system will not affect the stability of the inverters.

For clarification, it should be noted that the term "compensator" and "controller" are per definition two different concepts. A compensator is used to modify the performance characteristics of a system such that the required characteristics are obtained. A compensator is therefore an additional component that is added to the control system to alter the performance of the closed-loop system and compensate for the deficient performance [52]. A controller is a control system component that will react to the input of an error signal. This error signal is obtained from the difference between the reference signal and the output signal. The controller will then use the error signal to modify the system's output [52].

4.2.1 Phase-lead compensator

There are two main types of compensators widely used, namely a phase-lag compensator, and a phase-lead compensator. The phase-lead compensator is known for its positive phase that it will add to the uncompensated system [52]. The transfer function of a typical phase-lead compensator, as described by [52], is of the form:

$$D(s) = \frac{1 + a\tau s}{1 + \tau s}, \tag{4.1}$$

where $a > 1$. The bode plot for a phase-lead compensator can be seen in figure 4.1. The added phase can clearly be observed in the bode plot, but it will also increase the high-frequency gain of the system.

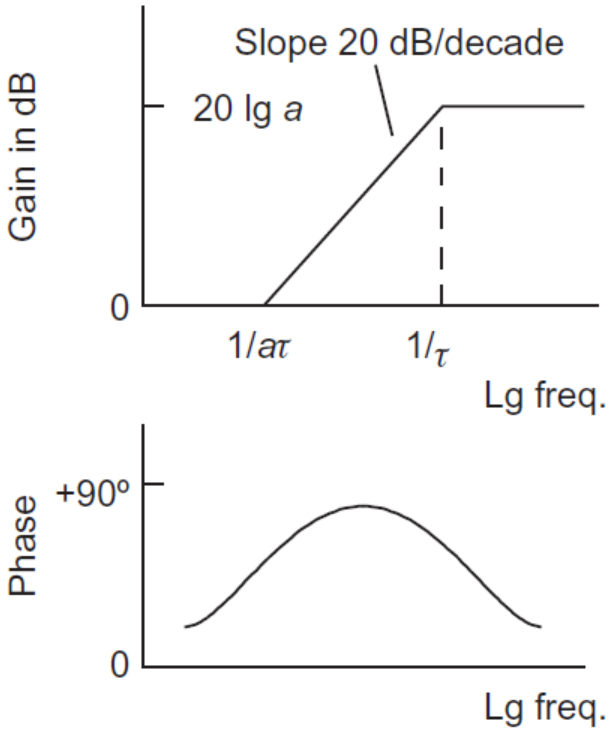

Figure 4.1: Bode plot of a phase-lead compensator. From [52].

The advantages and disadvantages of a phase-lead compensator are summarised in table 4.1 [53].

Table 4.1: Advantages and disadvantages of phase-lead compensator

Advantages	**Disadvantages**
The stability margins of the system are improved.	All the high-frequency noise in the system will be amplified.
The high-frequency performance of the system is also improved. This includes the response speed of the system.	Due to the high-frequency gain, large signals may be generated which can damage the system and/or result in the non-linear operation of the compensated system.

4.2.2 Phase-lag compensator

The phase-lag compensator is the opposite of the phase-lead compensator. The phase-lag compensator has a negative phase angle that it will subtract from the phase of the uncompensated system. The transfer function of the phase-lag compensator can be expressed as [52]

$$D(s) = \frac{1 + \tau s}{1 + a\tau s}, \tag{4.2}$$

where $a > 1$. The bode plot of the phase-lag compensator can be seen in figure 4.2. The phase is subtracted, which is the opposite of figure 4.1, while the gain of the system is reduced, which may result in a lower crossover frequency.

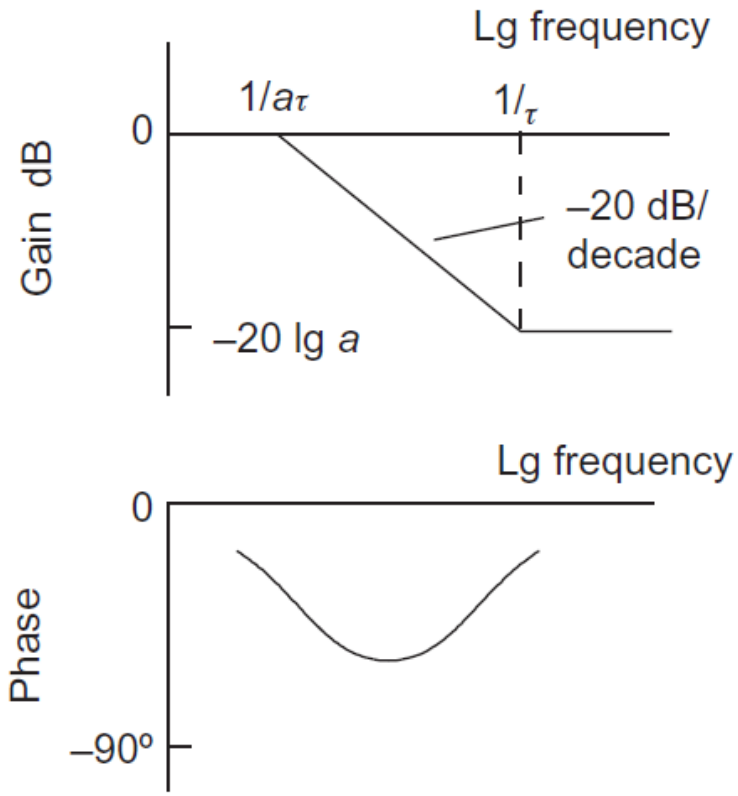

Figure 4.2: Bode plot of a phase-lag compensator. From [52].

Similar to the phase-lead compensator, the advantages and disadvantages of the phase-lag compensator are summarised in table 4.2 [53].

Table 4.2: Advantages and disadvantages of phase-lead compensator

Advantages	Disadvantages
The low-frequency characteristics of the system are maintained or improved.	The reduced bandwidth can become an issue in certain systems since it will slow the system's response.
The stability margins of the system are also improved.	The system transient response will gain one slow term.
The high-frequency elements are removed, which means that the bandwidth of the system is reduced. This may be an advantage in many applications.	There may exist some numerical challenges with filter coefficients.

4.2.3 Controller trade-off

Because the PI controller and the phase-lag compensator are essentially the same [52], a PI controller was chosen to be the controller that will be implemented on the inverters in the microgrid. As seen in figure 3.23, the step response of the inverter does contain high-frequency elements and it is known that the lack of inertia in inverters is one of the main causes of instability. Therefore, if a PI controller was to be used, the high-frequency elements will be removed while the bandwidth of the system will be reduced, which will slow the system's response. This can add a small amount of inertia to the inverter while maintaining stability [54].

4.3 Design methodology

There are two popular design methods which can be used to obtain an adequate controller for a system, namely the frequency-response design technique (also known as the bode-plot technique), and the root locus technique [53].

The root locus method will allow the addition of poles and zeros to the characteristic equation of the system by means of the controller. This will allow the placement of the poles and zeros of the system in a more appropriate location in the z-domain for the specific application. Consider a characteristic equation of a system to be

$$1 + KD(z)G(z) = 0, \tag{4.3}$$

where K is the gain that is to be varied. If the value of K varies, the root locus of the system will change which will allow for the poles and zeros of the system to move to the desired location [53]. The downside of this is that the exact location of the altered poles and zeros should be known in order to compensate for certain disturbances.

4.3.1 Frequency response

The design of the PI controller in this study will be done utilising the bode-plot technique. The reason for this is that the bandwidth and high-frequency elements of a 13th order system can be more easily controlled, whereas designing a controller for a 13th order system using the root locus method can become extremely complex. [55]. The frequency response of the state space model of the inverter, as expressed in (3.29), can be seen in figure 4.3.

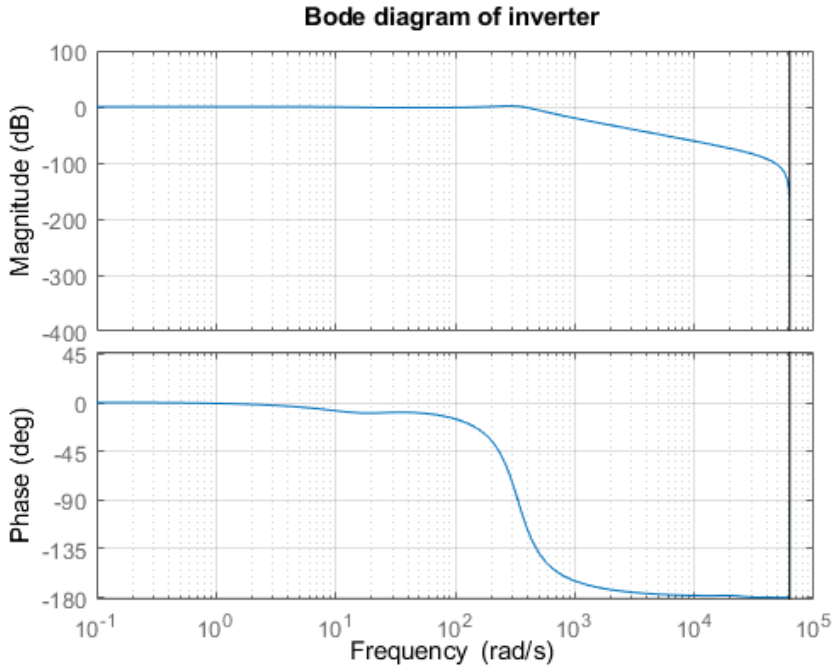

Figure 4.3: Bode diagram of the state-space model of an inverter.

The inverter does not have a high low-frequency gain, as seen in figure 4.3, but the system does contain some high-frequency elements which are not excessively attenuated. The bandwidth of the inverter is 431.63 rad/s (obtained from figure 4.3), which can be converter to Hertz using:

$$\begin{aligned} f_{bw} &= \frac{431.63}{2\pi} \\ &= 68.69 \text{ Hz}. \end{aligned} \tag{4.4}$$

Considering the step response in figure 3.23, the rise time of the state-space model is

$$t_{rss} = 5.3 \text{ ms}. \tag{4.5}$$

Since the step responses of the state-space model and the Simulink model are similar, it can be assumed that the rise time for the Simulink would also be close to 5.3 ms. Therefore, the bandwidth of the system can be calculated using the relationship between the bandwidth and the rise time. The relationship is presented in [56] to be

$$t_r = \frac{0.35}{BW}, \tag{4.6}$$

where t_r and BW represent the rise time and bandwidth respectively. Thus, the bandwidth of the system can be calculated using this relationship,

$$\begin{aligned} BW &= \frac{0.35}{t_{rss}} \\ &= 66.04 \text{ Hz}. \end{aligned} \tag{4.7}$$

This can be used as another verification that the state-space model is a representation of the Simulink model since the bandwidth calculated from the state-space model (bode plot) and the Simulink model (step response) are the same. According to [57], the bandwidth of the system should be less than 1/10 of the switching frequency (which is 2.7 kHz) to mitigate some of the switching harmonics. The bandwidth of the Simulink inverter is calculated to be 66 Hz, which is well below the threshold, therefore, the harmonics should be mitigated. As seen in figures 3.21 and 3.22, the harmonics in the system are low, but not totally mitigated.

4.3.2 Design criteria

In the preceding sections, it was decided that the PI controller would be used to control the inverter in the microgrid. The bandwidth of the system was also calculated, which will be used in this section to design the controller.

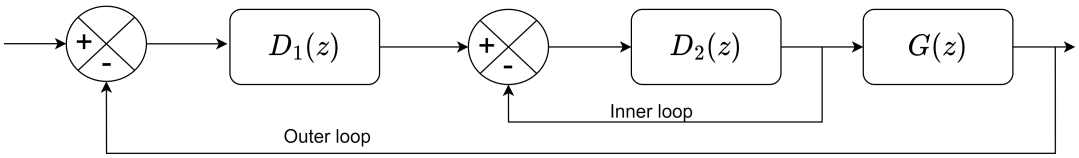

Figure 4.4: Cascaded control loops. Adapted from [52].

Consider the concept of cascaded control depicted in figure 4.4. This is the control setup for the inverters in this study; $D_2(z)$ is the internal controller of the inverter $G(z)$ which is embedded in the state-space model of the inverter. $D_1(z)$ is the external controller which is designed in this chapter. Since only the external controller has to be developed, the bandwidth of the inner controller can be used to determine the design parameters for the outer controller. Therefore, the bandwidth of the outer controller should be:

$$\frac{BW_{in}}{50} \leq BW_{out} \leq \frac{BW_{in}}{10}, \tag{4.8}$$

where BW_{in} and BW_{out} is the bandwidth of the inner controller and outer controller respectively [57]. By satisfying (4.8), the dual loop in the system can be decoupled, potentially simplifying the entire control structure [57]. The bandwidth of the inner control loop in the inverter (BW_{in}) was calculated to be 66.04Hz, therefore, according to (4.8), the bandwidth for the outer controller should be

$$1.32 \text{ Hz} \leq BW_{out} \leq 6.61 \text{ Hz}. \tag{4.9}$$

If the controller is designed in such a way that it satisfies (4.9), the system should be stable with slightly more inertia, which will mitigate high-frequency elements and reduce the Rate of Change of Frequency (ROCOF) [54].

4.3.3 Bilinear transformation

The Bilinear transformation that was used in section 3.5 will be used for the design of the digital controller. From [53] it is known that the Bode technique is based on the property that the stability boundary in the s-domain is the imaginary axis, but in the z-domain, the boundary is the unit circle. Therefore, by applying the bilinear transformation, the unit circle in the z-domain can be transformed to the imaginary axis in the w-plane.

The bilinear transformation is described by [53] as

$$w = \frac{2}{T}\frac{z-1}{z+1}, \tag{4.10}$$

where T is the sampling frequency. The transformation is realised by

$$\begin{aligned} w &= \frac{2}{T}\frac{z-1}{z+1}_{z=\varepsilon^{j\omega T}} \\ &= \frac{2}{T}\frac{\varepsilon^{j\omega T}-1}{\varepsilon^{j\omega T}+1} \\ &= \frac{2}{T}\frac{\varepsilon^{j\omega T/2}-\varepsilon^{-j\omega T/2}}{\varepsilon^{j\omega T/2}+\varepsilon^{-j\omega T/2}} \\ &= j\frac{2}{T}\tan\frac{\omega T}{2}. \end{aligned} \tag{4.11}$$

The mapping from the z-plane to the w-plane is illustrated in figure 4.5. This transformation was done prior to the design of the controller to ensure working in the correct plane. This transformation was also done by means of the *c2d* MATLAB function and not by hand.

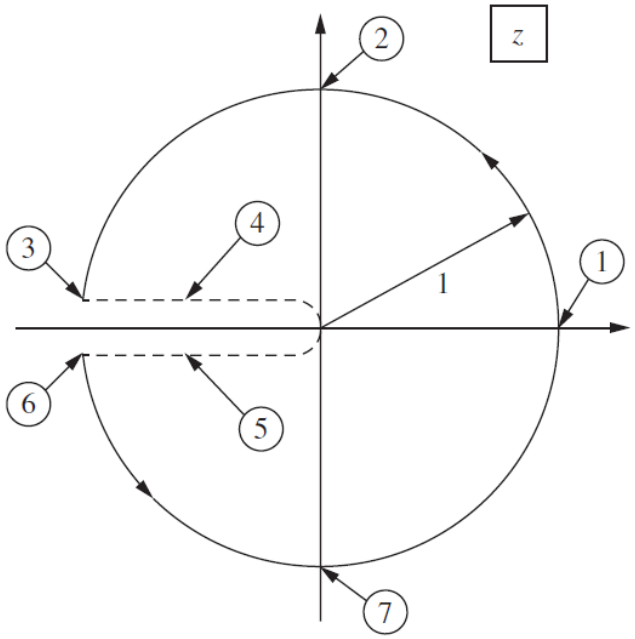

(a) Mapping in the z-plane

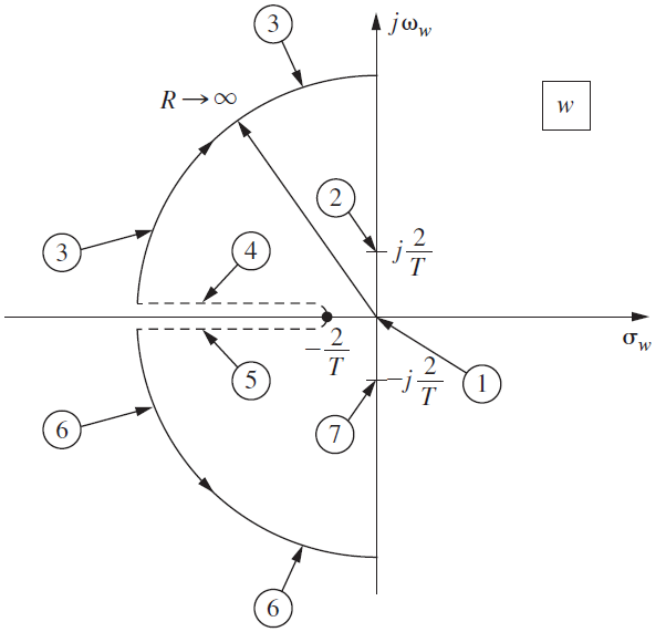

(b) Mapping in the w-plane

Figure 4.5: Mapping from the z-plane to the w-plane. From [53].

4.3.4 PI controller design

The design of the PI controller will be done in the w-plane, as discussed in the preceding section. The transfer function of a PID controller is given by [53]

$$D(w) = K_P + \frac{K_I}{w} + K_{Dw}, \tag{4.12}$$

where the K_D element is set to 0 for a PI controller. The frequency response of the PI controller is provided by [53]:

$$\begin{aligned} D(j\omega_w) &= K_P + j(K_D\omega_w - \frac{K_I}{\omega_w}) \\ &= |D(j\omega_w)|\varepsilon^{j\theta}. \end{aligned} \tag{4.13}$$

The design aims to choose $D(w)$ such that

$$D(j\omega_{w1})G(j\omega_{w1}) = 1\angle(-180^\circ + \phi_m), \tag{4.14}$$

at chosen frequency ω_{w1}. Therefore, from (4.13) and (4.14)

$$\theta = -180^\circ + \phi_m - \angle G(j\omega_{w1}), \tag{4.15}$$

where ϕ_m represents the phase margin. The design equations for the PID controller can now be written as [53]:

$$\begin{aligned} K_P = |D(j\omega_{w1})|\cos\theta &= \frac{\cos\theta}{|G(j\omega_{w1})|}, \\ K_D\omega_{w1} - \frac{K_I}{\omega_{w1}} &= \frac{\sin\theta}{|G(j\omega_{w1})|}. \end{aligned} \tag{4.16}$$

By equating the real and imaginary elements of the design equations, (4.16) will become [53]:

$$K_P + \frac{K_D\omega_{w1}^2(2/T)}{(2/T)^2 + \omega_{w1}^2} = \frac{\cos\theta}{|G(j\omega_{w1})|}, \tag{4.17}$$

and

$$\frac{K_D\omega_{w1}(2/T)^2}{(2/T)^2 + \omega_{w1}^2} - \frac{K_I}{\omega_{w1}} = \frac{\sin\theta}{|G(j\omega_{w1})|}. \tag{4.18}$$

For calculating the constants for a PI controller, the D-component will be set to 0, therefore, (4.17) and (4.18) can be used to calculate the K_P and K_I components directly:

$$K_P = \frac{\cos\theta}{|G(j\omega_{w1})|}, \tag{4.19}$$

and

$$K_I = -\frac{\omega_{w1}\sin\theta}{|G(j\omega_{w1})|}. \tag{4.20}$$

All of the equations are now defined, allowing the controller design to proceed. To design this PI controller, there are two inputs required for the design process, namely the frequency (ω_{w1}) of the controller, and the desired phase margin (ϕ_m). The frequency (ω_{w1}) is the frequency (in rad/s) at which the desired phase margin is obtained.

The process described above can be iterative since there are better combinations for phase margin and frequency than others, therefore, an algorithm was programmed into a MATLAB script which will calculate PI controllers for a given range of frequencies and phase margins. As per (4.9), the bandwidth of the system should be less than 6.61Hz, but more than 1.32Hz, therefore, these frequencies were converted to rad/s and used as the input frequency range:

$$8.29 \text{ rad/s} \leq BW_{out} \leq 41.53 \text{ rad/s}. \tag{4.21}$$

It should be noted that the bandwidth frequency indicates the frequency at the $-3dB$ point whereas ω_{w1} refers to the point at which the gain is equal to 0 dB. The 0 dB point is the point on the bode plot at which the phase margin is located, therefore, this range will not be 100% accurate, but it is a good starting point.

The algorithm that was used can be seen in figure 4.6. This algorithm was implemented in a MATLAB script in which possible options for controllers were calculated. The algorithm started by reading the ranges for the frequency (F) and phase margin (PM) from the MATLAB workspace. Frequency and phase margin local variables will then be created and set to the first value in the frequency and phase margin range. Once the local variables are set, they will be compared to the range's end values to ensure they are still in range.

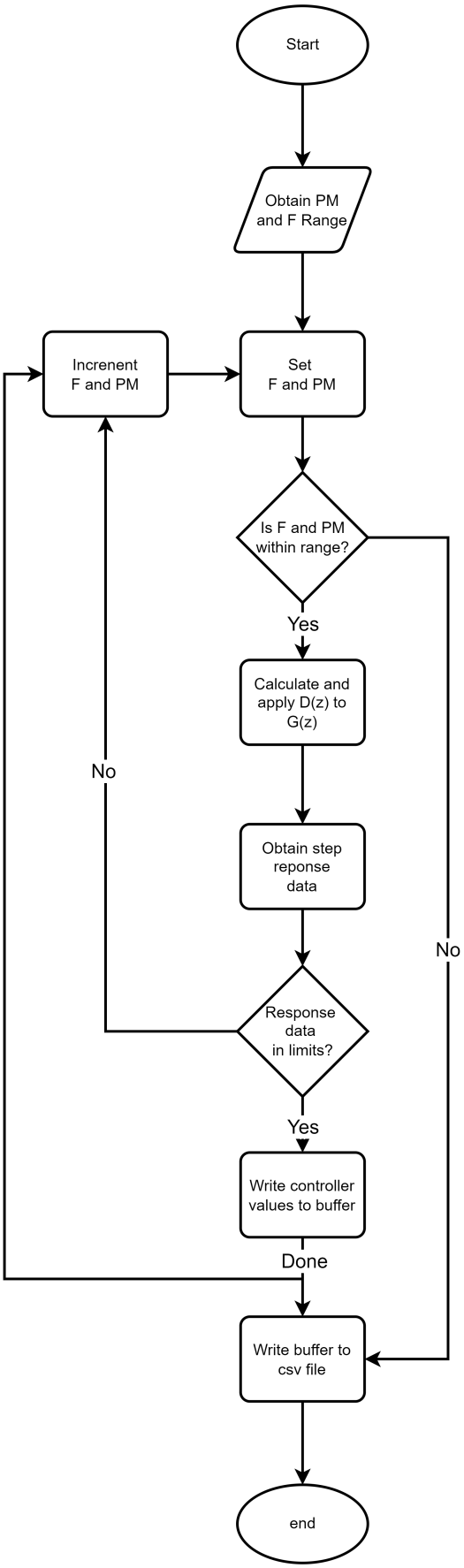

Figure 4.6: Algorithm being used for PI controller design.

Once it is confirmed that the phase margin and frequency values are still in range, the calculation of the PI controller will commence. This is done by calculating the K_P and K_I constants as discussed earlier in this section. Once the constants are known, the controller $D(z)$ is obtained which will be applied to the discrete state-space model of the inverter $G(z)$. The closed loop system of the compensated inverter $C(z)$ is then obtained by means of the *feedback* function in MATLAB. The feedback is assumed to be unity in this design.

The step response of the closed-loop system $C(z)$ is then obtained by means of the *step* function in MATLAB. The rise time and settling time data is then extracted from the step response using the *stepinfo* function. The settling time and rise time are then compared to the predefined thresholds to ensure the controller performs to specification. If the step response output data does not satisfy the requirements, the algorithm returns to the start, increments the phase margin and frequency, and repeats the entire process. If the step response output data does satisfy the requirements, the K_P and K_I values are added to a local buffer and the algorithm returns to the start for the next iteration. The data is stored in a local buffer to avoid having to write continuously to the *.csv* file.

This process will continue for all the values in the frequency and phase margin range. Once all the iterations have been done (the frequency and phase margin are out of range), the algorithm will break the iterative loop and write the buffer data to a *.csv* file. This is done by means of the *writecell* function in MATLAB. The output .csv file will contain all the possible controllers along with the corresponding phase margin, frequency, settling time, and rise time.

This algorithm will not provide the best controller, but it will provide possible controllers within the specified ranges which can be tested in different scenarios to determine which controller is the best for the inverter in the Simulink model. From the algorithm in figure 4.6, the best controller was chosen to be at the frequency and phase margin summarised in table 4.3.

Table 4.3: Design parameters for the digital PI controller

Parameter	**Value**	**Unit**
Frequency	11	radians/second
Phase margin	80	Degrees
Sampling time	50×10^{-6}	seconds

By utilising the before-mentioned design equations, the PI controller can be designed with the known frequency and phase margin. The gain and phase of the discrete state-space model at a frequency of 11 rad/s are:

$$\begin{aligned} G(j\omega_{w1}) &= G(j11) \\ &= 0.9431\angle(-7.9672). \end{aligned} \tag{4.22}$$

The phase is then calculated in degrees as well as in radians, which will be used in the calculation of K_P and K_I:

$$\begin{aligned} \theta &= 180 + 86 - (-7.9672) \\ &= -86.0328^\circ \\ &= -1.5016 \text{ radians.} \end{aligned} \tag{4.23}$$

The K_P and K_I values can now be calculated as:

$$\begin{aligned} K_P &= \frac{\cos(-1.5016)}{0.9431} \\ &= 0.0734, \end{aligned} \tag{4.24}$$

and

$$\begin{aligned} K_I &= 11\left(\frac{-\sin(-1.5016)}{0.9431}\right) \\ &= 11.6354. \end{aligned} \tag{4.25}$$

With the known controller gains and the sampling frequency of 50 µs, the transfer function of the PI controller can be presented by [53]:

$$\begin{aligned} D(z) &= K_P + K_I\frac{T}{2}\left[\frac{z+1}{z-1}\right] + K_D\left[\frac{z-1}{Tz}\right] \\ &= 0.0734 + 11.6354\left(\frac{50\ \mu\text{s}}{2}\right)\left[\frac{z+1}{z-1}\right] + 0 \\ &= \frac{0.0734z - 0.0731}{z-1}. \end{aligned} \tag{4.26}$$

This PI controller was implemented in MATLAB using the *feedback* function with unity feedback which produced the output in figure 4.7.

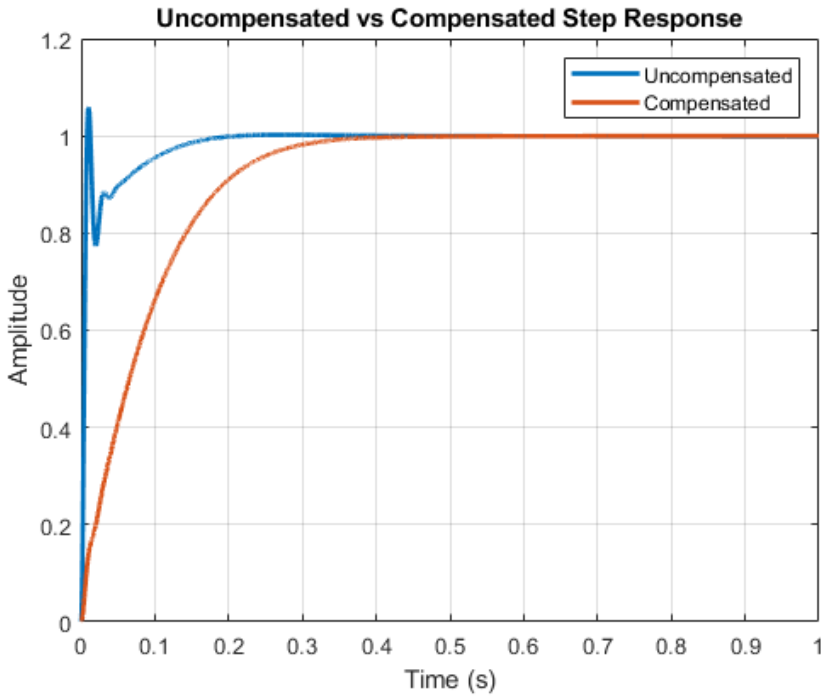

Figure 4.7: Uncompensated vs compensated step response of the discrete state-space model.

The compensated step response does not contain the same high-frequency elements that are present in the uncompensated state-space model. A complete analysis of the compensated step response will be done in section 4.5. The following section will detail the implementation of control in Simulink.

4.4 Controller implementation in Simulink

This section will describe how the control systems were implemented in the Simulink model. The centralised and decentralised control implementations are similar, but both will be discussed in this section.

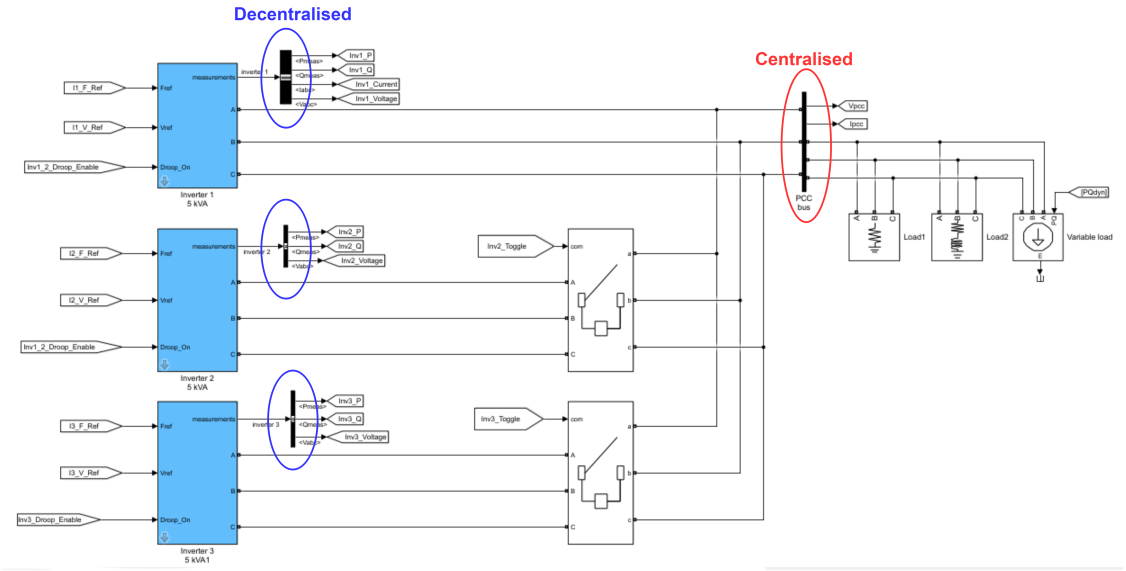

Figure 4.8: Illustration of the measurements taken for the different control techniques.

Figure 4.8 illustrates the locations in the Simulink where the measurements for the centralised and decentralised controller will be made. The centralised controller will only consider the measurements at the PCC (at the load) whereas the decentralised controller will consider the output of each inverter. The measurements in the following sections will refer to figure 4.8.

4.4.1 Centralised control implementation

The concept of the centralised controller implementation in this study can be seen in figure 4.9. Each of the three coloured blocks represents the three inverters in the Simulink model. As seen, the inverters already contain their internal control loops for the voltage and current. The outer control loop is the same controller that has been designed in this chapter. These internal control loops are the reason for the cascaded control system.

This implementation is simple in the sense that one PI controller will manipulate the control signals for multiple inverters. This may not be the best solution, but it is cost-effective and robust, which is a factor that is not necessarily present with more complex control techniques. The measurements for the PI controller are done at the PCC, or the load as seen in figure 4.8. These measurements are then compared to the reference inputs to obtain the error signal from which the adjustments will be made.

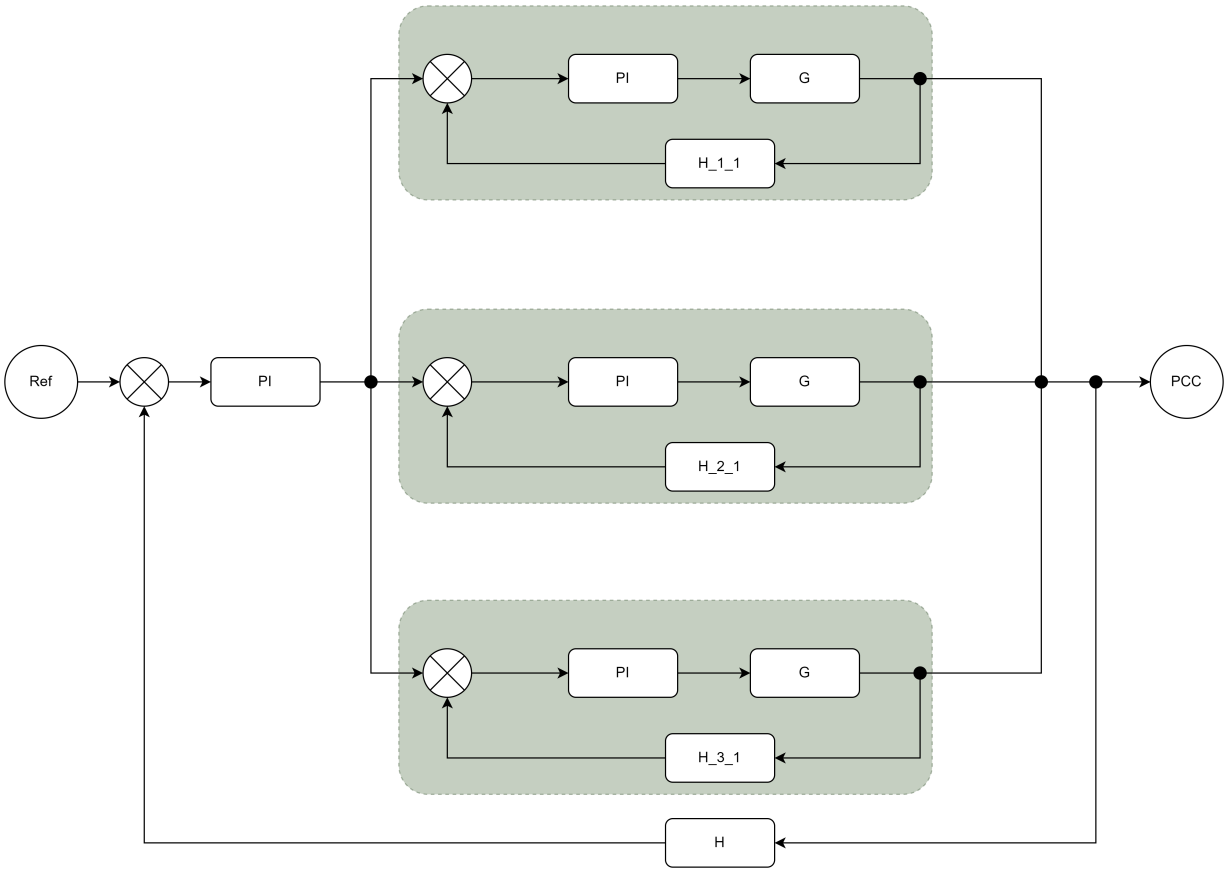

Figure 4.9: Block diagram of centralised control implementation.

The entire microgrid in figure 4.9 is controlled with one PI controller which will provide the same control signal for all the inverters in the microgrid. This will not allow the control system to control individual inverters, but it will control the entire system while all the inverters are connected to the microgrid. This was chosen based on the assumption that multiple inverters connected in parallel will behave the same as a single inverter. This assumption is supported by the step response in figure 4.10.

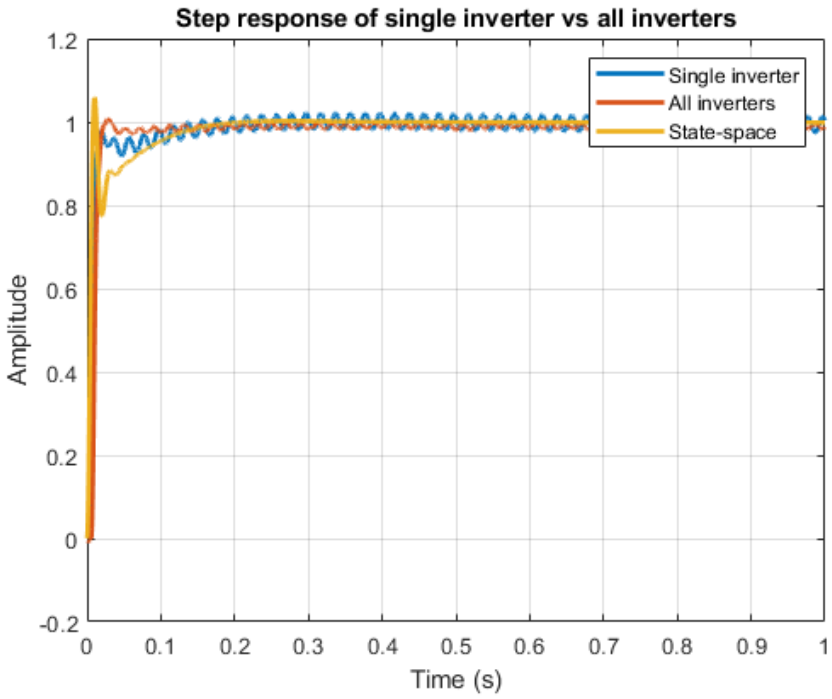

Figure 4.10: Step response of a single inverter vs multiple inverters

Figure 4.10 depicts the step response of a single inverter, many inverters (all of which are connected to the microgrid), and the step response of the state-space model. To accomplish the step response of many inverters, the control system was removed from the microgrid in the Simulink model and the step response was performed. The difference between this method and the single inverter method is that the measurement was performed at the PCC rather than at the output of a single inverter.

The single inverter and multiple inverter step responses differ somewhat at the start, but this is neglectable because the rest of the step response is nearly identical. Except for the start, both step responses are nearly identical to the state-space model. As a result, it can be assumed that the same controller will be able to control both a single inverter and the complete system.

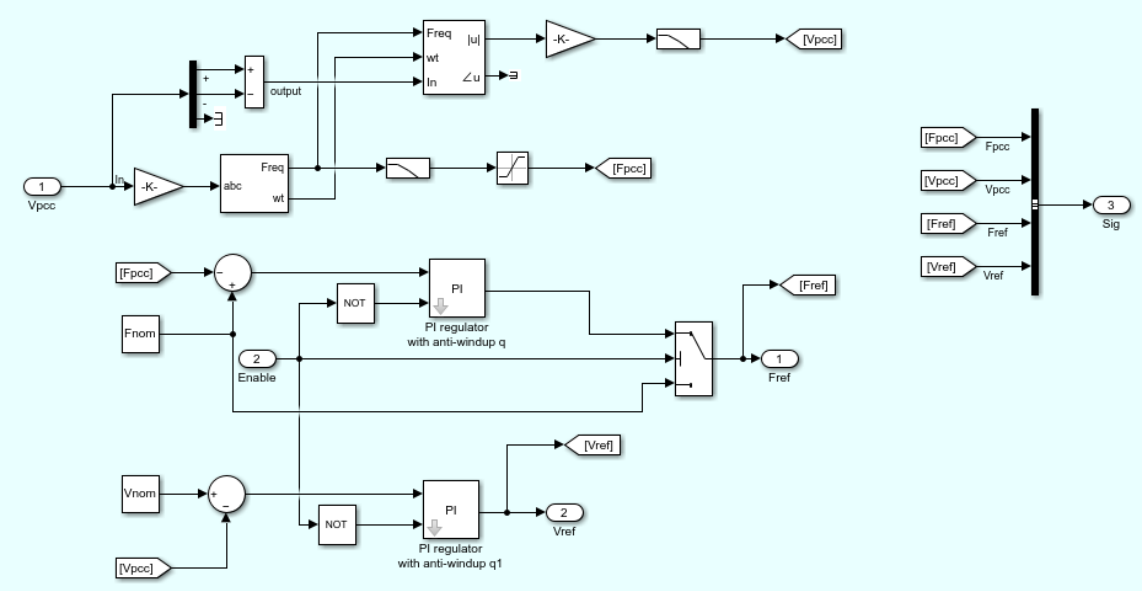

Figure 4.11: Centralised control implementation in the Simulink model

The block diagram shown in figure 4.11 represents the centralised controller for the microgrid. The V_{pcc} label on the left-hand side of the block diagram is the voltage input to the control system. This is the only input since the voltage magnitude and frequency can be obtained from the waveform. These values are then fed to the PI controller which calculates the compensated reference values for the voltage and frequency for the inverters. The output of the PI controller is the voltage V_{ref} and frequency F_{ref} reference values respectively, which are the inputs to the inverters.

All inverters in the microgrid receive the same voltage and frequency input values under this control system. As a result, if only a single inverter is affected by a disturbance, some inverters may be unable to maintain stability which may jeopardise the stability of the entire system.

4.4.2 Decentralised control implementation

The concept of decentralised control is illustrated in figure 4.12. As in figure 4.9, the coloured blocks represent the inverters in the microgrid, each with its own internal control system. The decentralised control technique is also considered cascaded control with the inner and outer control loop of each inverter.

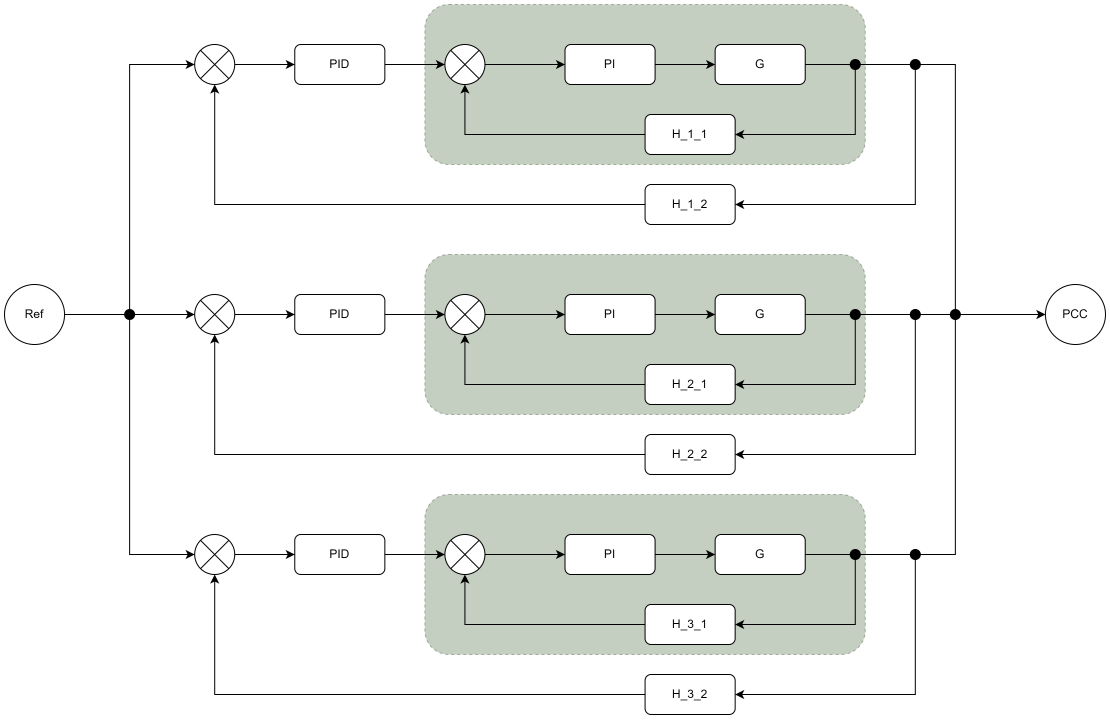

Figure 4.12: Block diagram of decentralised control implementation.

The implementation is also with PI controllers, which will maintain the simplicity of the control system. As seen in figure 4.12, the measurements for the control system are obtained from the output of each inverter. This will result in each inverter being controlled independently from the other, which may increase the stability of each inverter.

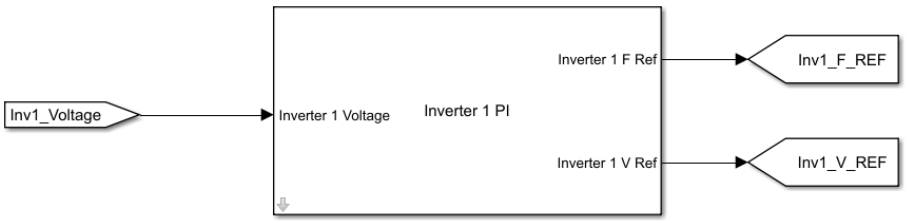

Figure 4.13: Decentralised control system of a single inverter

The block diagram in figure 4.13 illustrates the way in which the decentralised control system for a single inverter is implemented in the Simulink model. The output voltage of the inverter is the only input to the control system whereas the voltage and frequency reference values are the outputs.

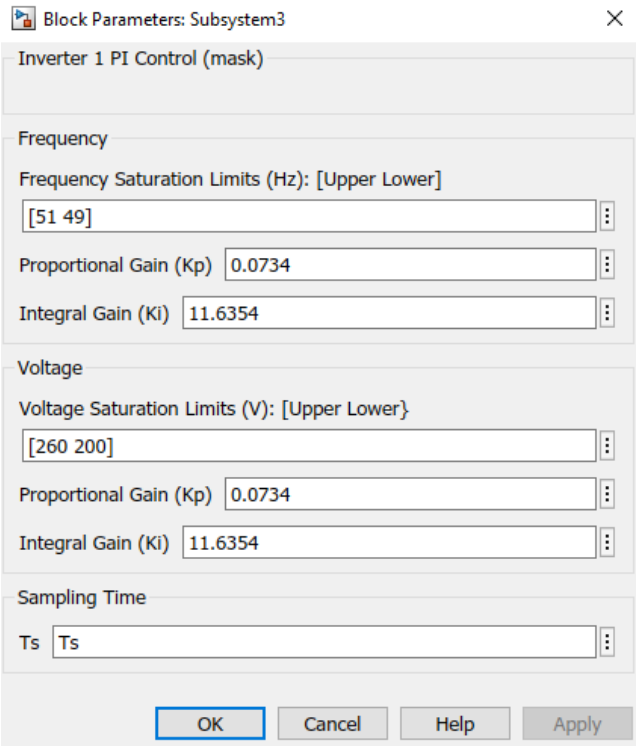

Figure 4.14: Input options of the decentralised controller for a single inverter.

The block parameters seen in figure 4.14 illustrate the different inputs that will define the decentralised controller for this specific inverter. The voltage and frequency saturation limits are used in the anti-windup to ensure the values are within a realistic range and to prevent the controller from malfunction due to too large values. The proportional and integral gains are also entered which will be used in the PI controller. The last parameter is the sampling time which is also used in the PI controller.

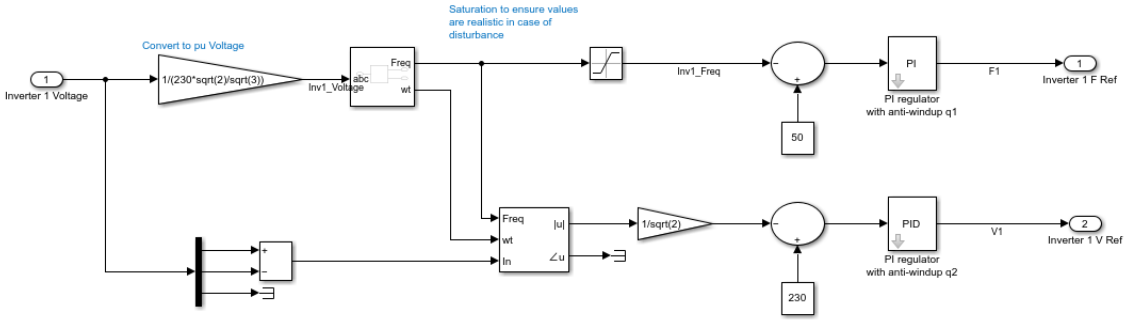

Figure 4.15: Decentralised control implementation for a single inverter.

When the mask in figure 4.13 is opened, the block diagram in figure 4.15 is revealed. The control loop is similar to the centralised controller since the inverter output voltage is the only input and the voltage and frequency reference values are the outputs. The control system for each inverter is the same, but the control signals to the inverters are the only elements that are not identical to each other. This control implementation allows for the control of each inverter independently, which will perform better if a disturbance only affects a single inverter.

4.4.3 Overload detection

The control system should be able to ensure microgrid stability in the face of significant load variations. As a result, an overload detection system was also included in the Simulink model. This was done to allow the microgrid to operate with the fewest number of inverters possible while still having the ability to add inverters if necessary.

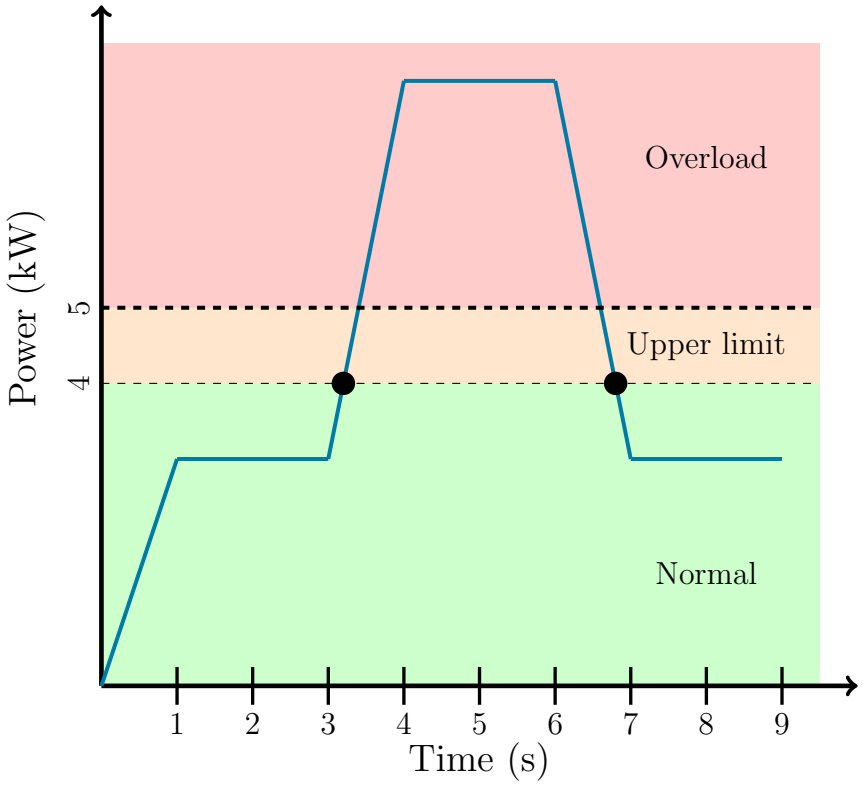

Figure 4.16: Inverter overload detection concept.

The concept of overload detection is illustrated in figure 4.16. The graph is the total power consumed if only one inverter is connected to the microgrid with a capacity of 5kVA, as implemented in the Simulink model. Once the load is connected (t=0), the load settles with a power consumption which is less than 4kW. A significant increase in the load is observed at t=3, which drives the load's power consumption above 5kW. If this happens, the system will become unstable since the single inverter does not have the capacity to supply the demanded power, therefore, the load should either be reduced or the capacity of the microgrid should be increased.

In this study, the load is not reduced to fit the capacity, the capacity of the microgrid is increased to fit the demand. Thus, as the microgrid's circumstances change, inverters should be added dynamically. The inverse is also true; if the load decreases to below the threshold, the added inverters will be removed as they are not needed anymore.

To realise this concept in the Simulink model, a threshold of 4 kW was defined, as seen in figure 4.16. This would imply that an inverter will be added if the demand exceeds 4 kW, even though a single 5 kW inverter is capable of meeting the demand. This band between 4 kW and 5 kW is known as the *Upper Limit*, and it serves as a buffer. If this buffer is removed and the demand is at 4.5 kW, any slight rise in load may create instability (exceeds 5 kW); however, if another inverter at 4 kW is added, the overall capacity is increased to 10 kW, which should be enough to compensate for any load changes.

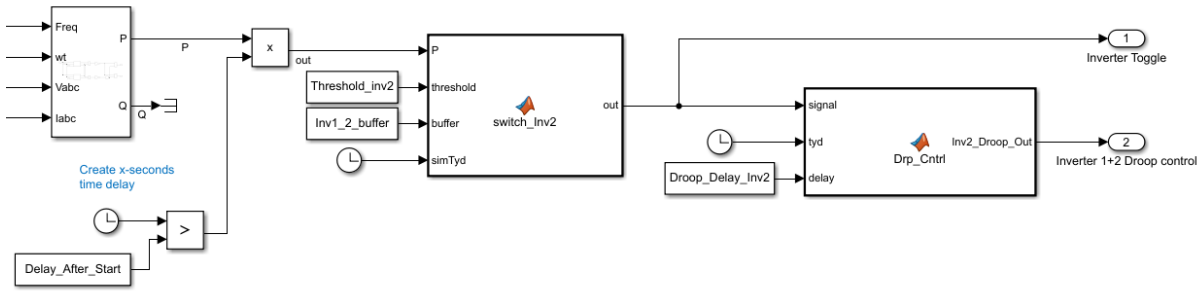

Figure 4.17: Implementation of the overload detection concept in Simulink

The implementation of this concept in figure 4.16 in Simulink can be seen in figure 4.17. The left-hand side of the implementation is not been included since it only consists of voltage and frequency measurements.

Once the power is obtained from the measurements, it is passed through a *product* block in Simulink, which will either multiply the power by 1 (allowing the power to be seen by the rest of the block diagram) or by 0, which will "disable" the power in the block diagram. The *Delay_After_Start* variable is obtained from the input parameters in figure 4.18, which is compared to the simulation time in order to provide the 1 or 0 to the product block. The purpose of this is to "disable" the overload detection for the first second to ensure inverters are not added due to startup spikes observed in the system.

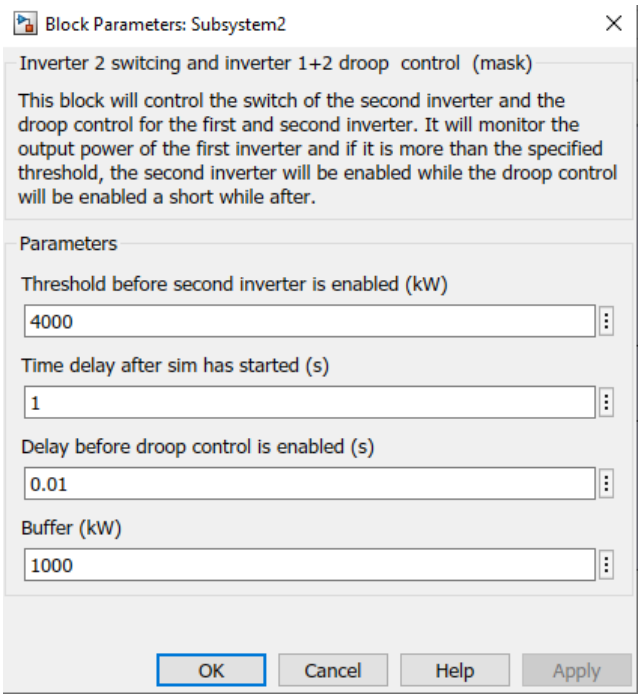

Figure 4.18: Input parameters to the overload detection control block in Simulink.

The power in figure 4.17 is then fed the first *MATLAB Function* block that contains the software for the overload detection. The values for the *Threshold_Inv2* and *Inv1_2_buffer* variables are also obtained from the input parameters in figure 4.18. The *Threshold_Inv2* variable represents the size of the *Normal* region in figure 4.16, while the *Inv1_2_buffer* variable is the size of the *Upper Limit* region. The internal software will then compare the input power to the threshold and if the power is within the normal range, the output will be 0 which will not include an additional inverter. If the input power exceeds the threshold, the output would be changed to 1, which will enable the three-phase circuit breakers in figure 3.3 to add an additional inverter.

If the required power is reduced to less than the threshold, the software will also disable the extra inverter. This is performed by comparing the input power to the threshold and removing the extra inverter if the threshold is crossed. The only difference between adding and removing inverters is the time delay attached to the removal. When the threshold is crossed and the inverter should be removed, the software will postpone this process for a short period of time to guarantee that the detection was not false, indicating a drop in the necessary power. If the software removes one inverter due to false detection, the system will become unstable because the load is still above the capability of one inverter, and the inverter will have to be added again. The addition and removal of an inverter in such a short period of time generate a large disturbance, which is enough to jeopardise the microgrid's stability.

The droop control is controlled in the second *MATLAB Function* block in figure 4.17 by providing the enable/disable signal to each inverter for the internal droop control system. This is performed by monitoring the output signal of the first block that will add or remove an inverter; once the signal to add an inverter is active, the droop control is deactivated for a short time before it is enabled. The disturbance introduced when inverters are added is significant, but by disabling the droop control for a short period of time, the disturbance can be reduced. This does not affect the load sharing performance of the system, which will be discussed in chapter 5.

This overload detection is used with both the centralised and decentralised controller should the application be to add inverters dynamically. If all the inverters are connected all the time, the overload detection will be removed. This will also be discussed in chapter 5.

4.5 PI controller verification

This section will verify that the PI controller designed in the preceding sections is operating to specification. Before proceeding to validation in Chapter 5, the controller will be evaluated on the mathematical state-space model and the Simulink model to ensure adequate performance.

The compensated step response of the state-space model can be seen in figure 4.7. The PI controller was implemented on the same Simulink model that was used to obtain the uncompensated step responses of a single inverter. The step response was performed to analyse the effect of the controller in the simulation model. The output of the step response can be seen in figure 4.19.

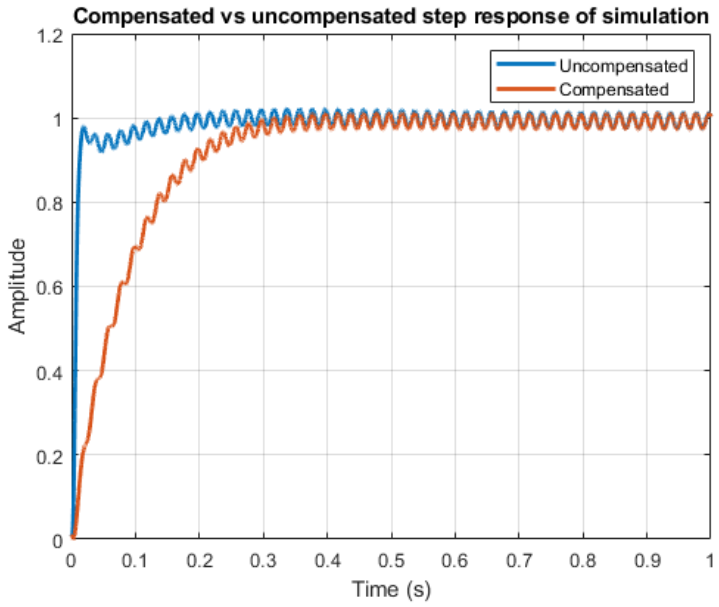

Figure 4.19: Uncompensated vs compensated step response of Simulink model.

The response in figure 4.19 is what is expected since the compensated output seems to have a lower bandwidth, which was part of the design requirements. The high-frequency elements at the start of the step response are also removed. The comparison between figure 4.7 and 4.19 can be seen in figure 4.20.

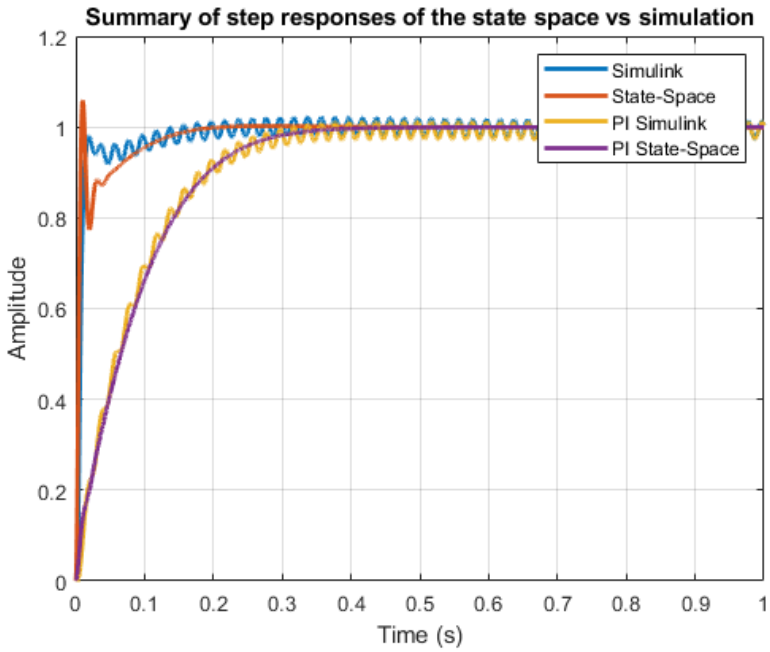

Figure 4.20: Comparison between the compensated and compensated responses for the state-space and Simulink models.

The step responses of the compensated and uncompensated state-space and Simulink models in figure 4.20 are confirmation that the mathematical approximation was successful. The responses of the state-space and Simulink are identical, which concludes that the state-space is a mathematical representative model of the Simulink model.

The design criteria in section 4.3.2 stated that the bandwidth of the system should be between 1.32 Hz and 6.61 Hz (see (4.9)). To ensure that the controller is accurate, compute the bandwidth of the compensated controllers to see if the controller meets the design requirements.

From figure 4.20, the rise time for the compensated system was calculated using the *stepinfo* function in MATLAB. Since the Simulink and state-space models are almost identical, only the rise time of the state-space model was calculated to be

$$t_r = 185.2 \text{ ms}. \tag{4.27}$$

By using (4.6), the bandwidth of the system can be calculated as

$$\begin{aligned} BW &= \frac{0.35}{185.2 \text{ ms}} \\ &= 1.89 \text{ Hz}. \end{aligned} \tag{4.28}$$

The frequency response of the compensated and uncompensated system can be seen in figure 4.21. The bandwidth for the compensated system calculated from the frequency response is

$$\begin{aligned} f_{bw} &= \frac{14.94 \text{ rad/s}}{2\pi} \\ &= 2.37 \text{ Hz}. \end{aligned} \tag{4.29}$$

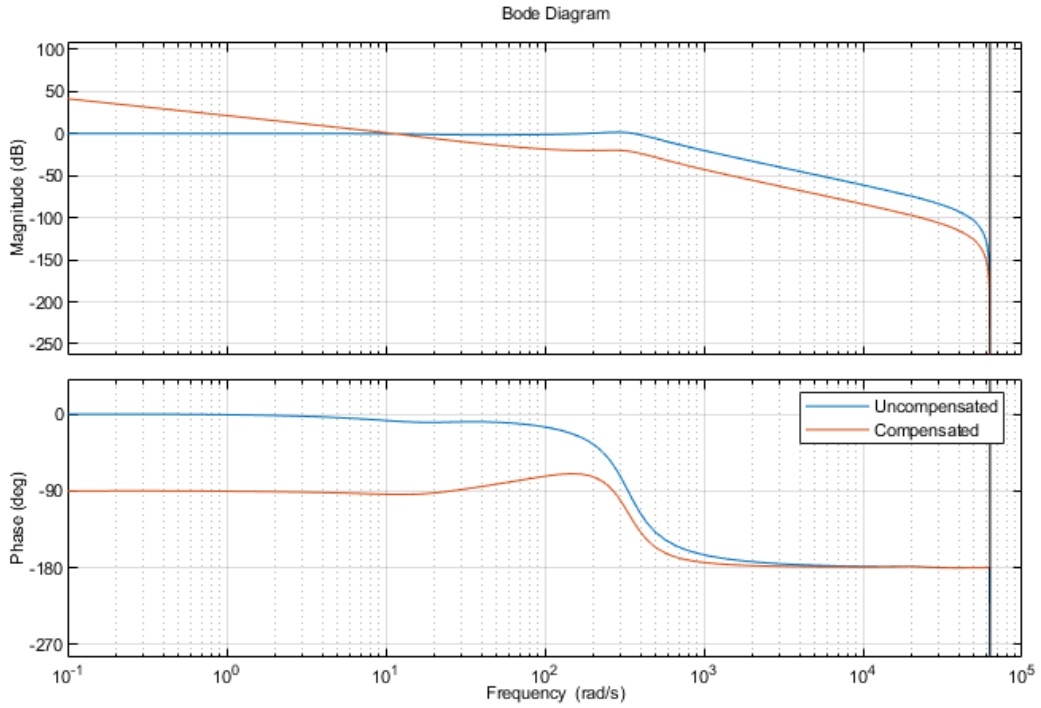

Figure 4.21: Bode plot of both the compensated and uncompensated state-space model.

The small deviation between the bandwidth calculated from the step response and frequency response is neglectable small since both are still within the design requirements. The phase margin of the system was also extracted from the frequency response in MATLAB, and documented in table 4.4.

Table 4.4: Summary of the phase margins of the two systems compared to the design requirement.

Phase margin of the systems		
System	**Phase Margin**	**Frequency**
Design requirement	86°	11 rad/s
Compensated	86°	11 rad/s
Uncompensated	77°	363 rad/s

A summary of the controller's bandwidth performance can be seen in table 4.5.

Table 4.5: Summary of the controller's performance for the compensated and uncompensated systems.

Summary of controller's performance		
Parameter	**Compensated**	**Uncompensated**
Rise Time	185.20 ms	5.30 ms
Bandwidth (Step response)	1.89 Hz	66.04 Hz
Bandwidth (Frequency response)	2.37 Hz	68.69 Hz
Design Requirement	1.32 Hz - 6.61 Hz	-

The bandwidth for the compensated system is within the design requirements, even with the small deviation between the step response and the frequency response. The phase margin requirement is also satisfied by the PI controller, therefore, since the controller performs to specification, it can be confirmed that this controller should be able to maintain a microgrid in stability.

4.6 Conclusion

This chapter depicted the control of the PI controller for the inverter in Simulink. The PI controller was chosen to be the best suited for this application after which some design criteria were documented. The frequency response design method was chosen to be the best since the bandwidth of the system was one of the prerequisites.

Once the controller was designed, the implementation of the controller in Simulink was discussed along with the implementation of the overload detection. This overload detection will add and/or remove inverters based on the demand of the load. The ripple in the output current was due to the harmonics in the system, but it can be neglected. During the verification of the control system, it became clear that the state-space model and the Simulink model have the same dynamics for the compensated and uncompensated systems. The bandwidth for the compensated systems was also calculated to be within the prerequisites.

Chapter 5

Controller evaluation

This chapter will detail the experimental design that was used to determine the performance of each controller. Different scenarios are developed in which the performance of each controller will be measured to finally find the best controller for each application/scenario.

5.1 Introduction

This chapter begins with an experimental design that will outline the approach for testing the control system designed in Chapter 4. The experimental design will explain the various scenarios that will be implemented in Simulink, as well as the desired outcomes for each scenario. The scenarios are developed in such a way that the system will be tested under extreme conditions in order to assess the robustness of the control system.

Thereafter, the results of the different scenarios are analysed. The challenges for each disturbance are discussed and the comparison between the different microgrid configurations is examined to determine which configuration performed the best after being subjected to a certain environment.

This chapter concludes with a discussion of the results. In the discussion, all the scenarios are compared to determine in which environment each controller will perform the best. Recommendations are also provided for the optimal operation of a microgrid which is subjected to unforeseen circumstances.

5.2 Experimental design

This section will describe the experimental design that was followed to create the different scenarios in which the stability of the microgrid was tested.

5.2.1 Purpose

The purpose of this experiment is to determine the system's voltage and frequency sensitivity with and without an integrated controller. This data will then be utilised to assess which control philosophy is best for a given configuration.

5.2.2 Hypothesis

The disturbance caused by the interaction between the different inverters (DERs) has a larger impact on the system's stability than fluctuations in load. Thus, the decentralised controller will be the best choice when considering an application where DERs must be added and/or removed.

5.2.3 Measurements to be captured

The following measurements should be obtained from each of the scenarios:

- For the system as a whole:
  - Output voltage of the entire system (measured at the PCC).
  - Output frequency of the entire system (measured at the PCC).
  - Output active and reactive power for the system as a whole.
- For each inverter:
  - Output voltage.
  - Output frequency.
  - Droop control.

- For the control comparison:
  - Error signals for all the control techniques.
  - Integral Squared Error (ISE) for each controller.
  - Integral Absolute Error (IAE) for each controller.

5.2.4 Variables to be changed in each scenario

The following variables will be altered to create different scenarios in which the system can be tested:

- Control philosophy (decentralised/centralised/no-control).
- Amount of inverters connected to the microgrid at any given time.
- The magnitude of the load connected to the microgrid. The magnitude can be varied at any given time.

5.2.5 Disturbances to be introduced

The different types of disturbances that will be introduced into the system are:

- Variation in load (abrupt changes in the magnitude of the load).
- Inverter addition and removal in the microgrid.

5.2.6 Experimental scenarios

These scenarios will test the system's ability to mitigate the disturbances mentioned in section 5.2.5. The output of each scenario will be evaluated to determine the sensitivity of the system and the performance of each controller. Each scenario will be performed three times with three different control configurations; no-control, centralised control, and decentralised control. The no-control scenario will be used as the benchmark against which the other control systems are measured.

5.2.7 Scenarios 1-3: Interaction between inverters

Scenarios 1, 2, and 3 comprise the no-control, centralised control, and decentralised control respectively. In this scenario, the only disturbance given to the system will be the change in the number of inverters connected to the system. The total number of inverters connected to the system will be changed at specified times to evaluate the system's response to this type of disturbance. The load will be fixed at 3 kW to ensure that only one inverter will be able to supply the load and to ensure the load does not affect the outcome of these scenarios.

These scenarios aim to:

- Determine the impact of a change in system configuration on overall system stability.
- Analyse the effect of each controller on the stability of the system in contrast to the no-control system.

5.2.8 Scenarios 4-6: Load changes on maximum-capacity microgrid

Scenarios 4, 5, and 6 comprise the no-control, centralised control, and decentralised control respectively. In this scenario, the only disturbance provided to the system will be the variations in the load's magnitude. All of the inverters will be connected to the system simultaneously (i.e. maximum system capacity) after which the magnitude of the load is increased and decreased over time.

These scenarios aim to:

- Determine the impact of a change in system load on overall system stability.
- Analyse the effect of each controller on the stability of the system in contrast to the no-control system.

5.2.9 Scenarios 7-9: Disturbances introduced to dynamically controlled system

Scenarios 7, 8, and 9 comprise the no-control, centralised control, and decentralised control respectively. Only one inverter will be connected to the microgrid in these scenarios, with a load that is within the capacity of a single inverter.

The load will then be increased to the point that it exceeds the capacity of a single inverter, at which point the dynamic control system will have to add more inverters to meet the demand.

This is considered the "worst case" scenario since both disturbances will be introduced into the system and must be managed by the control system. Given these disturbances, it will be assessed whether the control methodologies are adequate to ensure voltage- and frequency stability.

These scenarios aim to:

- Determine how both of these disturbances affect the overall stability of the microgrid.
- Analyse the effect of each controller on the stability of the system in contrast to the no-control system.

5.3 Results

The outcomes of the various scenarios outlined in section 5.2 will be discussed in this section. The advantages and disadvantages of each scenario will be examined, and the various control systems will be compared.

For all the scenarios in this section, a separate Simulink model was created and the output measurements were passed to the MATLAB workspace with the *to Workspace* block in Simulink. All die calculations and graphs presented in this section were done in a MATLAB script. The simulations will be referred to as scenarios throughout the rest of this section, as seen in table 5.1.

Table 5.1: Description of each scenario's simulation

Scenarios	Simulation description
Scenario 1	Interaction between inverters with no control.
Scenario 2	Interaction between inverters with centralised control.
Scenario 3	Interaction between inverters with decentralised control.
Scenario 4	Load changes with no control.
Scenario 5	Load changes with centralised control.
Scenario 6	Load changes with decentralised control.
Scenario 7	"Worst case" circumstances with no control.
Scenario 8	"Worst case" circumstances with centralised control.
Scenario 9	"Worst case" circumstances with decentralised control.

Some results are not presented in this chapter due to their relevance, but all outstanding results may be found in Appendix B.

5.3.1 Interaction between inverters

The different scenarios for the interaction between the inverters will be discussed in separate sections, each with its own discussion. A comparison between the three scenarios is done at the end of this section.

Table 5.2: Summary of events in scenarios 1-3

Time (s)	Event	Inverters connected
0	Simulation starts	1
4	Inverter is added	2
8	Inverter is added	3
12	Inverter is removed	2
16	Inverter is removed	1

The simulations performed in scenarios 1-3 are according to the events in table 5.2. The load will remain at 3 kW for the entire simulation, but the number of inverters connected to the microgrid will be changed.

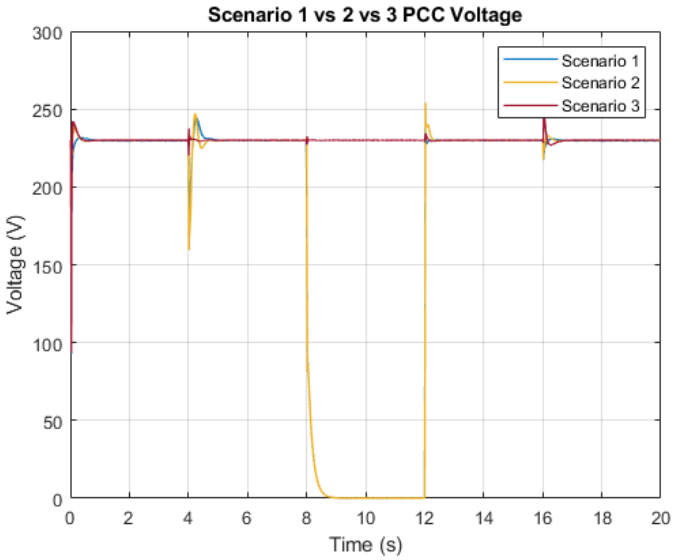

Figure 5.1: PCC voltage comparison for scenarios 1-3.

The output voltage for scenarios 1, 2, and 3 can be seen in figure 5.1. There is a spike in output voltage for scenarios 2 and 3, which is due to the compensation of the centralised and decentralised control systems. The no-control system (scenario 1) does not have the spike observed in the other scenarios, which indicates the lack of control in this case. Once the first inverter is added at $t = 4$, there exists a voltage spike for all the scenarios. This spike is the result of the introduced disturbance from the added inverter. The system does, however, returns to steady state despite the disturbance, but the centralised and decentralised system do ensure that steady state is reached faster, which indicates the significance of an external control system.

Once the second inverter is added to the microgrid, the bus voltage collapses. Voltage collapse is defined by [58] as the process by which the string of events that coincide with voltage instability leads to abnormally low voltages in a large part of the microgrid. The voltage is abnormally low for scenarios 1 and 2 during the time frame for which three inverters are connected to the microgrid. This voltage collapse is associated with voltage instability, as discussed in section 2.4.3. As soon as the third inverter is removed ($t = 12$), the voltage returns to a stable reading of 230 V.

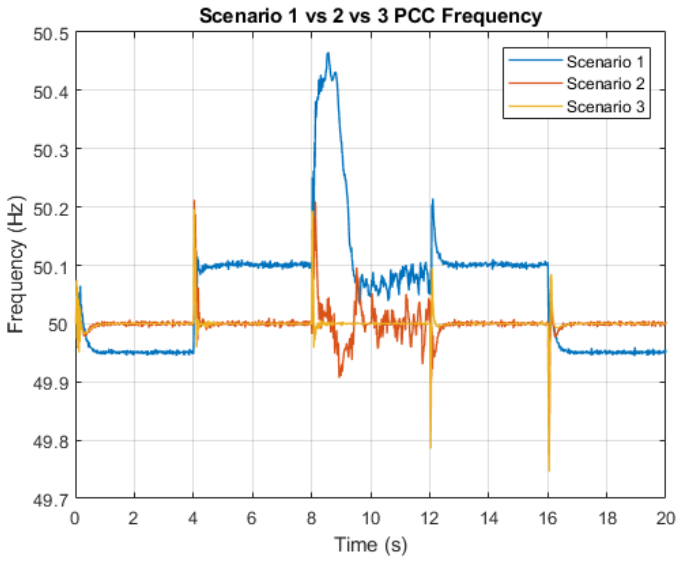

Figure 5.2: PCC frequency comparison for scenarios 1-3.

The frequency output for scenarios 1-3 can be seen in figure 5.2. The frequency for scenarios 2 and 3 is 50 Hz from the simulation started, which is the result of the centralised and decentralised controller respectively. The frequency for scenario 1 is not 50 Hz for the entire simulation since it varies around 50 Hz. This is the result of no control in scenario 1, which illustrates the need for an external control system.

All the scenarios are considered stable despite the first disturbance, but scenarios 1 and 2 become unstable when the second inverter is added. The frequency oscillations and voltage collapse are due to the same disturbance in the system. The instability in the microgrid is due to the synchronisation of the frequency between the inverters. Figure B.1 and B.2 shows the output frequency for each inverter in scenario 1 and 2 respectively. As seen, the frequency of each inverter is different when an extra inverter is added, meaning that the added inverter should synchronise with the bus frequency. This introduces an extra disturbance into the system, meaning that the microgrid should mitigate the disturbance from the interaction between the inverters and the disturbance of synchronisation.

If only two inverters are to be connected, the system can manage the disturbance, but as soon as three or more inverters are to be connected, instability will occur. The decentralised system's inverters are in sync before they are added, which removes the extra disturbance, therefore, more than two inverters can be added without compromising the stability of the microgrid.

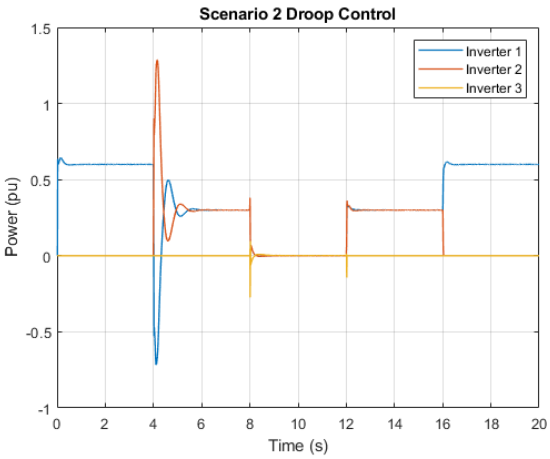

(a) Scenario 2 load sharing output

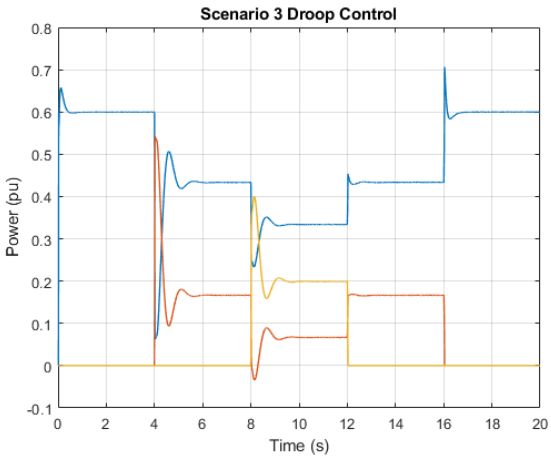

(b) Scenario 3 load sharing output

Figure 5.3: Load sharing output from scenarios 2 and 3.

The load sharing of the centralised (scenario 2) and decentralised (scenario 3) is depicted in figure 5.3. The load-sharing capabilities of the centralised controller are better than that of the decentralised controller, as seen in the output. The centralised controller shared the load ideally between the two inverters when the second inverter was added. The voltage collapse caused the power-sharing also to collapse during the time the third inverter was connected.

Once the second inverter is added, there is load sharing amongst the inverters in scenario 3, but it proved to be less effective than in scenario 2. Since each droop controller is independent of the other, the droop controller is dependent on the reference input to the inverter from which the droop output will be calculated. In the centralised controller, the reference input to all inverters is identical, hence, the droop controllers will behave the same and the load will be shared equally. In the decentralised controller, each inverter will receive a unique reference input, therefore, the droop controllers will have different outputs which will result in the load not being shared equally. The differences in reference inputs are caused by the differences in control topologies, as seen in figures 4.9 and 4.12 respectively.

The performance of the centralised controller was calculated using the Integral Squared Error (ISE) and the Integral Absolute Error (IAE). The ISE and IAE are presented by [59] as

$$ISE = \int_0^T e^2(t)dt, \tag{5.1}$$

and

$$IAE = \int_0^T |e(t)|dt, \tag{5.2}$$

where $e(t)$ and T are the error signal and time respectively. The error signal is the difference between the measured output of the system and the reference input to the controller.

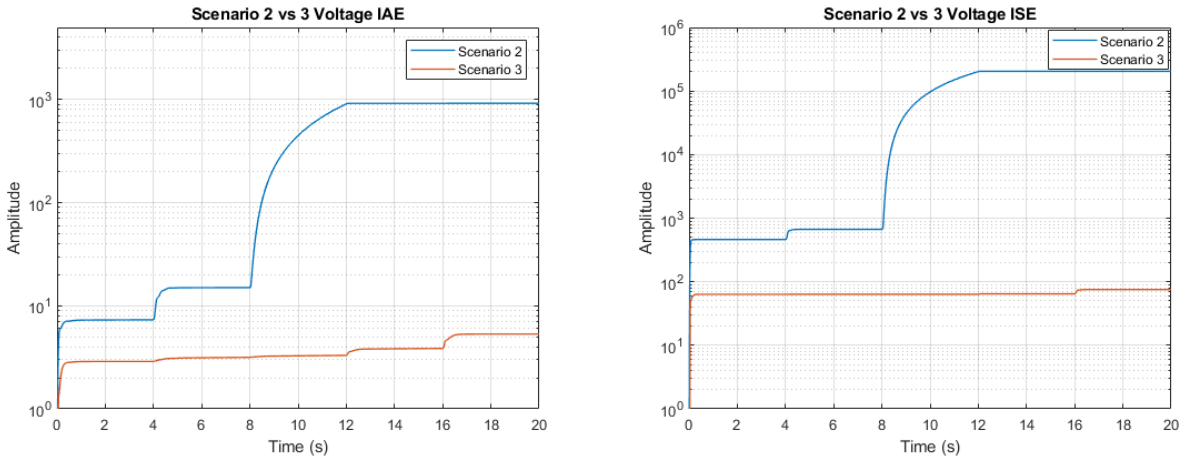

(a) IAE comparison of output voltage. **(b) ISE comparison of output voltage.**

Figure 5.4: ISE and IAE comparison of the PCC voltage from scenarios 2 and 3.

The ISE and IAE of the output voltage from scenarios 2 and 3 can be seen in figure 5.4. The shape of both the ISE and IAE are similar, but the magnitude of the ISE is significantly larger due to the square term. The reason for the steep increase between $t = 8$ and $t = 12$ is due to the voltage collapse. During this time, the error signal is significantly larger than during normal operation, which will result in a high output due to the integral term. Thus, the magnitude and duration of the error signal are considered by both the ISE and IAE.

The voltage collapse is the main reason for the poor performance of the centralised controller in scenario 2. Other than the voltage collapse, there is a slight difference between $t = 4$ and $t = 8$ on the IAE, meaning that the decentralised controller's ability to mitigate these kinds of disturbances is not as effective as the centralised controller if the centralised controller can maintain stability within the microgrid.

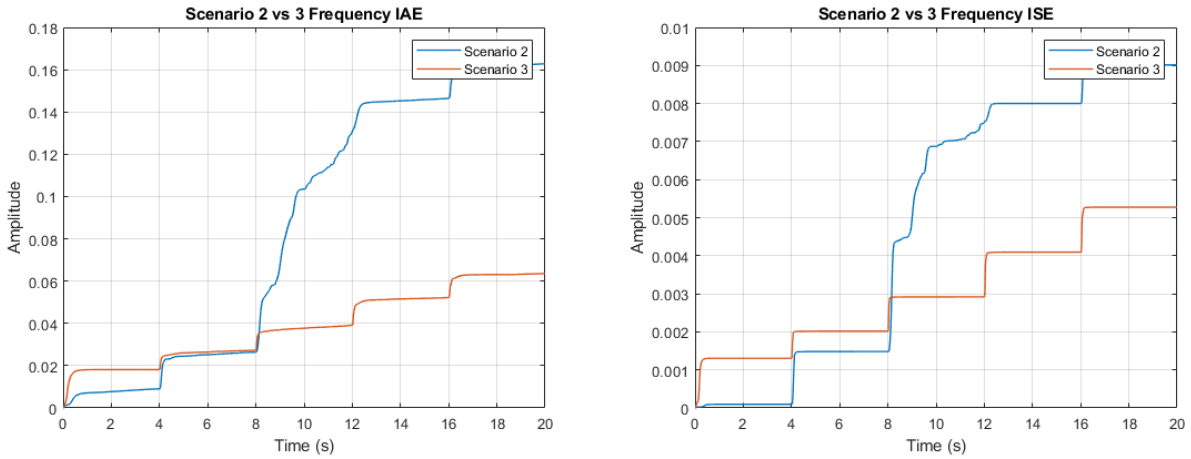

(a) IAE comparison of the output frequency.

(b) ISE comparison of the output frequency.

Figure 5.5: ISE and IAE comparison of the PCC frequency from scenarios 2 and 3.

The performance comparison for the frequency is visible in figure 5.5. The frequency comparison is closer than the voltage comparison, but the decentralised controller (scenario 3) is still the better-performing controller in the end. The centralised controller did, however, perform better than the decentralised controller from $t = 0$ to $t = 8$, which means that the centralised controller is better at mitigating disturbances when considering frequency. This, however, only holds if the system remains stable after the disturbance is introduced.

5.3.2 Load changes in maximum-capacity microgrid

The results of the three scenarios related to the changes in load will be detailed in this section. The differences between the control techniques will be presented at the end of this section. The simulations for scenarios 4-6 are done according to the events stipulated in table 5.3.

Table 5.3: Summary of events in scenarios 4-6

Time (s)	Event	Load connected
0	Simulation starts	3 kW
4	4 kW Load is added	7 kW
8	4 kW Load is added	11 kW
12	4 kW Load is removed	7 kW
16	4 kW Load is removed	3 kW

The time intervals for the events are the same as for scenarios 1-3, but this time, the load is increased or decreased (see section 5.2.8). All the inverters are connected from the beginning, meaning that there will be no disturbances associated with the interaction between the inverters; the only disturbances are those associated with the change in load.

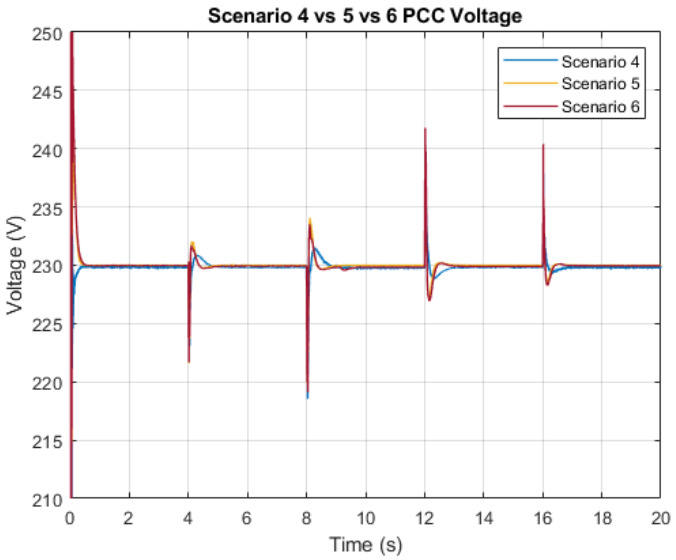

Figure 5.6: PCC voltage comparison for scenarios 4-6.

The voltage output of scenarios 4, 5, and 6 can be seen in figure 5.6. The output of the scenarios is almost similar, with all the scenarios classified as stable. There are slight differences between the scenarios such as the centralised and decentralised controllers caused a larger startup transient spike than the no-control system. This spike is due to the control system trying to stabilise the system at the start, and since the no control system does not consist of a control system, the system settles as guided by the internal control system of the inverters.

The voltage spike observed for each disturbance is also larger for the centralised and decentralised control systems. This is also due to the compensation of the added PI controllers. The no-control system also takes longer to recover from the disturbance, which is confirmation that the external control system does add value to the microgrid. From this output, it can be concluded that the centralised and decentralised controlled system, as well as the no control system, can maintain stability despite the disturbances from a change in load.

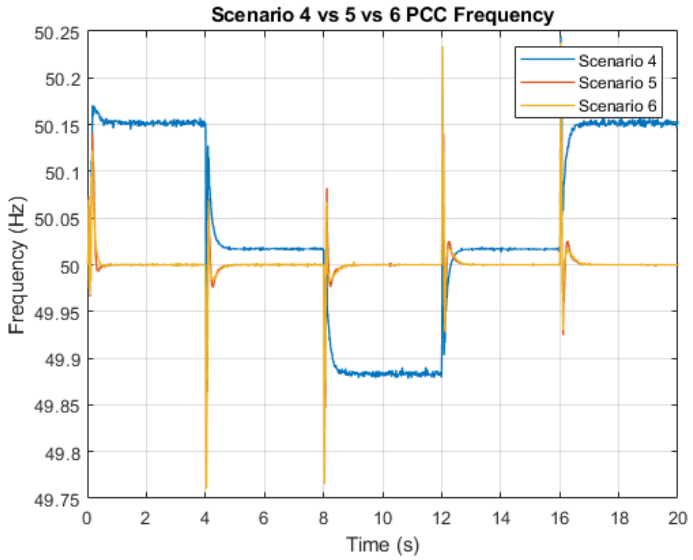

Figure 5.7: PCC frequency comparison for scenarios 4-6.

The output frequency is visible in figure 5.7. Since all the inverters are connected from the start, both the centralised and decentralised controllers can maintain the inverters' frequency at 50 Hz. The no-control system is, however, unable to maintain a stable frequency reading of 50 Hz, which is similar to the results found in scenarios 1-3.

The centralised and decentralised systems can return to steady state much faster than the no-control system; again due to the compensation of the external control system. The output of the centralised and decentralised controlled systems is identical, supporting the claim that a single inverter behaves the same as multiple inverters (see figure 4.10). This can be concluded since the centralised control system will control multiple inverters and the decentralised controller will only control a single inverter while both control systems comprise the same PI controller.

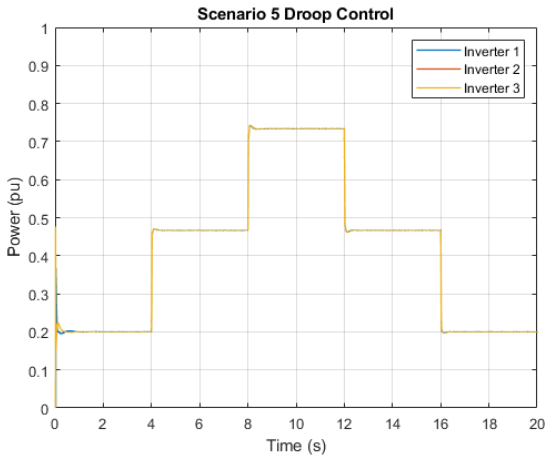

(a) Scenario 5 load sharing output

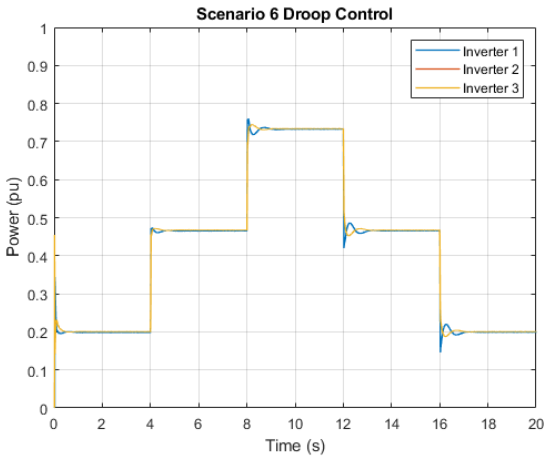

(b) Scenario 6 load sharing output

Figure 5.8: Load sharing output from scenarios 5 and 6.

The load sharing (droop control) output for both scenario 5 and 6 can be seen in figure 5.8. The load-sharing capabilities of the centralised controller (scenario 5) are still operating as expected, with all the inverters sharing the load equally. The decentralised system's (scenario 6) load-sharing capabilities are better than in scenario 3, but it is still not perfect. There are small deviations once the disturbance got introduced, but the load sharing becomes equal after a short while.

This difference between the centralised and decentralised system is observed due to the value of the input reference. For the centralised system, the input reference is the same for all the inverters despite the disturbance, but the decentralised system provides a different reference value to each inverter until the disturbance is mitigated, after which the reference values will also be the same for all the inverters, hence the equal load sharing.

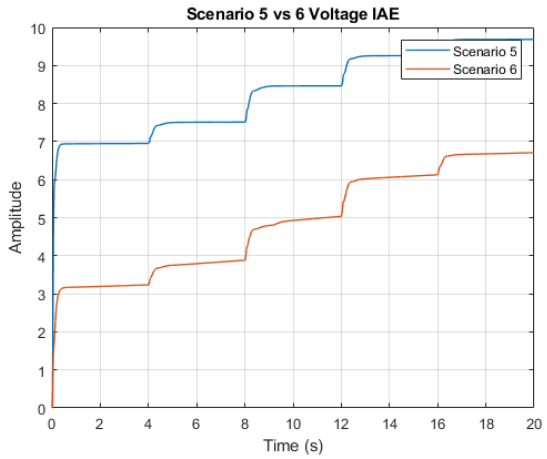

(a) IAE comparison of output voltage.

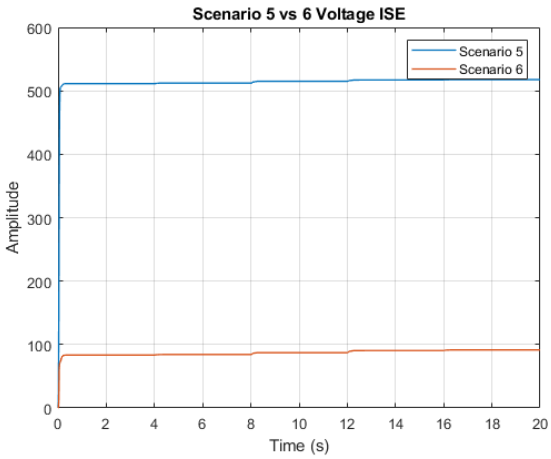

(b) ISE comparison of output voltage.

Figure 5.9: ISE and IAE comparison of the PCC voltage from scenarios 5 and 6.

The performance of the controllers based on the output voltage can be seen in figure 5.9. From the performance graphs, it is clear that the decentralised controller (scenario 6) performed better at maintaining the voltage at the reference value than the centralised controller (scenario 5). The effect of the disturbances from $t = 2$ onwards was similar for both controllers since the magnitude of each deviation is the same. The main difference occurred at the startup transient spike; the decentralised controller was able to suppress the spike more than the centralised controller. This is the only significant difference between the two controllers.

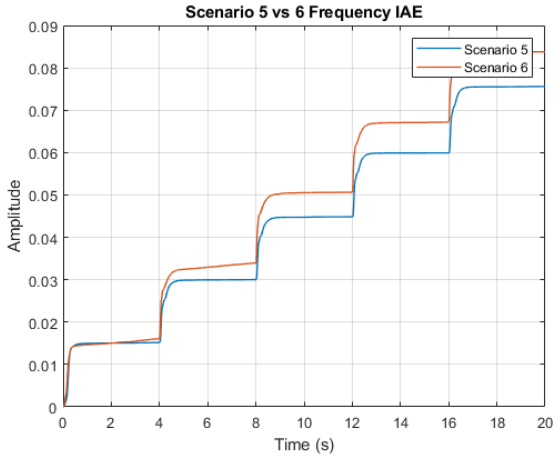

(a) IAE comparison of the output frequency.

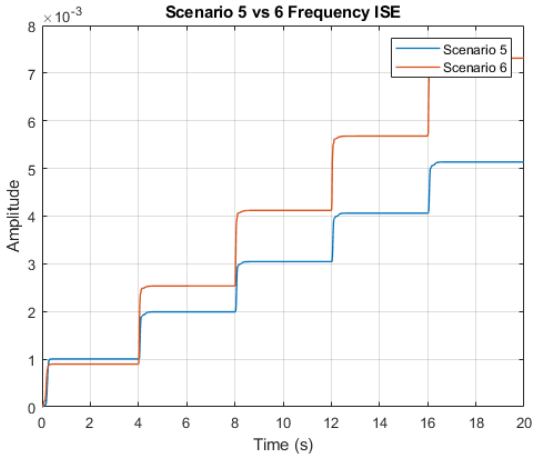

(b) ISE comparison of the output frequency.

Figure 5.10: ISE and IAE comparison of the PCC frequency from scenarios 5 and 6.

The performance of the controller for the output frequency is depicted in figure 5.10. In these results, the centralised controller (scenario 5) outperformed the decentralised controller (scenario 6). The deviations from the set point due to the disturbances were larger for the decentralised controller, hence the larger steps in figure 5.10. The startup transient did not seem to challenge either controller for the output frequency. Therefore, one can conclude that both the centralised and decentralised controller can maintain frequency stability despite the disturbances.

5.3.3 Dynamically controlled system

The results from the scenarios discussed in section 5.2.9 are presented in this section. Since this is the worst-case scenario, the load will will be varied along with the number of inverters connected to the PCC. The effect of both disturbances will be investigated in this section. The overload detection discussed in section 4.4.3 will be used to add and remove inverters as the magnitude of the load varies. The events for scenarios 7-9 are captured in table 5.4.

Table 5.4: Summary of events in scenarios 4-6

Time (s)	Event	Total Load	Inverters
0	Simulation starts	3 kW	1
4	4 kW Load and inverter are added	7 kW	2
8	4 kW Load and inverter are added	11 kW	3
12	4 kW Load and inverter are removed	7 kW	2
16	4 kW Load and inverter are removed	3 kW	1

The output voltage for scenarios 7-9 is presented in figure 5.11. At the start of the simulation, only one inverter is connected with a base load of 4 kW, meaning that the microgrid should be able to supply the demand. The three scenarios all present as stable, meaning that the output voltage is 230 V with a minimal steady-state error.

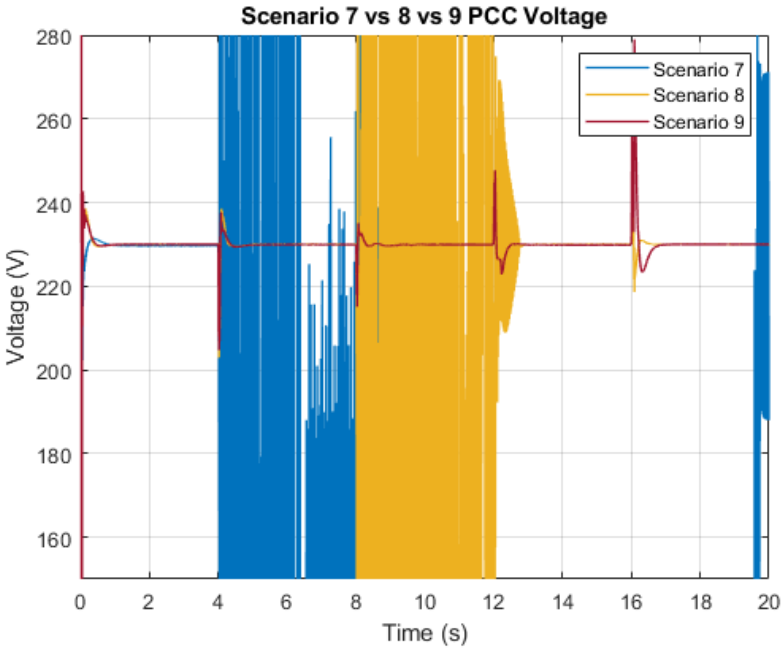

Figure 5.11: PCC voltage comparison for scenarios 7-9.

At $t = 4$s, the load is increased to 7 kW (see figure B.3), meaning that a single inverter is no longer adequate to supply the demanded power, therefore, the control system will add a second inverter. If this happens, there are two disturbances introduced into the microgrid; the first is the disturbance from the interaction between the inverters, and the second is from the abrupt change in load. In these scenarios, the load is increased to more than the capacity of the microgrid before the extra inverter is added, which means that the control system should stabilise the system until the capacity of the second inverter is available.

These two disturbances proved to be too severe for scenario 7 (no control) to retain stability. Once the second inverter is added, the system spirals out of control and never returns to a state of stability. The centralised controller can maintain stability when there are two inverters connected. The disturbance from the load and inverter is mitigated without compromising stability. As soon as the third inverter is added due to the high demand, the centralised controller can no longer maintain stability. The system becomes completely unstable and the control system is unable to counteract the disturbance. Once the third inverter is removed after the demand had decreased, the system returns to stability after a short time delay. This is the same behaviour for the centralised controller as observed in scenario 2 where the controller is unable to mitigate the disturbance if there are more than two inverters added.

The decentralised control system is again the only control system which can maintain stability despite the disturbances introduced. The first disturbance (when the second inverter is added at $t = 4$) caused a voltage spike, but it was able to return to a steady state relatively fast. Once the third inverter was added at $t = 8$, the control system again managed to retain stability. The decentralised controller also managed to maintain stability when the inverters were removed at $t = 12$ and $t = 16$ respectively. The voltage spikes that occurred when the inverters were removed were more severe than when the inverters were added, which is due to the fact that the system is no longer overloaded. The load is decreased meaning that it softened the severity of the disturbance.

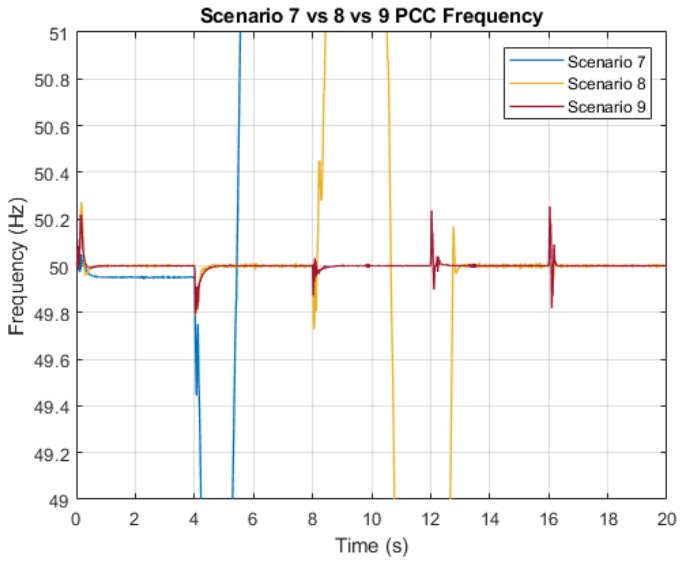

Figure 5.12: PCC frequency comparison for scenarios 7-9.

The output frequency for scenarios 7-9 is captured in figure 5.12. The frequency output mimics the behaviour seen in the output voltage since the no-control system is not able to maintain stability beyond a single disturbance. The centralised controller can maintain stability after the first disturbance, but not the second. The centralised controller is also able to maintain the output frequency at 50 Hz, which is better than the no-control system that could not maintain stability at the desired frequency.

The frequency spikes from the decentralised control system are not as severe as for the voltage, meaning that it was able to mitigate frequency deviations better than voltage deviations. This again proved that the decentralised controller is the most suitable controller when inverters are added and removed from the microgrid.

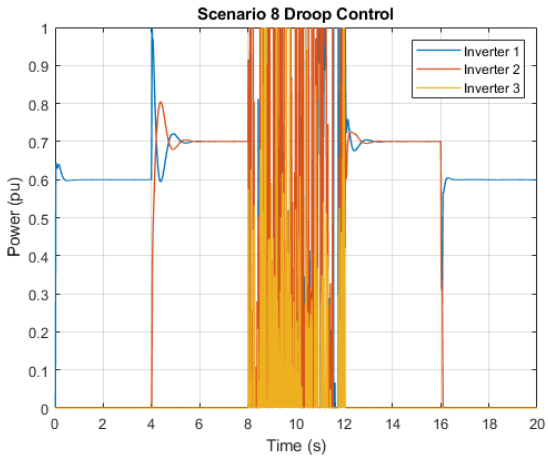

(a) Scenario 8 load sharing output

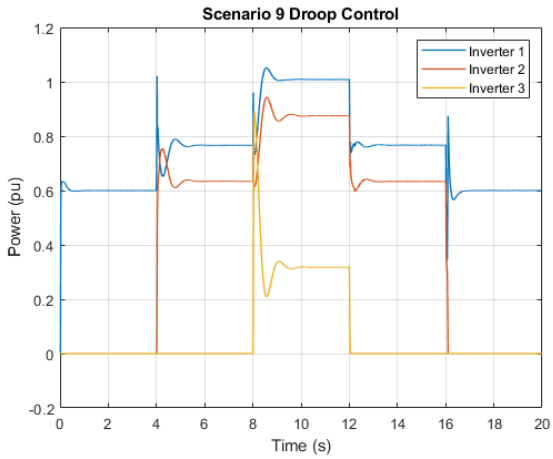

(b) Scenario 9 load sharing output

Figure 5.13: Load sharing output from scenarios 8 and 9.

The load-sharing output for scenarios 8 and 9 can be seen in figure 5.13. The centralised controller was able to share the load effectively between the two inverters after the second inverter was added. The system became unstable after the second disturbance, therefore, the droop controller was not operational.

The droop controller for the decentralised controller did share the load between the inverters, but it was not as effective as the centralised controller. When the third inverter was added, the load was shared unequally between all the inverters, but the first inverter still operated at its maximum, which is not ideal. Although the load sharing was not flawless, the droop controller did enough to prevent instability due to overloading.

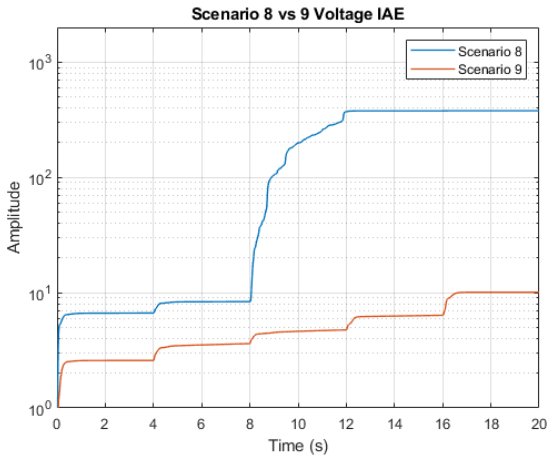

(a) IAE comparison of output voltage.

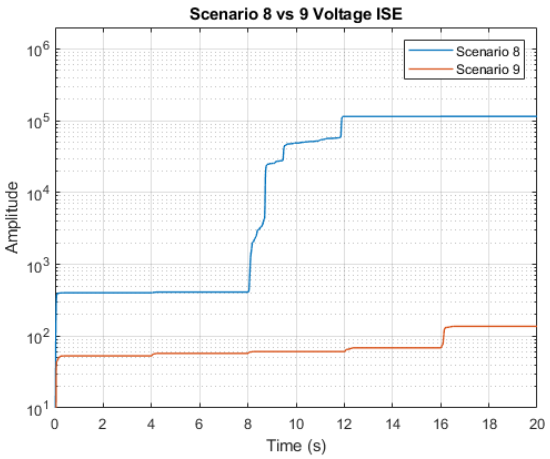

(b) ISE comparison of output voltage.

Figure 5.14: ISE and IAE comparison of the PCC voltage from scenarios 8 and 9.

The performance graphs for scenarios 8 and 9 can be seen in figures 5.14 and 5.15. The y-axis scale of these graphs was changed to a logarithmic scale to display the entire graph due to the large amplitude of the centralised controller's graphs. The decentralised controller outperformed the centralised controller from the start of the simulation, which was not the case in scenarios 5 and 6. The instability of the system caused the extreme high amplitude for the centralised controller's ISE and IAE.

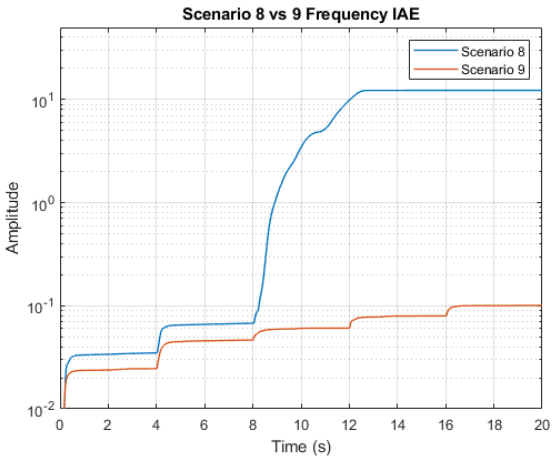

(a) IAE comparison of output frequency

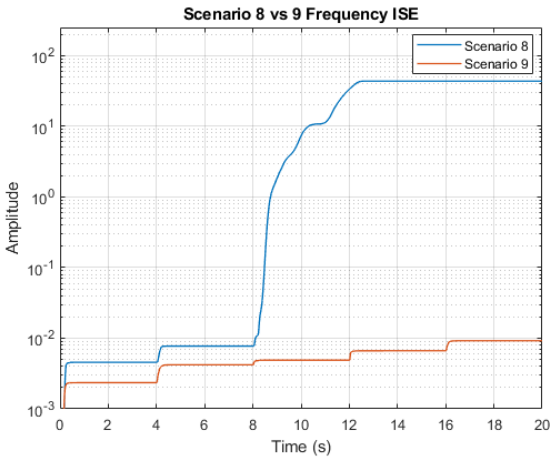

(b) ISE comparison of output frequency

Figure 5.15: ISE and IAE comparison of the PCC frequency from scenarios 8 and 9.

This section summarised the results from the worst-case scenarios, meaning that these scenarios are unlikely in physical applications, but not impossible. From these results, it can be concluded that an external controller is not optional for normal operation since the disturbances are too severe. The centralised controller can only be implemented in certain circumstances where there are not more than two inverters. The decentralised controller proved to be the most robust and can be implemented in any application.

This does, however, not mean that the decentralised controller is without flaws, but it will regain stability after a severe disturbance. The hard limits for the voltage and frequency deviations should be considered before installing a decentralised controller in a microgrid for such an application.

5.4 Discussion

Microgrids are usually implemented with an intended purpose, meaning the circumstances in which they will have to operate are usually known to a large extent. Therefore, the control system can be hand-picked for the specific application to ensure proper operation of the microgrid.

The scenarios discussed in the preceding sections aimed to present the challenges the different control techniques might face in certain unknown circumstances. The no-control systems (scenarios 1, 4, and 7) illustrated what would happen to the microgrid if there is not an external control system, and in all the scenarios, the need for an external controller is highlighted. Since an external control system is necessary, the control system should be selected so that it can withstand the disturbances that will be introduced into the microgrid.

From the simulation results, it can be concluded that the decentralised controller is overall the best performing and most robust controller since it is the only controller that could maintain stability in all scenarios. The disturbances associated with changes in load proved to be less significant than the disturbances associated with the interaction between the inverters. This is supported by the results which stated that the microgrid did not become unstable when subjected to load variance. The no-control and centralised control systems did, however, fail the stability test when the interaction between the inverters was tested. Thus, the latter disturbance has the most severe effect on the microgrid.

All the control systems struggled to manage the disturbances when both the load variance and interaction between the inverters were tested in the worst-case scenario. The decentralised control system was, however, the only controller to maintain stability, but at a cost. The output voltage and frequency for each inverter in scenario 9 is captured in figures B.4 and B.5 respectively. Although the output voltage of scenario 9 is considered stable, the output for each inverter illustrates some differences between the different inverters, which could potentially cause instability if subjected to more severe circumstances.

The performance measures used for the centralised and decentralised controllers were the ISE and IAE, which produced output graphs that can be compared with one another. To evaluate performance from a graph is rather difficult, therefore, the ISE and IAE were quantified to obtain a numerical value. This was done by calculating the area under the ISE and IAE graphs by means of the *trapz* function in MATLAB. The output would be a numerical value of the area, and the smaller the area, the better the performance of the controller.

Table 5.5: Comparison between the controllers' performance

	Integral Squared Error (ISE)		**Integral Absolute Error (IAE)**	
	Voltage	**Frequency**	**Voltage**	**Frequency**
Scenario 2 (C)	2.027×10^{6}	0.0985	9.2280×10^{3}	1.7231
Scenario 3 (D)	$\mathbf{1.316 \times 10^{3}}$	**0.0620**	**72.7826**	**0.7794**
Scenario 5 (C)	1.027×10^{4}	**0.0604**	166.3939	**0.8869**
Scenario 6 (D)	$\mathbf{1.742 \times 10^{3}}$	0.0817	**97.6816**	0.9849
Scenario 8 (C)	1.085×10^{6}	381.899	3.8041×10^{3}	112.4163
Scenario 9 (D)	$\mathbf{1.496 \times 10^{3}}$	**0.1082**	**106.6052**	**1.2179**

The numerical values of ISE and IAE are captured in table 5.5 where C and D represent centralised and decentralised control respectively. The results are grouped by disturbance as stipulated in section 5.2, where the bold values represent the superior performance. Scenarios 2 and 3 represent the disturbance from the interaction between the inverters. The centralised controller (scenario 2) was outperformed by the decentralised controller (scenario 3) for both the voltage and frequency. The poor performance of the centralised controller is due to the voltage collapse as discussed in the preceding sections.

Considering figure 5.5, the centralised controller was better at mitigating the disturbance when the second inverter was added, meaning that the centralised controller may be better for this type of disturbance should the microgrid remain in a stable state. The reason for considering the performance over the entire simulation instead of only one disturbance is to determine how the controller performs for all possible outcomes (such as the connection of more than two inverters).

Scenarios 5 and 6 represent the disturbance from the change in load. Both controllers were able to maintain stability in the microgrid despite the disturbances. The decentralised controller outperformed the centralised controller based on its ability to mitigate voltage deviations. The centralised controller was superior in militating frequency deviations. Therefore, according to the results, either of these controllers can be used to maintain stability in a microgrid when the only disturbance is the change in load.

Scenarios 8 and 9 represent the worst-case scenarios in which both disturbances were introduced. In the results, it is clear that the decentralised controller is the better option to implement on a multi-inverter microgrid since neither of the other scenarios was able to maintain stability. The decentralised controller is not flawless, but it can manage the disturbances quite well.

The results in table 5.5 provide a valuable overview of the performance of each controller, but it does not necessarily mean that the controllers have a positive influence on the system. Therefore, the outputs of the baseline scenarios (1, 4, and 7) were also quantified in order to determine how well the controllers can manage the microgrid. This quantification entailed that the offset from the desired set point (230 V and 50 Hz) was calculated for every point in time to obtain the set point error graph. The area under the graph was then calculated to provide the magnitude of the offset over the entire simulation, similar to the quantification of the ISE and IAE graphs.

Table 5.6: Comparison between Set Point (SP) errors for scenarios 1-9

	Voltage SP Error (V)	Frequency SP Error (Hz)
Scenario 1 (N)	917.606	1.847
Scenario 2 (C)	916.588	0.192
Scenario 3 (D)	**6.914**	**0.062**
Scenario 4 (N)	8.286	1.794
Scenario 5 (C)	**6.162**	0.086
Scenario 6 (D)	8.1789	**0.084**
Scenario 7 (N)	2354	388.337
Scenario 8 (C)	601.694	15.271
Scenario 9 (D)	**14.002**	**0.116**

The results are captured in table 5.6, where N, C, and D represent no-control, centralised control, and decentralised control respectively. For the first disturbance, scenarios 1 and 2 are quite similar due to the voltage collapse. The decentralised controller has the best influence on the system since the centralised controller failed the voltage stability test and only managed to keep the frequency relatively close to the set point. The performance of the no-control and centralised control for the voltage output is almost the same, meaning that the influence of the centralised controller can be neglected.

For the second disturbance (change in load), the centralised controller performed the best in terms of voltage control. The decentralised controller and the no-load controller's output are almost identical, meaning that the decentralised controller did not contribute to the mitigation of voltage deviations. The frequency, on the other hand, is much better with both the centralised and decentralised controllers.

In the worst-case scenario, both the centralised controller and the no-control system performed poorly. The decentralised controller outperformed both the other two scenarios. There is an improvement for the centralised output in contrast with the no-control system, but it is not worth exploring.

Taking all of the aforementioned findings into account, the conclusion can be drawn that an external controller should be implemented on a microgrid since the voltage, and especially the frequency, must be maintained to ensure proper functioning. The choice of external controller comes down to application; if the microgrid will be subjected to disturbances which include the addition and removal of inverters, the decentralised controller is the optimal choice. If there will be no change in the number of inverters connected and the only disturbance will originate from the load connected, it will not matter which controller is implemented since both performed almost equally. If the microgrid might experience both disturbances, the decentralised controller is again the optimal option. Therefore, overall, the most robust controller is the decentralised controller. It is not perfect and the controller should be improved before it will operate flawlessly, but the decentralised concept is the best topology to implement in the circumstances discussed.

5.5 Conclusion

This chapter started with an experimental design that depicted the different scenarios to be implemented in Simulink to evaluate the robustness of the control system. These scenarios were implemented for both the centralised and decentralised control systems, which provided a comprehensive understanding of the capabilities of the control system.

The results from the scenarios were analysed to determine the shortcomings of each control system in each simulation environment. The no-control, centralised control, and decentralised control scenarios were compared for each disturbance to determine which control system would be optimal for each disturbance.

From this analysis, it was found that the decentralised controller would be suitable for almost all the scenarios since it is the only control system capable of maintaining stability despite the disturbances introduced in this study. The centralised controller outperformed the decentralised controller in voltage control for some of the scenarios, but the centralised controller was not able to ensure stability for all operating conditions.

Chapter 6

Conclusion

This chapter serves as the conclusion of this dissertation. The key discoveries identified in this study are reported along with suggestions on how to improve the already-implemented structures in an islanded microgrid.

6.1 Conclusion

The global challenge of energy supply security is intensifying, necessitating the use of microgrids, specifically islanded microgrids. This introduced the challenge of microgrid stability in an islanded microgrid, which is currently being researched worldwide in an effort to overcome this challenge. The stability challenge is usually approached with extremely complex and expensive solutions which perform perfectly but are not feasible for all applications, therefore, the simple and cost-effective PI controller was implemented in this study to evaluate its capabilities on a multi-inverter microgrid.

Chapter 3 discussed the process that was followed in order to obtain a suitable model of a microgrid. The MATLAB example was used as the foundation from which all the modifications were done to ensure the model applies to this study. Since the model's dynamics were unknown, a generic microgrid state space model was derived in order to approximate the Simulink model. This state space model was then used in the controller design phase. The Simulink model consisted of all the elements required, as mentioned in the first objective in chapter 1. This concluded the first objective of this study, as depicted in section 1.3.1.

The second objective of this study was to identify the elements that may contribute to instability in the microgrid (section 1.3.2). Once the model development was done in chapter 3, the frequency response of the system was analysed in chapter 4, which concluded that the high-frequency elements in the system may cause stability challenges. Furthermore, the experimental simulations performed in chapter 5 concluded that the system is not able to maintain stability when subjected to certain circumstances, which is also added to the list of elements that may cause instability.

The third objective was to develop a suitable control system for this system (section 1.3.3). The control development process is detailed in chapter 4. The control system was realised with a PI controller since it will remove some of the high-frequency elements and add little inertia to the system. This would aid the stability of the microgrid in unfavourable circumstances, as mentioned in the second objective. This PI controller was then implemented in a centralised- and decentralised configuration, which was evaluated in the last objective.

The final objective was to evaluate the control systems based on their performance (section 1.3.4). The evaluation of the system was done by means of different predefined scenarios that will evaluate the control system's performance to maintain stability despite specific disturbances. The centralised and decentralised control system's performances were measured against a microgrid that does not have any external control.

During this evaluation, it was found that the decentralised control technique proved to be more effective than the centralised controller based on its ability to mitigate disturbances. The concept that each inverter is managed by an individual controller is the deciding factor between the centralised and decentralised control techniques. Although the decentralised control technique was superior for most of the scenarios discussed in this dissertation, it was not able to keep the output voltage and frequency spikes within the specified ranges, therefore, it still needs refinement. The disturbance associated with the interaction between the inverters also proved to be more severe than the disturbance from the change in load in the microgrid.

The centralised and decentralised control system was designed for a single inverter but implemented on a microgrid with more than one inverter. All of the inverters in the microgrid are identical, which is the reason why the control system could be developed from a single inverter. Despite the other inverters in the microgrid, the decentralised control system was able to maintain stability for up to three inverters that are connected at the same time.

The simple PI controller will be stable in most applications, but it cannot be applied in all applications as is. The fact that the decentralised control technique was the best performing only means that the concept of decentralised control should be explored before defaulting to the computationally expensive centralised controller.

Although stability was maintained by the decentralised controller, the performance measures discussed in section 1.4.4 were not all satisfied in all the scenarios. In some of the scenarios, the decentralised controller met these requirements; in another, the specified ranges were violated when the disturbances were introduced, but the operation following the disturbance was well within the prescribed ranges.

This study concluded that it is possible to mitigate extreme disturbances and regain stability with a simple control technique, therefore, the use of Artificial Intelligence (AI) and neural networks are not always needed for a specific application.

6.2 Future work

The aim of this study was not to solve the stability challenge in microgrids, but it was to investigate the performance of simple control techniques on multi-inverter microgrids. Therefore, the addition of advanced control techniques such as AI is unnecessary for the purpose of simple control techniques.

For future research, it is recommended to obtain data from a specific microgrid from which the mathematical models can be created. This will provide a more accurate approximation of a microgrid which could yield better results. The same centralised and decentralised control system can be implemented on the actual microgrid to compare the simulations and the real-life application. This also may provide more insight into the performance of the PI control system.

The control system can be optimised further to ensure the specified operating conditions are not violated when disturbances are introduced. This can be done by adding more complexity to the PI control system, change the PI controller to a PID controller, or add other means of compensation to the microgrid.

Since the PI controller was able to retain stability, its performance may be improved if the control system had access to data from the immediate future to prepare the microgrid for the events. The addition of Neural Networks may be able to realise this concept, because load data from a specific microgrid can be used to predict demand for that microgrid in the near future, allowing the control system to add or remove inverters prior to any disturbances to avoid the worst-case scenario.

Bibliography

[1] G. K. Gill, T. kaur Gill, and R. Singh, "Energy security - the issue of present time," in *2015 IEEE 10th Conference on Industrial Electronics and Applications (ICIEA)*. Auckland, New Zealand: IEEE, Jun. 2015, pp. 2065–2068.

[2] E. Hossain, E. Kabalcı, R. Bayindir, and R. Perez, "A comprehensive study on microgrid technology," *International Journal of Renewable Energy Research*, vol. 4, pp. 1094–1104, Jan. 2014.

[3] Y. Lim, H.-M. Kim, and T. Kinoshita, "Distributed load-shedding system for agent-based autonomous microgrid operations," *Energies*, vol. 7, pp. 385–401, Jan. 2014.

[4] M. Farrokhabadi, C. A. Canizares, J. W. Simpson-Porco, E. Nasr, L. Fan, P. A. Mendoza-Araya, R. Tonkoski, U. Tamrakar, N. Hatziargyriou, D. Lagos, R. W. Wies, M. Paolone, M. Liserre, L. Meegahapola, M. Kabalan, A. H. Hajimiragha, D. Peralta, M. A. Elizondo, K. P. Schneider, F. K. Tuffner, and J. Reilly, "Microgrid Stability Definitions, Analysis, and Examples," *IEEE Trans. Power Syst.*, vol. 35, no. 1, pp. 13–29, Jan. 2020.

[5] *The South African Grid Code (System Operation Code)*, NERSA Std., Aug. 2019.

[6] M. Ramezani and S. Li, "Voltage and frequency control of islanded microgrid based on combined direct current vector control and droop control," in *2016 IEEE Power and Energy Society General Meeting (PESGM)*, Jul. 2016, pp. 1–5.

[7] Liu and Wang, "Research on frequency control of islanded microgrid with multiple distributed power sources," *Processes*, vol. 8, p. 193, Feb. 2020.

[8] M. Griffiths and C. Coates, "Behaviour of microgrids in the presence of unbalanced loads," in *2007 Australasian Universities Power Engineering Conference*. Perth, Australia: IEEE, Dec. 2007, pp. 1–5.

[9] K. Chen and M. Baran, "Stability of a Community Microgrid in Islanded Mode: A Case Study," in *2018 9th IEEE International Symposium on Power Electronics for Distributed Generation Systems (PEDG)*, Jun. 2018, pp. 1–5.

[10] R. Christensen, "Analysis of Variance and Generalized Linear Models," in *International Encyclopedia of the Social & Behavioral Sciences*. Elsevier, 2015, pp. 659–664.

[11] A. Johansen, "Monte Carlo Methods," in *International Encyclopedia of Education*. Elsevier, 2010, pp. 296–303.

[12] X. Ma, Y. Wang, and J. Qin, "Generic model of a community-based microgrid integrating wind turbines, photovoltaics and CHP generations," *Applied Energy*, vol. 112, pp. 1475–1482, 2013.

[13] J. Wang, C. Zhao, A. Pratt, and M. Baggu, "Design of an advanced energy management system for microgrid control using a state machine," *Applied Energy*, vol. 228, pp. 2407–2421, Oct. 2018.

[14] A. Thakar and M. Pala, "Modelling and Transient Stability Analysis of Microgrid," in *2019 IEEE 5th International Conference for Convergence in Technology (I2CT)*, Mar. 2019, pp. 1–5.

[15] T. Kousksou, P. Bruel, A. Jamil, T. El Rhafiki, and Y. Zeraouli, "Energy storage: Applications and challenges," *Solar Energy Materials and Solar Cells*, vol. 120, pp. 59–80, Jan. 2014.

[16] N. S. Chouhan and M. Ferdowsi, "Review of energy storage systems," in *41st North American Power Symposium*. Starkville, MS, USA: IEEE, Oct. 2009, pp. 1–5.

[17] G. Graditi, R. Ciavarella, M. Valenti, G. Ferruzzi, and G. Zizzo, "Frequency stability in microgrid: Control strategies and analysis of BESS aging effects," in *2016 International Symposium on Power Electronics, Electrical Drives, Automation and Motion (SPEEDAM)*, Jun. 2016, pp. 295–299.

[18] J. Shen, C. Jiang, and B. Li, "Controllable Load Management Approaches in Smart Grids," *Energies*, vol. 8, no. 10, pp. 11 187–11 202, Oct. 2015.

[19] B. Moran, "Microgrid load management and control strategies," in *2016 IEEE/PES Transmission and Distribution Conference and Exposition (T D)*, May 2016, pp. 1–4.

[20] M. Pasetti, S. Rinaldi, and D. Manerba, "A Virtual Power Plant Architecture for the Demand-Side Management of Smart Prosumers," *Applied Sciences*, vol. 8, no. 3, p. 432, Mar. 2018.

[21] G. Invernizzi and G. Vielmini, "Challenges in Microgrid Control Systems Design. An application case," in *2018 AEIT International Annual Conference*. Bari, Italy: IEEE, Oct. 2018, pp. 1–6.

[22] R. Kljajić, P. Marić, H. Glavaš, and M. Žnidarec, "Microgrid Stability: A Review on Voltage and Frequency Stability," in *2020 IEEE 3rd International Conference and Workshop in Óbuda on Electrical and Power Engineering (CANDO-EPE)*, Nov. 2020, pp. 000 047–000 052.

[23] M. Anwar, M. I. Marei, and A. A. El-Sattar, "Generalized droop-based control for an islanded microgrid," in *2017 12th International Conference on Computer Engineering and Systems (ICCES)*, Dec. 2017, pp. 717–722.

[24] R. Belkacemi, S. Zarrabian, A. Babalola, and R. Craven, "Experimental transient stability analysis of MicroGrid systems: Lessons learned," in *2015 IEEE Power Energy Society General Meeting*, Jul. 2015, pp. 1–5.

[25] G. A. Alizadeh, T. Rahimi, M. H. Babayi Nozadian, S. Padmanaban, and Z. Leonowicz, "Improving Microgrid Frequency Regulation Based on the Virtual Inertia Concept while Considering Communication System Delay," *Energies*, vol. 12, no. 10, p. 2016, May 2019.

[26] N. Jayawarna, X. Wu, Y. Zhang, N. Jenkins, and M. Barnes, "Stability of a MicroGrid," in *2006 3rd IET International Conference on Power Electronics, Machines and Drives - PEMD 2006*, Apr. 2006, pp. 316–320.

[27] S. Arif and T. Aziz, "Study of Transient Stability with Battery Energy Storage Systems in Renewable Integrated Islanded Microgrid," in *2017 IEEE International WIE Conference on Electrical and Computer Engineering (WIECON-ECE)*, Dec. 2017, pp. 266–269.

[28] F. Luo, Y. M. Lai, K. H. Loo, C. K. Tse, and X. Ruan, "A generalized droop-control scheme for decentralized control of inverter-interfaced microgrids," in *2013 IEEE International Symposium on Circuits and Systems (ISCAS)*, May 2013, pp. 1320–1323.

[29] G. Delille, B. Francois, and G. Malarange, "Dynamic Frequency Control Support by Energy Storage to Reduce the Impact of Wind and Solar Generation on Isolated Power System's Inertia," *IEEE Trans. Sustain. Energy*, vol. 3, no. 4, pp. 931–939, Oct. 2012.

[30] F. Chen, R. Burgos, D. Boroyevich, and W. Zhang, "A nonlinear droop method to improve voltage regulation and load sharing in DC systems," in *2015 IEEE First International Conference on DC Microgrids (ICDCM)*, Jun. 2015, pp. 45–50.

[31] L. Jia, C. du, C. Zhang, and A. Chen, "An improved droop control method for reducing current sensors in DC microgrid," Oct. 2017, pp. 4645–4649.

[32] H. Karimi-Davijani and O. Ojo, "Dynamic operation and control of a multi-DG unit standalone Microgrid," in *ISGT 2011*. Anaheim, CA, USA: IEEE, Jan. 2011, pp. 1–7.

[33] P. Kant, P. Singhal, M. K. Mahto, and D. Jain, "Control strategies for DC Microgrids: An overview," in *2022 2nd International Conference on Power Electronics & IoT Applications in Renewable Energy and Its Control (PARC)*. Mathura, India: IEEE, Jan. 2022, pp. 1–6.

[34] F. Li, R. Li, and F. Zhou, *Microgrid Technology and Engineering Application*. San Diego, CA, USA: Elsevier Science Publishing Co Inc, 2015.

[35] S. Manson, K. G. Ravikumar, and S. K. Raghupathula, "Microgrid Systems: Design, Control Functions, Modeling, and Field Experience," p. 9.

[36] F. Khavari, A. Badri, A. Zangeneh, and M. Shafiekhani, "A comparison of centralized and decentralized energy-management models of multi-microgrid systems," in *2017 Smart Grid Conference (SGC)*. Tehran: IEEE, Dec. 2017, pp. 1–6.

[37] W. Zhong, M. A. A. Murad, M. Liu, and F. Milano, "Impact of Virtual Power Plants on Power System Short-Term Transient Response," *Electric Power Systems Research*, vol. 189, Dec. 2020.

[38] K. Tazi, F. M. Abbou, and F. Abdi, "Multi-agent system for microgrids: Design, optimization and performance," *Artif Intell Rev*, vol. 53, no. 2, pp. 1233–1292, Feb. 2020.

[39] C. Colson, M. Nehrir, and R. Gunderson, "Multi-agent Microgrid Power Management," *IFAC Proceedings Volumes*, vol. 44, no. 1, pp. 3678–3683, Jan. 2011.

[40] S. K. Sahoo, A. K. Sinha, and N. K. Kishore, "Control Techniques in AC, DC, and Hybrid AC–DC Microgrid: A Review," *IEEE J. Emerg. Sel. Topics Power Electron.*, vol. 6, no. 2, pp. 738–759, Jun. 2018.

[41] A. Kulasekera, R. Gopura, K. T. M. U. Hemapala, and N. Perera, "A review on multi-agent systems in microgrid applications," ser. 2011 IEEE PES International Conference on Innovative Smart Grid Technologies-India, ISGT India 2011, Dec. 2011.

[42] A. L. Dimeas and N. D. Hatziargyriou, "Agent based control of Virtual Power Plants," in *2007 International Conference on Intelligent Systems Applications to Power Systems*. Kaohsiung, Taiwan: IEEE, Nov. 2007, pp. 1–6.

[43] A. Kantamneni, L. E. Brown, G. Parker, and W. W. Weaver, "Survey of multi-agent systems for microgrid control," *Engineering Applications of Artificial Intelligence*, vol. 45, pp. 192–203, Oct. 2015.

[44] K. Nouman, Z. Asim, and K. Qasim, "Comprehensive Study on Performance of PID Controller and its Applications," in *2018 2nd IEEE Advanced Information Management,Communicates,Electronic and Automation Control Conference (IMCEC)*. Xi'an: IEEE, May 2018, pp. 1574–1579.

[45] L. Rundqwist, "Anti-reset Windup for PID Controllers," *IFAC Proceedings Volumes*, vol. 23, no. 8, Part 4, pp. 453–458, Aug. 1990.

[46] S. Shcherbovskykh, K. Kozlowski, and D. Pazderski, "Evaluation of integral anti-windup feedback coefficient for PI regulator," in *2018 IEEE 9th International Conference on Dependable Systems, Services and Technologies (DESSERT)*. Kyiv, Ukraine: IEEE, May 2018, pp. 74–77.

[47] K. Sakai and Y. Ishida, "An Improved Anti-windup Control Using a PI Controller," in *2015 3rd International Conference on Artificial Intelligence, Modelling and Simulation (AIMS)*. Kota Kinabalu, Malaysia: IEEE, Dec. 2015, pp. 197–201.

[48] MathWorks, *Islanded Operation of an Inverter-based Microgrid Using Droop Control Technique*, (2022), accessed: Feb. 12, 2022. [Online]. Available: https://www.mathworks.com/help/sps/ug/power-Microgrid-IslandedOperation-DroopControl.html;jsessionid=1f2d82e997b489e58ff3249b92ba

[49] N. Pogaku, M. Prodanovic, and T. C. Green, "Modeling, analysis and testing of autonomous operation of an inverter-based microgrid," *IEEE Transactions on Power Electronics*, vol. 22, no. 2, pp. 613–625, Mar. 2007.

[50] C. J. O'Rourke, M. M. Qasim, M. R. Overlin, and J. L. Kirtley, "A Geometric Interpretation of Reference Frames and Transformations: Dq0, Clarke, and Park," *IEEE Trans. Energy Convers.*, vol. 34, no. 4, pp. 2070–2083, Dec. 2019.

[51] C. Hu, Y. Wang, S. Luo, and F. Zhang, "State-space model of an inverter-based microgrid," in *2018 3rd International Conference on Intelligent Green Building and Smart Grid (IGBSG)*, Apr. 2018, pp. 1–7.

[52] W. Bolton, *Instrumentation and Control Systems*, third edition ed. Kidlington, England: Newnes, 2021.

[53] C. L. Phillips, H. T. Nagle, and A. Chakrabortty, *Digital Control System Analysis & Design*, fourth edition, global edition ed. Harlow, Essex, England: Pearson Education Limited, 2015.

[54] T. I. Reigstad and K. Uhlen, "Virtual Inertia Implementation in Variable Speed Hydropower Plant," in *2019 Modern Electric Power Systems (MEPS)*. Wroclaw, Poland: IEEE, Sep. 2019, pp. 1–6.

[55] S. M. Cherati, N. A. Azli, S. M. Ayob, and A. Mortezaei, "Design of a current mode PI controller for a single-phase PWM inverter," in *2011 IEEE Applied Power Electronics Colloquium (IAPEC)*. Johor Bahru, Malaysia: IEEE, Apr. 2011, pp. 180–184.

[56] M. Szirtes, R. Cselko, and I. Berta, "Developing a Filtering Algorithm for Partial Discharge Location Approximation Using the Emitted Electromagnetic Signals of Corona Discharges," *IEEE Trans. on Ind. Applicat.*, vol. 57, no. 1, pp. 932–940, Jan. 2021.

[57] D. Zhou and F. Blaabjerg, "Bandwidth oriented proportional-integral controller design for back-to-back power converters in DFIG wind turbine system," *IET Renewable Power Generation*, vol. 11, no. 7, pp. 941–951, Jun. 2017.

[58] A. A. Eajal, A. H. Yazdavar, E. F. El-Saadany, and K. Ponnambalam, "On the Existence of Voltage Collapse in Islanded Microgrid," in *2018 IEEE Electrical Power and Energy Conference (EPEC)*. Toronto, ON: IEEE, Oct. 2018, pp. 1–6.

[59] R. C. Dorf and R. H. Bishop, *Modern Control Systems*, thirteenth edition ed. Hoboken: Pearson, 2016.

Appendix A

Summary of variables used in the inverter modelling

A summary of all the parameters used in the derivation of a symbolic state-space model in chapter 3 is presented in this appendix.

Table A.1: Summary of variables used in section 3.3

Variable	Description
L_f	Inductance of low-pass filter
C_f	Capacitance of low-pass filter
L_c	Coupling inductance
v_{odq}	Output voltage
v_{od}	d-component of output voltage
v_{oq}	q-component of output voltage
i_{odq}	Output current
i_{od}	d-component of output current
i_{oq}	q-component of output current
ω_c	Cut-off frequency of low-pass filter
$\tilde{p}$	Instantaneous active power

Continued on next page

Table A.1 – *Continued from previous page*

$\tilde{q}$	Instantaneous reactive power
m_p	Frequency droop gain
n_q	Voltage droop gain
F	Feed-forward gain
K_{pv}	Proportional gain of inverter's internal voltage controller
K_{iv}	Integral gain of inverter's internal voltage controller
K_{pc}	Proportional gain of inverter's internal current controller
K_{ic}	Integral gain of inverter's internal current controller
L_c	Coupling inductance
ω_n	Natural frequency
v_{bdq}	Bus voltage
v_{bd}	d-component of bus voltage
v_{bq}	q-component of bus voltage

Appendix B

Simulation results

This appendix will provide some of the output graphs from the simulations done in chapter 5. All of the output graphs in this appendix are discussed in the relevant sections in chapter 5.

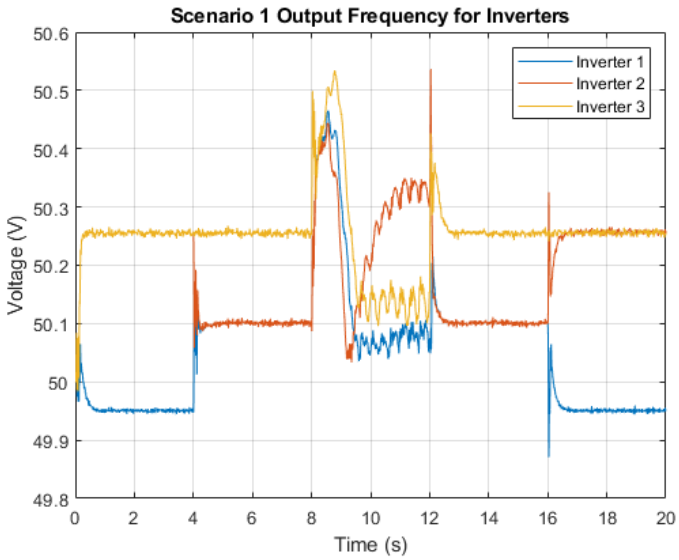

Figure B.1: Output frequency for each inverter in scenario 1.

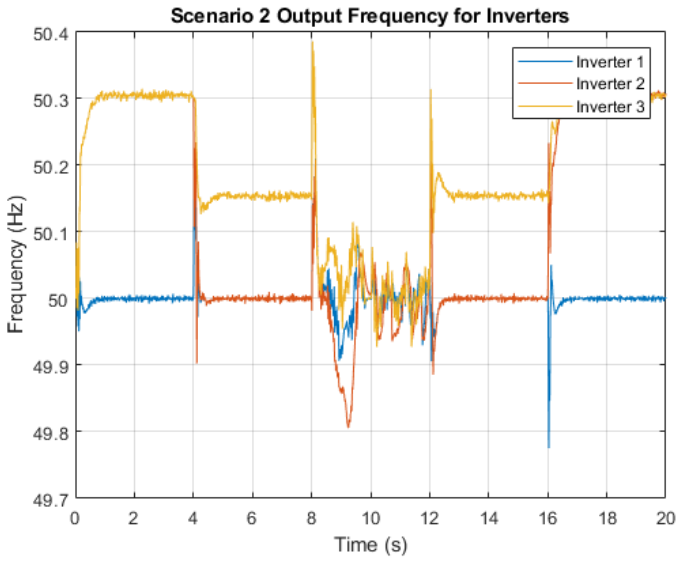

Figure B.2: Output frequency for each inverter in scenario 2.

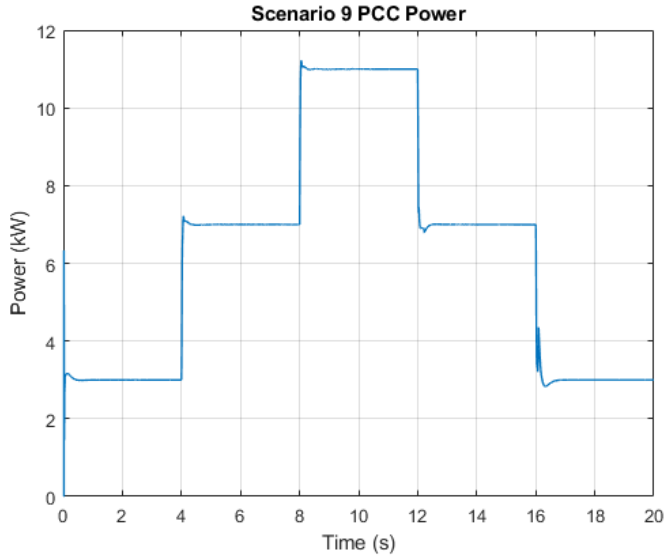

Figure B.3: PCC power from scenario 9.

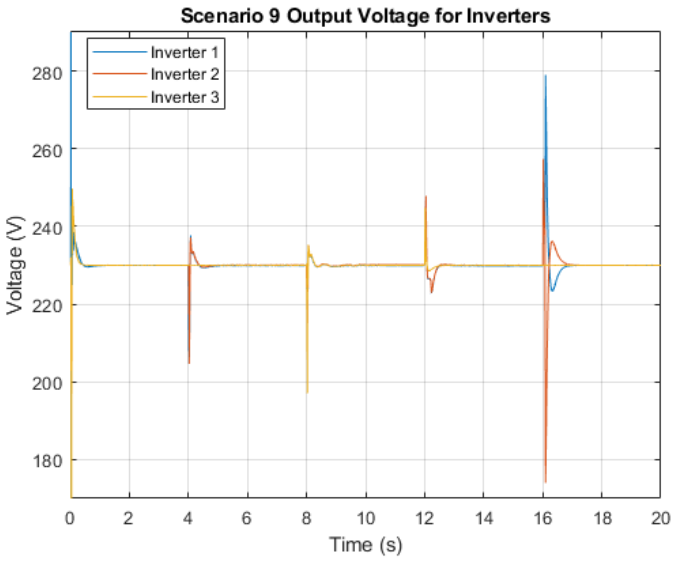

Figure B.4: Output voltage for each inverter from scenario 9.

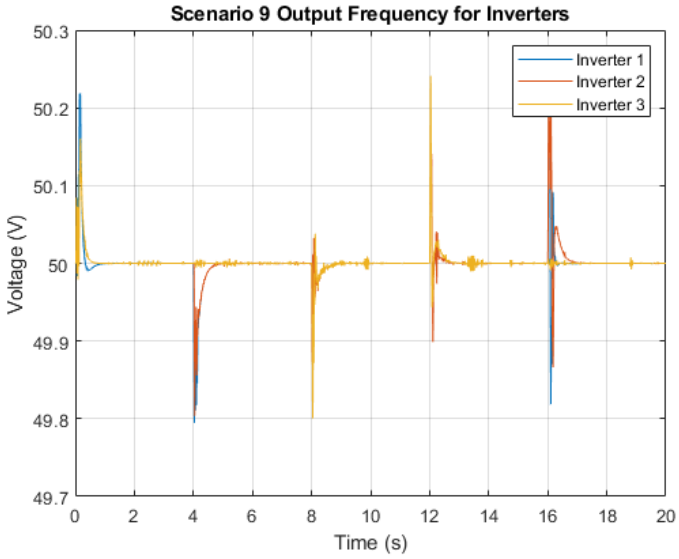

Figure B.5: Output frequency for each inverter from scenario 9.